UNIVERSITY OF CALIFORNIA
SANTA CRUZ

Linking hydrologic and biogeochemical cycling across scales: Implications for nutrient and water resource management

A dissertation submitted in partial satisfaction
of the requirements for the degree of

DOCTOR OF PHILOSOPHY

in

EARTH SCIENCES

by

Galen Gorski

September 2020

The Dissertation of Galen Gorski
is approved:

_____
Professor Andrew T. Fisher, Chair

_____
Dr. Adina Paytan

_____
Professor Noah Finnegan

_____
Quentin Williams
Vice Provost and Dean of Graduate Studies

TABLE OF CONTENTS

LIST OF FIGURES AND TABLES

Chapter 1: Field and laboratory studies linking hydrologic, geochemical, and microbiological processes and enhanced denitrification during infiltration for managed aquifer recharge

Chapter 2: Denitrification during infiltration for managed aquifer recharge: Infiltration rate controls and microbial response

Chapter 3: Mapping potential for denitrification during infiltration with machine learning informed by field and laboratory experiments

Chapter 4: Hydrologic regimes drive nutrient export behavior in human impacted watersheds

ABSTRACT

Linking hydrologic and biogeochemical cycling across scales: Implications for nutrient and water resource management

Galen Gorski

The effective management of water resources faces unprecedented pressures from growing demand and shifting climate among other stressors. Widespread issues of both water quantity and water quality affect many regions. One common problem facing many areas is the excess supply of nitrate (NO_3) to receiving bodies such as aquifers, rivers, streams, and estuaries. Excess nitrate is linked to human activity and can have detrimental effects of human and ecosystem health. Addressing these issues and ensuring that humans and ecosystems have sufficient supplies of clean water requires a more complete understanding of the complex linkages between water quantity and quality across space and time. In this dissertation, I present four original studies across a range of scales investigating the flow of water across and through landscapes that have been altered by human activity. In each study I ask the fundamental question *how does the magnitude, timing, and/or rate of water flow affect key water quality parameters?* Chapters One, Two, and Three focus on investigating water quality improvements during managed aquifer recharge (MAR), a technique for improving groundwater supply and quality through targeted infiltration. In Chapter One, measurements of water quality parameters during controlled

percolation experiments revealed that soil amendments could enhance nitrate removal during infiltration. In Chapter Two, column studies conducted on soil cores collected from MAR sites demonstrated that the rate of infiltration and the presence of a soil amendment were key factors controlling nitrate removal and affecting microbial community composition during MAR. In Chapter 3, we synthesized data from various scales to develop a novel, spatial model of nitrate removal during MAR based on soil and fluid properties. Finally, in Chapter Four, similar concepts are applied to the analysis of nitrate mobilization in streams and rivers of agricultural watersheds to analyze the patterns and timing of delivery of nitrate. Taken together, the studies serve to elucidate fundamental linkages between the hydrologic cycle and key biogeochemical cycles that have profound impacts on our understanding of water resource management for the health and well-being of humans and ecosystems.

ACKNOWLEDGEMENTS

No Ph.D. is a solo task, I am forever grateful to the many who have helped me along the way, and I hope to pay it forward in the future. Listed below are some of the many who have supported me, but there have been many more along the way.

I feel privileged to have been a part of the UC Santa Cruz Earth and Planetary Science Department, which was an amazing place to learn, develop and grow as a scientist and person. I would like to thank my advisor, Andy Fisher, for his patience, enthusiasm and unflagging demonstration of what it means to be a good mentor. I would also like to thank my co-advisor Adina Paytan, and committee member Noah

Finnegan for their guidance through my time in Santa Cruz. Margaret Zimmer has been a valuable mentor and collaborator and working with her and her group has enriched my experience in the EPS department greatly. The hydrogeology group, past and present, has been an amazing source of collaboration and friendship and I would especially like to thank Adam Price, Araceli Serrano, Jenny Pensky, Sarah Beganskas, Kyle Young, Walker Weir, Hannah Dailey, Paige Borges, and Victor Bautista. Our research in the department would not be possible without the tireless and often unheralded work of Amy Kornberg, Jade Loftus, and Jennifer Fish who make the department run.

I would like to thank my parents, Mary Sue and Mark, whose dedication, encouragement and emphasis on education throughout my life has opened innumerable doors for me. I would also like to thank my brothers, Adam and Bradley, for their support and guidance. I am very lucky to have an incredible network of extended family and friends, who have supported me in big ways and small throughout my PhD. Lastly, my amazing, intelligent, and strong girlfriend Tori has been an incredible partner through it all, and I couldn't have done it without her.

Chapter One

FIELD AND LABORATORY STUDIES LINKING HYDROLOGIC, GEOCHEMICAL, AND MICROBIOLOGICAL PROCESSES AND ENHANCED DENITRIFICATION DURING INFILTRATION FOR MANAGED RECHARGE

Published: Gorski G., Fisher A. T., Beganskas S., Weir W., Redford K., Schmidt C., and Saltikov C., (2019) Field and laboratory studies linking hydrologic, geochemical, and microbiological processes and enhanced denitrification during infiltration for managed recharge. *Environmental Science and Technology.* 53, 9491-9501.
doi: 10.1021/acs.est.9b01191

ABSTRACT

We present linked field and laboratory studies investigating controls on enhanced nitrate processing during infiltration for managed aquifer recharge. We examine the influence of carbon-rich permeable reactive barriers (PRBs) made of woodchips or biochar, placed in the path of infiltrating water to stimulate microbial denitrification. In field studies with infiltration at 0.2-0.3 m/day and initial concentration of [NO_3-N] = 20-28 mg/L, we observed that woodchips promoted 37±5.6% nitrate removal (primarily via denitrification), and biochar promoted 33±15% nitrate removal (via denitrification and physical absorption effects). In contrast, unamended soil at the same site generated <4% denitrification. We find that the presence of a carbon-rich PRB has a modest effect on the underlying soil microbial community structure at this site, indicating that existing consortia have the capability to carry out denitrification given favorable conditions. In laboratory studies using intact cores from the same site, we extend the results to quantify how infiltration rate influences denitrification, with and without a carbon-rich PRB. We find that the influence of both PRB materials is diminished at higher infiltration rates (>0.7 m/day), but can still result in denitrification, despite short fluid residence times in saturated soils. These results demonstrate a quantitative relationship between infiltration rate and denitrification that depends on the presence and nature of a PRB. Combined results from these field and laboratory experiments, with complementary studies of denitrification during infiltration through other soils, suggest a framework for understanding linked hydrologic and chemical controls on microbial denitrification

(and potentially other redox-sensitive processes) that could improve water quality during managed recharge.

1.1 Introduction

Managed aquifer recharge (MAR) is an important technique for sustaining groundwater supplies and mitigating the impact of increased demand, climate change, and shifting land use (Wada et al., 2010). MAR projects collect and infiltrate excess surface water flows using a variety of techniques including stream-bank filtration, dry wells, and dedicated infiltration basins (Bouwer, 2002). Water for MAR can be derived from non-pristine sources such as storm water (Beganskas and Fisher, 2017), treated wastewater (Schmidt et al., 2011b) or other excess surface flows (Grau-Martínez et al., 2018); in some cases, these source waters can contain contaminants that threaten groundwater quality. In addition, infiltrating water is subject to physical, geochemical, and microbiological processing, which can improve or degrade water quality (Bekele et al., 2011; Dallman and Spongberg, 2012; Ganot et al., 2018; Groffman et al., 2006; Tedoldi et al., 2016).

Nitrate (NO_3) is a common and pervasive contaminant in both groundwater (Burow et al., 2010) and surface water (Carpenter et al., 1998; Kaushal et al., 2011), and elevated concentrations have been linked to toxicity in humans and negative environmental effects on ecosystems (Gurdak and Qi, 2004; Vitousek et al., 1996). Nitrate can be removed through microbial denitrification (Korom, 1992), a multi-step process that (if run to completion) converts nitrate to inert N_2 gas through a series of

reactive intermediates. Denitrification requires an electron donor (often in the form of organic carbon), takes place under suboxic to anoxic conditions, and can be affected by additional factors such as soil pH, temperature, saturation, and vegetation (Seitzinger et al., 2006).

Earlier studies have demonstrated the feasibility of enhancing denitrification with carbon-rich permeable reactive barriers (PRBs) made of materials such as woodchips, biochar, or compost (Bock et al., 2015; Schipper and Vojvodić-Vuković, 2001). These materials are often used in denitrification bioreactors, a broad class of systems designed to reduce nitrate concentrations in agricultural runoff (Robertson and Merkley, 2008), treated wastewater (Christianson et al., 2016), contaminated groundwater (Schipper et al., 2005), and other settings (Schipper et al., 2010).

PRBs can be applied in conjunction with MAR to improve water quality during infiltration, particularly by enhancing denitrification. For example, a PRB made of vegetal compost and woodchips was installed in an MAR system to promote denitrification during infiltration of diverted river water, resulting in 30-40% nitrogen removal on some days, but negligible removal or addition on other days (Grau-Martínez et al., 2018). Controlled percolation experiments using water with elevated [NO_3] demonstrated that adding a woodchip PRB to coarse-grained soils (>90% sand) led to enhanced denitrification during rapid infiltration (Beganskas et al., 2018). This study also noted a negative correlation between rates of infiltration and denitrification, with tests run at infiltration rates up to 1.9 m/day. While these studies show promise in using a PRB to enhance denitrification during infiltration for MAR, the notable

variability in the occurrence and extent of denitrification highlights sensitivity to chemical and hydrologic conditions. This makes it difficult to design and operate MAR systems beyond the specific sets of parameters and conditions documented at each site.

MAR systems operate across a range of soil substrates and fluid chemistries, and understanding the complex interactions between soil characteristics (e.g. grainsize distribution, soil organic matter), hydrologic conditions (e.g., infiltration rate, saturated zone thickness, fluid residence time) and chemical constraints (e.g., abundance and/or availability of electron donors) during infiltration is important for maximizing water quality benefits during MAR, and avoiding resource degradation. While a subset of these factors has been investigated (e.g., increased carbon on denitrification in bioreactors), few studies have combined co-located measurements of hydrologic, geochemical, and microbiological data in order to elucidate the fundamental processes that control denitrification at rapid infiltration rates that are typical for MAR systems.

In this study we present co-located physical, geochemical, and microbiological observations from linked field and laboratory studies using intact soil cores from the same site, to quantify how horizontal PRBs made from carbon-rich materials (woodchips or biochar) can enhance denitrification during infiltration for MAR. We are particularly interested in quantifying the dependence of denitrification on infiltration rate with and without a PRB. The field and laboratory studies link hydrologic conditions and the nature of carbon-rich PRB materials to concomitant geochemical and microbiological changes during infiltration. Laboratory studies are particularly useful in this context for extending field results to different flow rates. We

present data from new experiments, combine these results with those from other studies, and propose a conceptual framework for understanding denitrification during infiltration leading to MAR, including a dependence on flow rate, with and without a carbon-rich PRB.

1.2 Materials and methods

1.2.1 Study site

The study site for this project was an active ranch in the Pajaro Valley near Watsonville CA, adjacent to Monterey Bay and the Pacific Ocean (Figure 1-S1), where installation of an MAR infiltration system is planned that will collect stormwater runoff from >1000 acres of farmland and rangeland. Soils at the site are representative of soils in the southeastern portion of the valley, comprising mainly flood plain, alluvial, and fluvial deposits adjacent to the Pajaro River, the primary drainage channel for the valley. Other infiltration and recharge projects are operating nearby or being considered for installation (Beganskas et al., 2019a; Beganskas and Fisher, 2017).

1.2.2 Experimental design and operation – Field studies

Field percolation studies emulated continuous infiltration that would occur during MAR operation, using an experimental design similar to that applied in an earlier study of coarser soils in the same region (Beganskas et al., 2018) (Figure S-1A). The current study differs from earlier work in several respects, including testing of adjacent materials in the field and lab. Three square plots with an area of 1 m^2 were hand excavated to 1-m depth. Lateral flow through the sides of the plots was limited by

installing fiberglass walls on plot sides, caulking corner joints, and backfilling the annulus around the walls with activated bentonite.

One plot was used as a control to test native soil conditions (*NS-Perc*), and the other two plots were augmented with 40-cm-thick PRBs made of woodchips (*WC-Perc*) or biochar (*BC-Perc*), installed above the plot base. During each test, water with elevated [NO_3] was applied to the plot through an inlet hose supplied by a nearby groundwater well. Water level was controlled with an automated inflow management system that used a float switch connected to a solenoid valve. The system maintained saturated conditions below the base of the plot and prevented overtopping the plot walls. Tests were run sequentially, each for 14-15 continuous days to establish saturated, quasi-stable conditions in the subsurface below the plot base.

1.2.3 Physical hydrology – Field studies

Infiltration testing generally results in a large fraction of horizontal flow, especially around the edges of the test plot. Fluid measurement and sampling instrumentation for this study was placed within a 0.4-x-0.4 m central area within each plot, where the vertical component of infiltration was expected to be greatest.

The tests were designed to facilitate independent measurements of total infiltration and the vertical component of infiltration near the center of the plot. Total infiltration was measured by recording the change in water stage over time during each infiltration cycle (the period of time when there was no flow into the plot and water was infiltrating into the subsurface). Temperature loggers were installed in thermal

probes, at depths of 5 and 20 cm below the base of the plot (bpb), to measure the vertical component of infiltration using heat as a tracer(Hatch et al., 2006).

1.2.4 Experimental design and operation – Lab studies

Intact soil cores (60 cm X 10 cm ID) for laboratory testing were collected adjacent to field test locations using a custom hammer coring system (Figure 1-S2). After cores were transported to the lab, woodchips, biochar, or coarse sand (1-2 mm, well rounded, ≥95% silica, used as a control) was added to the top of the cores as a PRB layer (~30 cm thick, similar to that used for field testing), and the cores were sealed and inverted for testing. These tests are referred to as *WC-Col*, *BC-Col*, and *NS-Col,* respectively.

A solution of local tap water and NO_3 (~30 mg/L N-NO_3) was pre-mixed in a 550 L tank, then pumped through the columns in an upward flow direction so that saturated conditions could be maintained across a range of flow rates; this approach has been taken in earlier studies (Della Rocca et al., 2006; Gibert et al., 2008; Halaburka et al., 2017; Healy et al., 2012; Moon et al., 2008). Results from column tests are presented for two analysis periods of quasi-stable flow, AP1 and AP2 (Figure 1-S4). AP1 lasted from infiltration day (ID)-32 to ID-52, when the vertical rate was ~0.17 m/day, overlapping with vertical infiltration rates observed in the field percolation experiments. The pumping rate was increased to ~0.72 m/day and flow was allowed to stabilize for 18 days with AP2 occurring from ID-71 to ID-94 (Figure 1-S4).

1.2.5 Fluid sampling and analysis

For field tests, two nests of fluid sampling piezometers (screens 10 cm long) were installed in the soil below each field plot to sample infiltrating fluid, with screened

depths centered at 30, 55, and 80 cm bpb (Figure 1-1A). Another fluid sampler was installed in each plot to sample water before it infiltrated. In *WC-perc* and *BC-perc*, an additional fluid sampler was placed within the PRB layer. During laboratory tests, influent and effluent samples were collected from each core. Fluid samples were collected during both percolation and laboratory experiments every 1-2 days.

All fluid samples were analyzed for nitrogen species (NO_3, NO_2 and NH_4), and dissolved organic carbon (DOC). A subset of the field fluid samples was analyzed for $\delta^{15}N$ and $\delta^{18}O$ of NO_3.

Net changes in solutes for each day were calculated as:

$$\Delta[N]=([NO_3\text{-}N]+[NO_2\text{-}N]+[NH_4\text{-}N])_{depth} - ([NO_3\text{-}N]+[NO_2\text{-}N]+[NH_4\text{-}N])_{surface} \quad [1.1]$$

$$\Delta[DOC]= [DOC]_{depth} - [DOC]_{surface} \quad [1.2]$$

where Δ[N] and Δ[DOC] are net changes in inorganic nitrogen and DOC concentrations (mg/L). For field studies, *surface* and *depth* refer to the inflowing water and water sampled from the 80-cm piezometer respectively, unless otherwise stated. For lab studies, *surface* and *depth* refer to the influent and effluent, respectively, corresponding to the same infiltration flow direction as in the field. Δ[N] accounts for inter-conversion of N between species but neglects common gaseous forms of N such as NO, N_2O and N_2, intermediate and final products of denitrification.

The mass of nitrogen removed from the system as Δ[N] was converted to a rate of mass loss:

$$\Delta N_L = (\Delta[N] \times IR_V) \quad [1.3]$$

where ΔN_L = load reduction (g-N•m^{-2}•day^{-1}), and $\Delta N_L < 0$ indicates a net removal of nitrogen. IR_V is the vertical infiltration rate for field tests and the measured flow rate for the laboratory studies. We use vertical infiltration rates, as these values represent conditions near the center of the plots (where fluid samples were collected, and thermal probes were deployed), and this allows the most direct comparison between field and lab experiments. In order to distinguish differences in Δ[N] and ΔN_L between experimental treatments and between flow rates, single-tailed t-tests were conducted in experimental results. To distinguish differences with depth within experiments, single factor ANOVA tests were performed. For both tests, results were considered significant when $p < 0.05$.

1.2.6 Sediment sampling and analysis

Sediment samples were collected before and after each field and lab experiment and analyzed for 1) soil texture 2) total organic carbon (TOC) and total nitrogen (TN), and 3) phylogenetic sequencing of microbial DNA. Microbial samples were collected using sterile techniques and were immediately placed in a liquid nitrogen field dewar for storage. DNA samples were kept at -80°C until extraction.

1.2.7 DNA extraction and phylogenetic sequencing

Methods for microbial analysis of soil samples were similar to those applied in an earlier study in the Pajaro Valley (Beganskas et al., 2018). Briefly, soil DNA was extracted with a PowerSoil DNA Isolation Kit (QIAGEN). The Qubit 4 Fluorometer (Invitrogen) was used to quantify DNA extracts. PCT amplicons (~550 bp) were

generated from PCRs with soil DNA and 16S rRNA gene primers targeting the V4 and V5 variable regions. The PCR amplicon sequencing pipeline used in this study was adapted from Illumina MiSeq platform protocol for 16S metagenomic libraries (Beganskas et al., 2018). The overall pipeline included steps for the primary PCR using 16S rRNA primers (Klindworth et al., 2013), PCR clean-up, library preparation (adding unique sequencing indices [barcodes] to each PCR amplicon), normalizing DNA concentrations of each library, and library pooling. The pooled library was sequenced on the Illumina MiSeq (600 cycles v3 PE300 flow cell kit) at the University of California, Davis Genome Center. The raw sequence reads have been uploaded to the National Center for Biotechnology Information Sequence Read Archive (accession number: PRJNA523645).

1.2.8 Phylogenetic data processing

To analyze differences in microbial community structure, soil samples were grouped based on experimental conditions (see supporting tables). Samples were grouped into six categories based on 1) experiment (field or laboratory) 2) treatment (NS, WC or BC) and 3) whether they were collected before or after infiltration. Within each group, samples collected from 10 and 30 cm depth were grouped and selected for comparison, as these depths showed the most significant nutrient cycling.

1.3 Results

1.3.1 Field studies

The first six days of field percolation tests comprised an "initialization period," when the soil system was saturating, and biogeochemical cycling adapted to new storage and flow conditions (Figure 1-2). During the subsequent "analysis period," total infiltration rates were relatively stable, and nutrient concentrations developed consistent patterns relative to the initialization period.

1.3.1.1 Soils and infiltration rates

Soil samples from the three field plots had median clay, silt, and sand fractions consistent with textural characterization of loam (Figure 1-S5). However, some samples from *NS-Perc* and *WC-Perc* were sandy loam, whereas some samples from *BC-Perc* were finer, particularly in the upper 20 cm-bpb, including silt loam. All soil samples showed consistent TOC (0.3-0.9 %-wt) and TN (0.04-0.08 %-wt); there was no systematic variation with depth or soil treatment, and no systematic difference between samples collected before and after the tests (Figures 1-S6 and 1-S7).

Mean total infiltration rates were 2.40, 0.78, and 0.28 m/day for *NS-Perc*, *WC-Perc*, and *BC-Perc* respectively (Figure 1-2A). The difference in these infiltration rates is best explained by local soil heterogeneity, as plots were constructed on adjacent areas (separated laterally by 3-4 m), using identical configurations and materials. In addition to differences in soil texture, macropores can lead to large variations in hydraulic properties. Similar spatial differences in infiltration rates have been observed during

earlier tests in sandy deposits (Beganskas et al., 2018) and in measurements made in active managed recharge systems (Beganskas and Fisher, 2017; Racz et al., 2012).

Vertical infiltration rates for *NS-Perc* and *WC-Perc* were consistent throughout the experiments (IR_V = 0.20 and 0.21 m/day respectively) whereas vertical infiltration rates for *BC-Perc* were higher (IR_V = 0.36 m/day) and peaked near ID-11 (IR_V = 0.60 m/day), exceeding total infiltration rates for several days (Figure 1-2A). Vertical infiltration rates are point measurements, whereas total infiltration rates are calculated by mass balance and applied to the full plot area. When vertical infiltration rates exceed total infiltration rates, this likely indicates a response to highly conductive infiltration paths, perhaps root tubules or burrows (Beganskas and Fisher, 2017; Clark et al., 2004). It is unlikely that water flowed quickly down the side of the probe as the annulus around the thermal probes was filled with silica slurry when the probes were installed. Because these transient rates are not representative of broader infiltration conditions, and nutrient load is calculated explicitly using the vertical infiltration rate (equation [1.3]), we do not include data from these days (ID-9 to ID-13) in the assessment of ΔN_L. However, we include a longer infiltration record (ID-7 to ID-15) for analysis of Δ[N] and Δ[DOC], as these values are calculated using only the differences between observed concentrations at the surface and at depths.

1.3.1.2 Nutrient changes

The water supply for field percolation tests had elevated [NO_3-N] throughout the experiments, ranging from 20 to 28 mg/L (Figure 1-2B). Variability in the surface concentration resulted from pulling this water from a nearby supply well. Influent

[NO_2-N] was below detection in influent in 7 of 21 samples (always ≤0.8 mg/L), and [NH_4-N] was below detection in all influent samples except one (0.1 mg/L; see SI Tables). Pore fluid analyses indicated the smallest systematic shift in [N] during *NS-Perc* (Δ[N] = -1.0 ± 1.4 mg/L), whereas Δ[N] during *WC-Perc* and *BC-Perc* showed greater changes (Δ[N] = -8.8 ±2.5 mg/L and -7.1 ±3.3 mg/L respectively; Table S-1 and Figure 1-2C), indicating more nitrate removal ($p < 0.05$). Δ[N] was more variable during *BC-Perc*, ranging from -10.2 mg/L on ID-9 to -3.9 mg/L on ID-12, but *WC-Perc* and *BC-Perc* showed statistically similar Δ[N] ($p > 0.05$).

WC-Perc showed consistent load reduction, with ΔN_L values between -1.5 and -2.5 g-N•m^{-2}•day^{-1} (Figure 1-2D), and *BC-Perc* showed ΔN_L values similar to *WC-Perc* ($p > 0.05$), ΔN_L = -2.2 to -1.4 g-N•m^{-2}•day^{-1}. Surface [DOC] was consistent during individual percolation tests but was lower during *NS-Perc and WC-Perc* (2.0 and 3.0 mg/L respectively) than during *BC-Perc* (5.1 mg/L). Δ[DOC] was greatest in *WC-Perc* with an average of 10.4±1.3 mg/L compared to 3.8±3.0 mg/L for *BC-Perc* and 0.7±2.0 mg/L *for NS-Perc* (Table 1-1 and Figure 1-2C).

NS-Perc showed no consistent change with depth in either [DOC] or [N] (Table S3, Figure 1-3A). In contrast, *WC-Perc* and *BC-Perc* showed significant changes with depth in both [N] and [DOC]. *WC-Perc* showed Δ[N] = -3.6 mg/L from the surface to the PRB, and Δ[N] = -7.7 mg/L from the surface to 30 cm-bpb (Figs. 1-2 and 1-3). [DOC] exhibited similar patterns with depth with the opposite sign: large Δ[DOC] within the PRB (4.5 mg/L) and at 30 cm-bpb (8.0 mg/L relative to the surface; Figure 1-3B).

BC-Perc showed Δ[N] = -12.7 mg/L and Δ[DOC] = 10.6 mg/L from the surface to PRB, indicating large nitrate removal within the PRB. However, these values showed opposite shifts below the PRB with Δ[N] = 6.0 mg/L and Δ[DOC] = -6.4 mg/L from the PRB to 30 cm-bpb (Figure 1-3C).

1.3.1.3 Stable isotopes of NO_3

Nitrogen and oxygen stable isotopes showed a progressive enrichment with depth on days when nitrate removal was detected (Figure 1-3 and 1-S8), suggesting that denitrification was a primary mechanism responsible for nitrate removal (Kendall and Caldwell, 1998; Mariotti et al., 1988). DNRA was likely not a significant pathway for NO_3 removal, as there was no pore fluid increase in $[NH_4^+]$ associated with lowered $[NO_3]$. Additionally, we observed no systematic increase in soil TN after any treatment, suggesting that $[NH_4^+]$ was not sorbed onto soil in measurable quantities (Figure 1-S7). However, it remains possible that $[NH_4^+]$ was being actively processed with little or no change to its standing stock; ongoing studies seek to identifying potential nitrogen processing pathways using soil microbial transcriptomics.

We find average enrichment factors of ε_N = -11.44‰ and ε_O = -8.32‰, with a ratio of $\varepsilon_N/\varepsilon_O$ 1.38 for *WC-Perc*, and an average ε_N = -4.83‰ and ε_O = -3.63‰ with a ratio of $\varepsilon_N/\varepsilon_O$ 1.33 for *BC-Perc*. $\varepsilon_N/\varepsilon_O$ ratios reported elsewhere for bacterial denitrification range from 0.9 to 2.1 (Bottcher, 1990; Otero et al., 2009). Commonly reported ε_N values for field studies of microbial denitrification range from -4 to -30‰ (Pauwels et al., 2000; Vogel et al., 1981), and results in the present study fall near the less negative end of this range. Relatively fewer ε_O factors have been reported in the

literature, but ε_O factors from this study (-8.32 and -3.63‰) are broadly consistent with reported values for denitrification of -2 to -18‰ (Mengis et al., 1999; Otero et al., 2009).

1.3.2 Lab studies

1.3.2.1 Soils and infiltration rate

Sediments collected for laboratory column experiments showed a similar grain size distribution to those from the percolation tests *NS-Perc* and *WC-Perc* (Figure 1-S5). Similarly, initial soil TOC and TN values in the soil columns were consistent with field samples (Figures 1-S6 and 1-S7).

Infiltration rates were 0.17, 0.18 and 0.18 m/day for the three columns during AP1 (Table 1-1 and Figure 1-S4), overlapping with IR_V during field experiments (Figure 1-2A). Infiltration rates were raised to 0.70-0.74 m/day during AP2 for the laboratory experiments (Table 1-1), near the upper end of values measured during field tests, and that were found to enhance denitrification during earlier measurements in an active MAR system (Schmidt et al., 2011b).

1.3.2.2 Nutrient changes

Influent water for all laboratory studies were drawn from the same source, although the composition varied somewhat because the supply tank had to be refilled. Surface [N] and [DOC] were generally higher than those observed in the field. Δ[N] values during AP1 exhibited similar patterns to those measured in the field, with *NS-Col* showing less N removal than did *WC-Col* or *BC-Col* (Table 1-1, Table 1-S1, Figure 1-S9). [DOC] also exhibited similar patterns to those observed in the field, with higher

[DOC] following passage through the PRB, and no consistent change in [DOC] during passage through native soil.

For *WC-Col* and *BC-Col*, higher infiltration rates during AP2, led to less N removal (lower magnitude Δ[N]), than at lower infiltration rates during AP1 (Table 1-S2). However, Δ[N] values were similar during AP1 and AP2 for *NS-Col* ($p < 0.05$) (Table 1-S2 and Figure 1-S9).

1.3.3 Microbiological changes

Groups of microorganisms that are thought to contribute to soil nitrogen and carbon cycling were found in both field and lab samples, including the Nitrospira family, capable of nitrite reduction (Koch et al., 2015) and *Azoacorus*, a denitrifier which has been isolated from activated sludge (Hagman et al., 2008). Additionally, all sample groups included ammonia-oxidizing archaea of the phylum Thaumarchaeota (Spang et al., 2012) with a relative abundance of 3-5%. *Marmoricola*, within the order Propionibacteriales showed increases in relative abundance after *WC-Perc*, *BC-Perc*, *NS-Col*, and *BC-Col*, they are capable of reducing NO_3 using acetic acid and propionoic acid as carbon sources (Dastager et al., 2008). Small increases in the Sphingomonadaceae family, which contain species know to reduce nitrate(Takeuchi et al., 2001) and utilize a wide variety of C sources (Anderson et al., 2011), were observed after *BC-Perc* and *BC-Col*.

Comparison of grouped soil samples before and after each test revealed no systematic shifts in the relative abundance of the most common phyla (Figure 1-S10). This result contrasts distinctly with results from an earlier study in sandy soils

(Beganskas et al., 2018), where there were significant shifts in microbial ecology following infiltration. However, beta (between-sample) diversity plots for the current experiments show weak grouping of *WC-Perc* and *BC-Perc* compared to samples collected before the field studies began (Figure 1-4B). No such grouping was evident with samples collected from the laboratory studies.

1.4 Discussion

1.4.1 Effect of PRB on denitrification during infiltration

In the field studies, both *WC-Perc* and *BC-Perc* showed statistically significant increases in [DOC] and decreases in [N], whereas *NS-Perc* showed no change with depth in either [DOC] or [N] (Table 1-S3). Although both biochar and woodchips were associated with enhanced nitrate removal, their mechanisms for doing so appear to be different. It is generally understood that woodchips enhance denitrification through the release of organic carbon[19, 20, 22, 25], a portion of which is available for capable microbial communities to utilize as an electron donor for cellular processes. This increases rates of microbial respiration, which depletes oxygen concentrations, leading to the consumption of nitrate.

During *WC-Perc*, there was an increase in [DOC] within the PRB and a concomitant decrease in [N] (Figure 1-3B), accompanied by a fractionation of the residual NO_3 pool to values more enriched in $\delta^{15}N$ and $\delta^{18}O$ in a ratio indicative of denitrification (Figures 1-3B and 1-S8). Additionally, these patterns continued below the PRB, at 30 cm-bpb, where additional [DOC] increases were observed, along with

even greater nitrogen removal and isotopic fractionation. These patterns persisted to depths of 55 and 80 cm-bpb, although differences were smaller with depth (Figure 1-3B). These trends suggest that woodchips provide benefit by enhancing denitrification within the PRB, and that benefit is carried into the underlying soil by the infiltrating water, in effect extending the thickness of the zone where enhanced nitrogen processing can occur. These results are consistent with tests done in coarser soils, which show denitrification occurring both within and below a woodchip PRB during rapid infiltration (Beganskas et al., 2018).

In contrast, biochar appears to promote denitrification *within* but not *beneath* the PRB. During *BC-Perc*, we observed a large increase in [DOC] within the PRB associated with a large decrease in [N] and an enrichment of residual NO_3 $\delta^{15}N$ and $\delta^{18}O$ (Figure 1-3C), all consistent with denitrification. However, below the PRB, [N] increased and [DOC] decreased, with no fractionation of residual NO_3 isotopes (Figure 1-3C). This suggests that increases in [N] observed below the PRB could be associated with physical processes such as absorption/desorption, which do not appreciably fractionate stable isotopes (Clough and Condron, 2010; Kameyama et al., 2012).

This pattern suggests that, unlike the woodchip PRB, the biochar PRB did not enhance denitrification beneath the PRB layer. Biochar can affect soil N and C cycling through many mechanisms (Clough and Condron, 2010; Kameyama et al., 2012), for example its high specific surface area (Atkinson et al., 2010) has been shown to provide an abundance of locations for microbial communities to colonize, which could help to explain high rates of cycling within the PRB (resulting in NO_3 isotopic shifts) that are

not continued within the underlying soil. The strong fractionation of residual NO_3 within the biochar PRB might have been enhanced by the separation of NO_3 into distinct pools: adsorbed and non-adsorbed. The extent to which these pools may form and be processed by different microbial consortia, and/or along different pathways, remains to be tested.

1.4.2 Effect of infiltration rate on denitrification during infiltration

The effect of infiltration rate on denitrification is best elucidated by comparing AP1 and AP2 during laboratory columns studies, where the infiltration rate was more easily controlled. All three treatments showed higher magnitude Δ[N] (more N removal) at lower infiltration rates (Tables 1-1 and 1-S2). These results are consistent with the understanding that higher infiltration rates result in greater penetration of oxygen and less favorable conditions for denitrification. Previous studies have identified fluid residence time as a primary control on nitrogen removal within bioreactor systems (Greenan et al., 2009; Halaburka et al., 2017; Hoover et al., 2016), but conditions in those systems are fundamentally different from those that occur during infiltration for MAR. In particular, residence times under saturated conditions during the present study are short compared to those commonly seen in bioreactors, on the order of hours. In addition, the present study shows how the infiltration rate dependence of denitrification is influenced by the presence and type of a PRB carbon source.

Figure 1-4A shows the relationship between Δ[N] and infiltration rate, demonstrating that both biochar and woodchip PRBs have pronounced influence at

lower infiltration rates. At higher infiltration rates, the biochar and woodchips had no discernable effect compared to the native soil (Table 1-S1). Distinct relationships between Δ[N] and infiltration rate are suggested based on the presence and composition of a PRB (Figure 1-4A), but additional work will be needed to assess the monotonic (possibly nonlinear) nature of these relations.

The consistently low ΔN_L values for the NS experiments across all infiltration rates (Table 1-1, Figure 1-S9) are comparable to measurements of denitrification during controlled percolation studies and active MAR operations ($\Delta N_L \sim 0.20$ g-N/day•m^{-2}) in coarser-grained soils. For WC and BC treatments, lower infiltration rates are associated with higher magnitude ΔN_L (more N load reduction) than during higher infiltration rates (Table 1-1, Figure 1-S9). This dependence appears to be similar to that for Δ[N], but because ΔN_L is the product of Δ[N] and infiltration rate, ΔN_L values are neither maximized at low infiltration rates nor at high infiltration rates (due to low Δ[N]). Instead, there is likely an intermediate range of infiltration rates that result in maximum ΔN_L, as a function of the nature of the carbon source, soil properties, and other factors. As ΔN_L is of primary concern for the health of aquifers and surface water bodies through the reduction of export loads, it should prove beneficial to quantify this relationship under a suite of natural and managed conditions.

1.4.3 Effect of infiltration on microbial ecology

Observed nitrate load reduction during biochar and woodchip PRB field and laboratory experiments, coupled with relatively modest changes in the diversity and relative abundance of soil microbial communities before and after each test, suggest

that sufficient microorganisms capable of carrying out denitrification during infiltration were present in the soil before the start of infiltration. The change in [N] (and ΔN_L) is likely the result of these preexisting microorganisms increasing their activity in response to changes in environmental conditions (i.e. water saturation, availability of carbon, development of suboxic/anoxic conditions). The presence of microorganisms that have previously been identified as important in nitrogen and carbon cycling in soils is consistent with this interpretation. Sphingomonadaceae, a family with many genera capable of nitrate reduction (Takeuchi et al., 2001), was observed in all samples. Other researchers have observed increases in its relative abundance in the presence of woodchips (Beganskas et al., 2018) and biochar (Xu et al., 2014) and have interpreted those increases as a signal of the family's importance to soil nitrogen and carbon cycling. Similarly, the order Burkholderiales and family Bradyrhizobiaceae were present in all sample groups and have been identified as potentially important groups carrying out key steps of denitrification in both amended (Anderson et al., 2011) and unamended (Liu et al., 2017) soils.

The immense complexity and interconnectedness of soil microbial ecology make it unlikely that changes in nutrient cycling can be directly connected to changes in individual groups of microorganisms without more detailed investigations, including studies focused on functional activity and soil metagenomics and metatranscriptomics. Additional work is underway that explores these topics, and should help to elucidate microbial controls on denitrification (and nutrient cycling more broadly) during infiltration for MAR.

1.4.4 Physical and chemical controls on denitrification during infiltration

By combining the results from the current study with similar studies carried out in coarse-grained soil (Beganskas et al., 2018; Schmidt et al., 2011b), we have developed a conceptual model that illustrates how two primary factors may affect denitrification during infiltration: (1) the presence or absence of a bioavailable carbon source, and (2) soil texture and associated influence on pore fluid storage and flow rate (Figure 1-5).

The effect of the woodchip PRB (Figure 1-5C and 1-5D) is two-fold; first the PRB supplies carbon (and potentially habitat and/or other benefits) to microbial communities that have the capacity to accomplish denitrification. Second, at dynamic steady state during infiltration, a saturated zone develops in the shallow soil above an inverted water table. Considerable geochemical processing occurs within this zone, including denitrification, under suitable conditions. The addition of a PRB increases the thickness of the saturated zone without having a significant impact on the rate of infiltration, because PRB materials tend to be large relative to the underlying native soil. The increase in saturated thickness, in turn, increases the residence time of fluid within this zone.

The second factor, soil texture, has a primary influence on both the rate of infiltration and the thickness of the saturated zone. Coarser soils tend to have higher infiltration rates than finer soils, resulting in a lower residence time for a given saturated thickness. But in addition, coarser soils tend to also be better drained, leading to a shallower inverted water table at the base of the saturated zone. We did not measure

the saturated thickness during field percolation tests in the present study, but have found that shallow piezometers tend to recover samples to greater depths in finer grained soils than in coarse grained soils (Figure 1-S11), a trend consistent with other field studies (Beganskas et al., 2018; Schmidt et al., 2011b). Thus fluids infiltrating coarser soils tend to have a shorter residence time within the saturated zone compared to that in finer soils, both because the infiltration rate is faster and because the saturated zone is thinner.

We hypothesize that these two processes will tend to reinforce differences in conditions that are most favorable for denitrification (Fig. 1-5). Oxygen infiltrating with surface water into shallow soils can reach the base of the saturated zone if the fluid is moving too quickly for soil microbes to consume it and/or because the saturated zone is thin. Both of these conditions are more likely to occur in coarse soils than in fine soils. In finer soils, the saturated zone is likely to be thicker to begin with, compared to coarser soils, and this plus the slower rate of infiltration tends to result in a commensurately longer fluid residence time in the saturated zone, and thus conditions that are more favorable to denitrification. Adding a carbon-rich PRB makes denitrification more favorable for both coarse and fine soils (Fig. 5), by helping to speed the rate of biological consumption of available oxygen, but the extent to which this favorability is expressed depends on the details of saturated zone thickness and infiltration rate (and thus residence time), and the availability of nitrate and a bioavailable carbon supply.

Both woodchips and biochar demonstrate potential to enhance nitrate removal

during infiltration, but [N] processing associated with a woodchip PRB is more clearly associated in the present study with denitrification. In contrast, while a biochar PRB may also provide a sink for nitrate, much of the Δ[N] apparent from field and laboratory tests with biochar may have resulted from absorption or denitrification that occurs mainly within the PRB layer. It may be that a PRB assembled from a mixture of woodchips and biochar would be particularly beneficial, as it could both slow the movement of nitrate by adsorption and provide habitat for microbial consortia that accomplish denitrification (among other functions).

These results, in combination with other studies, suggests that infiltration for managed recharge could be optimized for improvements to both water supply and water quality. Given the long-term challenges in many basins associated with managing loads of salts and nutrients, there may be benefits to considering MAR systems as providing opportunities to improve water quality, not just avoid degradation, but sustaining resources for the long term. Many questions remain about the complex interplay between physical and chemical conditions and processes that could stimulate naturally occurring microbiological communities in the subsurface to consume and process carbon and nutrients during MAR. While each infiltration and recharge project is subject to specific goals and considerations, and a variety of water quality concerns involving redox-sensitive solutes, defining quantitative links between biogeochemical cycling and physical hydrologic processes can lead to improved practices, helping to enhance resources under a range of natural and managed conditions.

ACKNOWLEDGEMENTS

We gratefully acknowledge the laboratory and field assistance of A. Paytan, R. Franks, D. Sampson, H. Dailey, E. Adelstein, T. Weathers, P. Karim, M. Cribari, D. van den Dries, T. Stewart, A. Yoder, K. Young, J. Cox, A. Serrano and J. Pensky. We would like to thank E. and J. Kelly, S. Dobbler, T. Marg, K. Camara, C. Coburn and B. Lockwood for their key guidance and cooperation on conducting the field studies.

FUNDING SOURCES

This project was funded by the Gordon and Betty Moore Foundation grant GBMF5595, UC Water Security and Sustainability Research Initiative (UCOP Grant # 13941), the National Science Foundation Graduate Research Fellowship Program, and from the Recharge Initiative (http://www.rechargeinitiative.org/).

ABBREVIATIONS

MAR, managed aquifer recharge; PRB, permeable reactive barrier; bpb, below plot base; NS, native soil; WC, woodchips; BC, biochar; DOC, dissolved organic carbon; OTU, operational taxonomic unit; DNRA, dissimilatory nitrate reduction to ammonia; ST, saturated thickness; DZ, denitrification zone

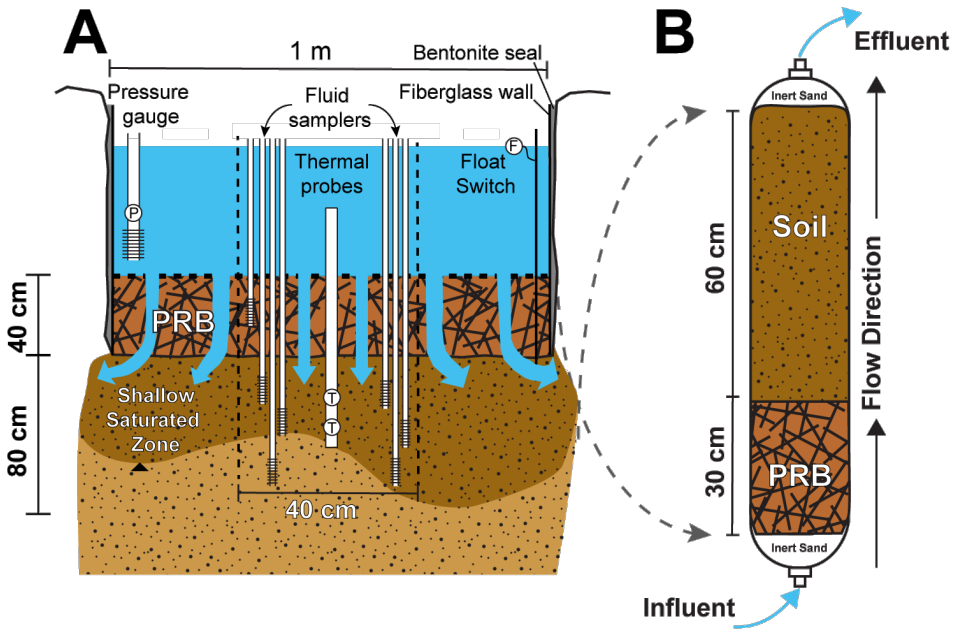

Figure 1-1 Field and laboratory experimental configurations. A Cross section of layout and plot construction for field percolation studies, with instrumentation installed within the central 0.16 m^2 of the plot. PRB layer was installed for tests with woodchips (WC-Perc) and biochar (BC-Perc). For native soil test NS-Perc, the plot construction was identical except no PRB layer was installed. **B** Laboratory column studies were designed to simulate the saturated zone within the field studies with identical layering. Columns were inverted for testing to maintain saturated conditions under different infiltration rates, retaining the same flow direction as used for field tests.

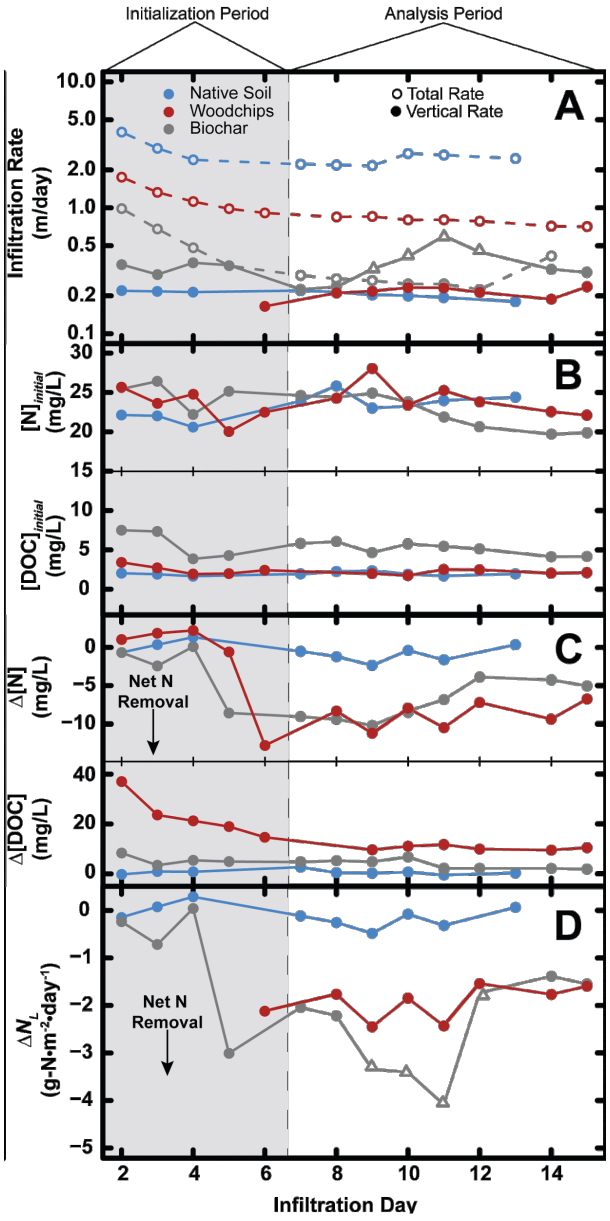

Figure 1-2 Results from field percolation experiments for three soil treatments showed enhanced nutrient cycling in both *WC-Perc* (red) and *BC-Perc* (gray) compared to *NS-Perc* (blue). Experiments were divided into initialization period (gray) and analysis period (white). **A** Total (open circles with dashed lines) and vertical (closed circles with solid lines) infiltration rates. **B** Surface [N] and [DOC]. **C** Δ[N] and [DOC] between surface and 80 cm fluid sampler. **D** Daily ΔN_L measurements for each treatment as defined by Eq. 3. Open triangles in **A** and **D** indicate the data was not used for calculations.

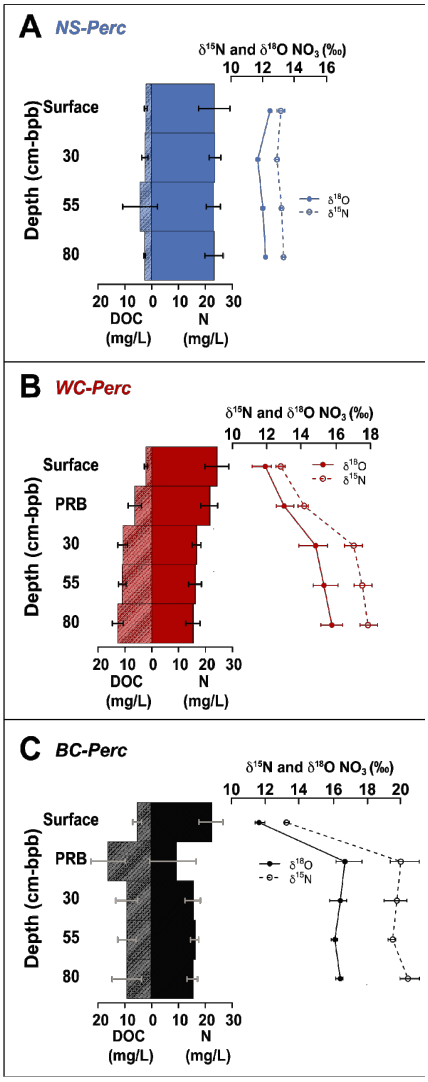

Figure 1-3 Average nutrient concentrations during the analysis period of field percolation experiments at measured depths show considerable differences between each soil treatment in [DOC], [N] and residual NO_3 $\delta^{15}N$ and $\delta^{18}O$. Increases in [DOC] are shown on the left of the bar plot and increases to [N] are shown on the right of the bar plot. Bars show the range of nutrient and isotope measurements during the analysis period. **A** *NS-Perc* showed negligible changes with depth ([N] and [DOC], $p > 0.05$). Changes in [N] and [DOC] with depth are significant for *WC-Perc* and *BC-Perc* (single factor ANOVA, $p < 0.05$), but are insignificant for *NS-Perc* (Table S3). **B** During *WC-Perc* there was a progressive decrease in [N] and increase in [DOC] both within and below the PRB and a fractionation in both $\delta^{15}N$ and $\delta^{18}O$([N] and [DOC], $p < 0.05$). **C** *BC-Perc* showed a decrease in [N] and increase in [DOC] within the PRB accompanied by an enrichment in $\delta^{15}N$ and $\delta^{18}O$, followed by a decrease in [DOC] and an increase in [N] with no isotope fractionation below the PRB ([N] and [DOC], $p > 0.05$).

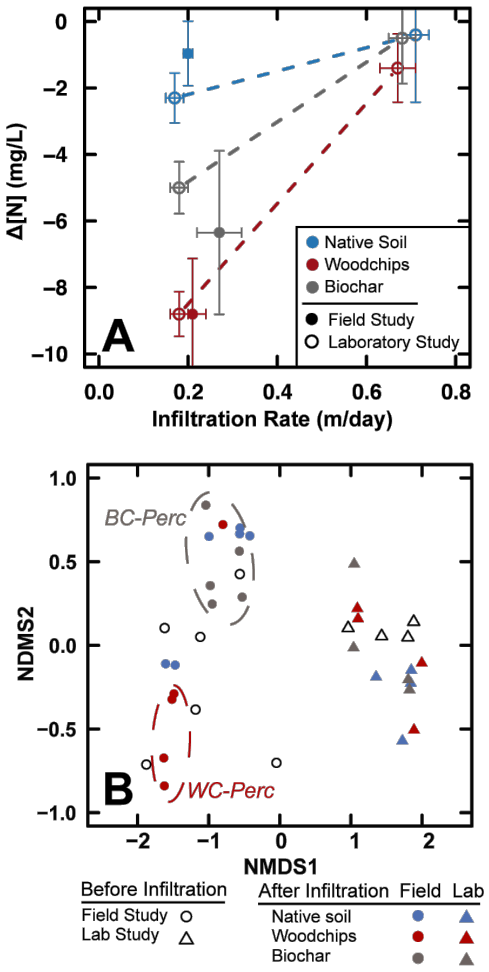

Figure 1-4 Combination of laboratory and field studies. **A** Δ[N] measurements across a range of vertical infiltration rates for field studies (closed circles) and laboratory studies (open circles) show that both woodchips and biochar are associated with greater magnitude Δ[N] at lower infiltration rates compared to higher infiltration rates during both field and laboratory testing. Additionally, both woodchips and biochar show greater magnitude Δ[N] compared to native soil treatments at lower infiltration rates (Tables 1-1, 1-S1, and 1-S2), but the difference is not significant at higher infiltration rates. Error bars show one standard deviation. **B** Beta (between sample) diversity of soil microbial community from before (open shapes) and after (closed shapes) each experiment, shows a weak grouping of *WC-Perc* and *BC-Perc* samples (red and gray closed circles). No such grouping is apparent for *NS-Perc* (blue closed circles) or laboratory studies (triangles). Beta diversity was calculated using Bray Curtis distances with non-metric multidimensional scaling (NMDS) for ordination.

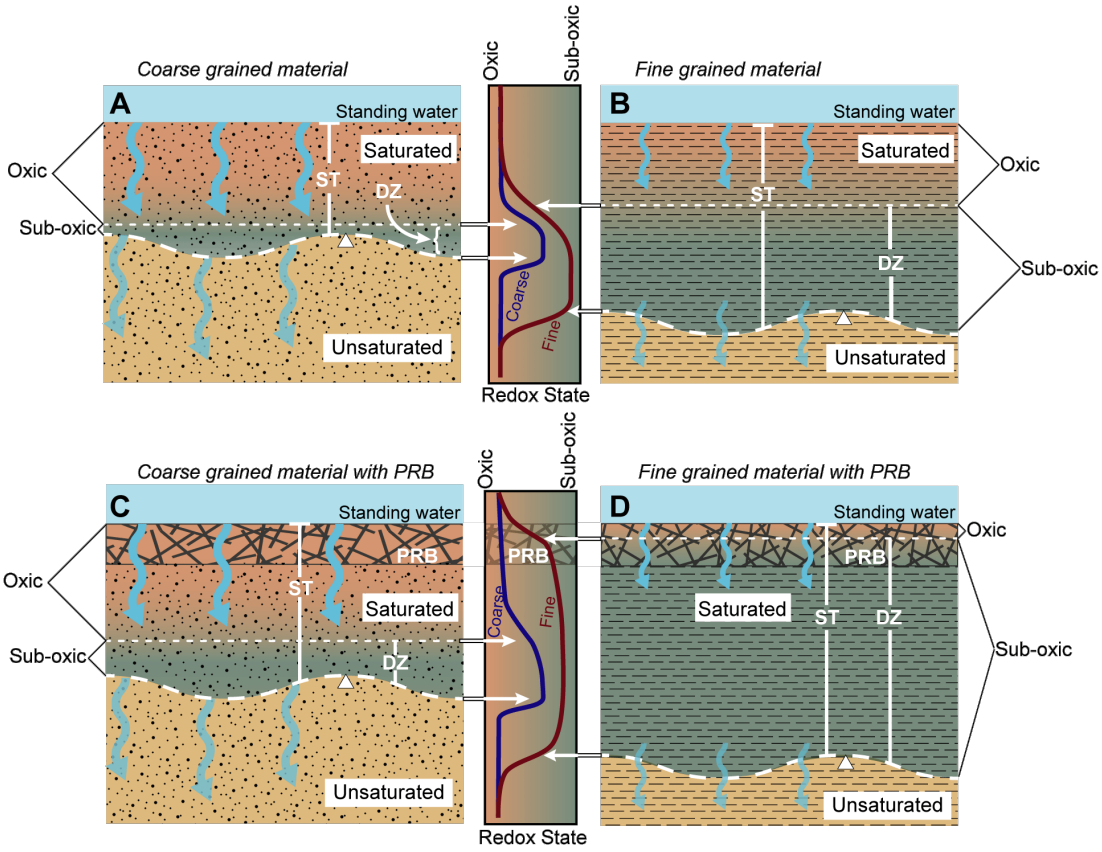

Figure 1-5 Schematic representation of primary factors controlling denitrification during infiltration through coarse-grained soil (**A** and **C**) and fine-grained soil (**B** and **D**) with (**C** and **D**) and without (**A** and **B**) a woodchip PRB. Patterns are generalized based on results from this study and similar studies done in coarser-grained soils, showing the relative thicknesses of the saturated thickness (ST) and the denitrification zone (DZ). Central plots show generic curves illustrating depth profiles of the relative redox conditions for coarse- (blue) and fine-grained (red) soils. Oxic conditions favor O_2 as the primary e- acceptor, whereas sub-oxic to reducing conditions are more favorable to NO_3. Orange areas indicate oxic zones in which denitrification is not favored, and green areas indicate sub-oxic (reducing) conditions under which denitrification is favored.

Table 1-1 Summary of experimental conditions and key results for all experiments

Experiment	Treatment	Analysis Period	Total Infiltration Days	Analysis Days[a]	Total Infiltration Rate	Vertical Infiltration Rate	Surface [N]	Depth[c] [N]	Surface [DOC]	Depth[c] [DOC]	Δ[N]	ΔN_L
			n	n	m/day	m/day	mg/L	mg/L	mg/L	mg/L	mg/L	g/day/m^2
Field	NS	A	13	6	2.4	0.2	24.1	23.1	2	2.7	-1	-0.2
					-0.22	-0.01	-1	-1.5	-0.2	-1.1	-1	-0.2
Laboratory	NS	AP1	19	12	-	0.17	31.5	29.3	27.6	30.9	-2.3	-0.4
						-0.02	-0.6	-0.6	-1.5	-2.9	-0.9	-0.1
Laboratory	NS	AP2	23	10	-	0.74	31.7	31.3	30.8	30.5	-0.4	-0.3
						-0.03	-1.3	-2.2	-5.5	-4.7	-2	-1.4
Field	WC	A	15	7	0.78	0.21	24.2	15.4	2.1	12.5	-8.8	-1.9*
					-0.06	-0.03	-2	-1.2	-1.5	-1	-1.7	-0.4
Laboratory	WC	AP1	19	12	-	0.18	31.4	22.6	27.4	37.1	-8.8*	-1.6*
						-0.02	-0.6	-0.9	-1.5	-3.1	-0.7	-0.2
Laboratory	WC	AP2	23	10	-	0.7	31.7	30.2	30.6	31.5	-1.4	-1
						-0.04	-1.3	-1.6	-5.2	-4.6	-1	-0.7
Field	BC	A	15	8(4)[b]	0.28	0.27	22.5	15.3	5.1	8.9	-7.1	-1.8*
					-0.06	-0.05	-2.2	-0.7	-0.8	-2.4	-2.5	-0.3
Laboratory	BC	AP1	19	13	-	0.18	31.5	26.5	27.2	31.2	-5.0*	-0.9*
						-0.02	-0.6	-1	-1.9	-2.5	-0.8	-0.2
Laboratory	BC	AP2	23	11	-	0.71	31.6	31.1	30.6	30.6	-0.5	-0.4
						-0.03	-1.3	-1.4	-5.2	-5.4	-1.4	-1

[a]Number of days in which fluid samples were collected during each analysis period

[b] For BC-Perc 8 days (ID-7 – ID-15) were used in reported values for Total Infiltration Rate, [N], [DOC], and Δ[N], but 4 days (ID-7–ID-8, and ID-14–ID-15) in the reported values for Vertical Infiltration Rate, and ΔN_L, this excludes days in which vertical infiltration rates exceeded total infiltration rates, see section 1.3.1.1 for explanation.

[c]Depth for field experiments indicates fluid samplers at the deepest piezometer (80 cm), while depth for laboratory experiments indicates samples collected from the column effluent

*Indicates single-tailed t-test revealed significant difference ($p < 0.05$) between treatment (WC or BC) and control (NS) within the analysis period

References

Anderson, C.R., Condron, L.M., Clough, T.J., Fiers, M., Stewart, A., Hill, R.A., Sherlock, R.R., 2011. Biochar induced soil microbial community change: Implications for biogeochemical cycling of carbon, nitrogen and phosphorus. Pedobiologia (Jena). 54, 309–320. https://doi.org/10.1016/j.pedobi.2011.07.005

Atkinson, C.J., Fitzgerald, J.D., Hipps, N.A., 2010. Potential mechanisms for achieving agricultural benefits from biochar application to temperate soils: A review. Plant Soil 337, 1–18. https://doi.org/10.1007/s11104-010-0464-5

Beganskas, S., Fisher, A.T., 2017. Coupling distributed stormwater collection and managed aquifer recharge: Field application and implications. J. Environ. Manage. 200, 366–379. https://doi.org/10.1016/j.jenvman.2017.05.058

Beganskas, S., Gorski, G., Weathers, T., Fisher, A.T., Schmidt, C., Saltikov, C., Redford, K., Stoneburner, B., Harmon, R., Weir, W., 2018. A horizontal permeable reactive barrier stimulates nitrate removal and shifts microbial ecology during rapid infiltration for managed recharge. Water Res. 144, 274–284. https://doi.org/10.1016/j.watres.2018.07.039

Beganskas, S., Young, K.S., Fisher, A.T., Harmon, R., 2019. Runoff Modeling of a Coastal Basin to Assess Variations in Response to Shifting Climate and Land Use : Implications for Managed Recharge. Water Resour. Manag. https://doi.org/https://doi.org/10.1007/s11269-019-2197-4 Runoff

Bekele, E., Toze, S., Patterson, B., Higginson, S., 2011. Managed aquifer recharge of treated wastewater: Water quality changes resulting from infiltration through the vadose zone. Water Res. 45, 5764–5772. https://doi.org/10.1016/j.watres.2011.08.058

Bock, E., Smith, N., Rogers, M., Coleman, B., Reiter, M., Benham, B., Easton, Z.M., 2015. Enhanced Nitrate and Phosphate Removal in a Denitrifying Bioreactor with Biochar. J. Environ. Qual. 44, 605. https://doi.org/10.2134/jeq2014.03.0111

Bottcher, J., 1990. Using isotope fractionation of nitrate-nitrogen and nitrate-oxygen

for evaluation of microbial denitrification in a sandy aquifer. J. Hydrol. 114, 413–424.

Bouwer, H., 2002. Artificial recharge of groundwater: Hydrogeology and engineering. Hydrogeol. J. 10, 121–142. https://doi.org/10.1007/s10040-001-0182-4

Burow, K.R., Nolan, B.T., Rupert, M.G., Dubrovsky, N.M., 2010. Nitrate in groundwater of the United States, 1991-2003. Environ. Sci. Technol. 44, 4988–4997. https://doi.org/10.1021/es100546y

Carpenter, A.S.R., Caraco, N.F., Correll, D.L., Howarth, R.W., Sharpley, A.N., Smith, V.H., 1998. Nonpoint pollution of surface waters with phophorous and nitrogen. Ecol. Appl. 8, 559–568.

Christianson, L.E., Lepine, C., Sharrer, K.L., Summerfelt, S.T., 2016. Denitrifying bioreactor clogging potential during wastewater treatment. Water Res. 105, 147–156. https://doi.org/10.1016/j.watres.2016.08.067

Clark, J.F., Hudson, G.B., Davisson, M.L., Woodside, G., Herndon, R., 2004. Geochemical Imaging of Flow Near an Artificial Recharge Facility, Orange County, California. Ground Water 42, 167–174. https://doi.org/10.1111/j.1745-6584.2004.tb02665.x

Clough, T.J., Condron, L.M., 2010. Biochar and the Nitrogen Cycle: Introduction. J. Environ. Qual. 39, 1218. https://doi.org/10.2134/jeq2010.0204

Dallman, S., Spongberg, M., 2012. Expanding Local Water Supplies: Assessing the Impacts of Stormwater Infiltration on Groundwater Quality. Prof. Geogr. 64, 232–249. https://doi.org/10.1080/00330124.2011.600226

Dastager, S.G., Lee., J.C., Ju, Y.J., Park, D.J., Kim, C.J., 2008. Marmoricola bigeumensis sp. nov., a member of the family Nocardioidaceae. Int. J. Syst. Evol. Microbiol. 58, 1060–1063. https://doi.org/10.1099/ijs.0.65576-0

Della Rocca, C., Belgiorno, V., Meriç, S., 2006. An heterotrophic/autotrophic denitrification (HAD) approach for nitrate removal from drinking water. Process Biochem. 41, 1022–1028. https://doi.org/10.1016/j.procbio.2005.11.002

Ganot, Y., Holtzman, R., Weisbrod, N., Russak, A., Katz, Y., Kurtzman, D., 2018. Geochemical Processes During Managed Aquifer Recharge With Desalinated Seawater. Water Resour. Res. 54, 978–994. https://doi.org/10.1002/2017WR021798

Gibert, O., Pomierny, S., Rowe, I., Kalin, R.M., 2008. Selection of organic substrates as potential reactive materials for use in a denitrification permeable reactive barrier (PRB). Bioresour. Technol. 99, 7587–7596. https://doi.org/10.1016/j.biortech.2008.02.012

Grau-Martínez, A., Folch, A., Torrentó, C., Valhondo, C., Barba, C., Domènech, C., Soler, A., Otero, N., 2018. Monitoring induced denitrification during managed aquifer recharge in an infiltration pond. J. Hydrol. 561, 123–135. https://doi.org/10.1016/j.jhydrol.2018.03.044

Greenan, C.M., Moorman, T.B., Parkin, T.B., Kaspar, T.C., Jaynes, D.B., 2009. Denitrification in wood chip bioreactors at different water flows. J. Environ. Qual. 38, 1664–1671. https://doi.org/10.2134/jeq2008.0413

Groffman, P.M., Altabet, M. a., Bohlke, J.K., Butterbach-Bahl, K., David, M.B., Firestone, M.K., Giblin, A.E., Kana, T.M., Nielsen, L.P., Voyteck, M. a., 2006. Methods for Measuring Denitrification : Ecol. Appl. 16, 2091–2122. https://doi.org/10.1890/1051-0761(2006)016[2091:MFMDDA]2.0.CO;2

Gurdak, J.J., Qi, L., 2004. Vulnerability of Recently Recharged Groundwater in the High Plains Aquifer To Nitrate Contamination. Environ. Sci. Technol. 36, 6004–6012. https://doi.org/10.1021/es300688b

Hagman, M., Nielsen, J.L., Nielsen, P.H., Jansen, J.C., 2008. Mixed carbon sources for nitrate reduction in activated sludge-identification of bacteria and process activity studies. Water Res. 42, 1539–1546. https://doi.org/10.1016/j.watres.2007.10.034

Halaburka, B.J., Lefevre, G.H., Luthy, R.G., 2017. Evaluation of Mechanistic Models for Nitrate Removal in Woodchip Bioreactors. Environ. Sci. Technol. 51, 5156–5164. https://doi.org/10.1021/acs.est.7b01025

Hatch, C.E., Fisher, A.T., Revenaugh, J.S., Constantz, J., Ruehl, C., 2006. Quantifying surface water-groundwater interactions using time series analysis of streambed thermal records: Method development. Water Resour. Res. 42, 1–14. https://doi.org/10.1029/2005WR004787

Healy, M.G., Ibrahim, T.G., Lanigan, G.J., Serrenho, A.J., Fenton, O., 2012. Nitrate removal rate, efficiency and pollution swapping potential of different organic carbon media in laboratory denitrification bioreactors. Ecol. Eng. 40, 198–209. https://doi.org/10.1016/j.ecoleng.2011.12.010

Hoover, N.L., Bhandari, A., Soupir, M.L., Moorman, T.B., 2016. Woodchip Denitrification Bioreactors: Impact of Temperature and Hydraulic Retention Time on Nitrate Removal. J. Environ. Qual. 45, 803–812. https://doi.org/10.2134/jeq2015.03.0161

Kameyama, K., Miyamoto, T., Shiono, T., Shinogi, Y., 2012. Influence of Sugarcane Bagasse-derived Biochar Application on Nitrate Leaching in Calcaric Dark Red Soil. J. Environ. Qual. 41, 1131. https://doi.org/10.2134/jeq2010.0453

Kaushal, S.S., Gro, P.M., Band, L.E., Elliott, E.M., Shields, C.A., Kendall, C., 2011. Tracking Nonpoint Source Nitrogen Pollution in Human-Impacted Watersheds. Environ. Sci. Technol. 45, 8225–8232. https://doi.org/10.1021/es200779e

Kendall, C., Caldwell, E.., 1998. Isotope Tracers in Catchment Hydrology. Elsevier, Amsterdam.

Klindworth, A., Pruesse, E., Schweer, T., Peplies, J., Quast, C., Horn, M., Glöckner, F.O., 2013. Evaluation of general 16S ribosomal RNA gene PCR primers for classical and next-generation sequencing-based diversity studies. Nucleic Acids Res. 41, 1–11. https://doi.org/10.1093/nar/gks808

Koch, H., Lücker, S., Albertsen, M., Kitzinger, K., Herbold, C., Spieck, E., Nielsen, P.H., Wagner, M., Daims, H., 2015. Expanded metabolic versatility of ubiquitous nitrite-oxidizing bacteria from the genus *Nitrospira*. Proc. Natl. Acad. Sci. 112, 11371–11376. https://doi.org/10.1073/pnas.1506533112

Korom, S.F., 1992. Natural denitrification in the saturated zone: A review. Water

Resour. Res. 28, 1657–1668. https://doi.org/10.1029/92WR00252

Liu, Yuanyuan, Liu, C., Nelson, W.C., Shi, L., Xu, F., Liu, Yunde, Yan, A., Zhong, L., Thompson, C., Fredrickson, J.K., Zachara, J.M., 2017. Effect of Water Chemistry and Hydrodynamics on Nitrogen Transformation Activity and Microbial Community Functional Potential in Hyporheic Zone Sediment Columns. Environ. Sci. Technol. 51, 4877–4886. https://doi.org/10.1021/acs.est.6b05018

Mariotti, A., Landreau, A., Simon, B., 1988. 15N isotope biogeochemistry and natural denitrification process in groundwater: Application to the chalk aquifer of northern France. Geochim. Cosmochim. Acta 52, 1869–1878. https://doi.org/10.1016/0016-7037(88)90010-5

Mengis, M., Schiff, S.L., Harris, M., English, M.C., Aravena, R., Elgood, R.J., MacLean, A., 1999. Multiple geochemical and isotopic approaches for assessing ground water NO3- elimination in a riparian zone. Ground Water. https://doi.org/10.1111/j.1745-6584.1999.tb01124.x

Moon, H.S., Shin, D.Y., Nam, K., Kim, J.Y., 2008. A long-term performance test on an autotrophic denitrification column for application as a permeable reactive barrier. Chemosphere 73, 723–8. https://doi.org/10.1016/j.chemosphere.2008.06.065

Otero, N., Torrentó, C., Soler, A., Menció, A., Mas-Pla, J., 2009. Monitoring groundwater nitrate attenuation in a regional system coupling hydrogeology with multi-isotopic methods: The case of Plana de Vic (Osona, Spain). Agric. Ecosyst. Environ. 133, 103–113. https://doi.org/10.1016/j.agee.2009.05.007

Pauwels, H., Foucher, J.C., Kloppmann, W., 2000. Denitrification and mixing in a schist aquifer: Influence on water chemistry and isotopes. Chem. Geol. 168, 307–324. https://doi.org/10.1016/S0009-2541(00)00201-1

Racz, A.J., Fisher, A.T., Schmidt, C.M., Lockwood, B.S., Huertos, M.L., 2012. Spatial and Temporal Infiltration Dynamics During Managed Aquifer Recharge. Ground Water 50, 562–570. https://doi.org/10.1111/j.1745-6584.2011.00875.x

Robertson, W.D., Merkley, L.C., 2008. In-Stream Bioreactor for Agricultural Nitrate Treatment. J. Environ. Qual. 38, 230–238. https://doi.org/10.2134/jeq2008.0100

Schipper, L.A., Barkle, G.A., Vojvodić-Vuković, M., 2005. Maximum Rates of Nitrate Removal in a Denitrification Wall. J. Environ. Qual. 4, 1270–1276. https://doi.org/10.2134/jeq2005.0008

Schipper, L.A., Robertson, W.D., Gold, A.J., Jaynes, D.B., Cameron, S.C., 2010. Denitrifying bioreactors - An approach for reducing nitrate loads to receiving waters. Ecol. Eng. 36, 1532–1543. https://doi.org/10.1016/j.ecoleng.2010.04.008

Schipper, L.A., Vojvodić-Vuković, M., 2001. Five years of nitrate removal, denitrification and carbon dynamics in a denitrification wall. Water Res. 35, 3473–3477. https://doi.org/10.1016/S0043-1354(01)00052-5

Schmidt, C.M., Fisher, A.T., Racz, A.J., Lockwood, B.S., Huertos, M.L., 2011. Linking denitrification and infiltration rates during managed groundwater recharge. Environ. Sci. Technol. 45, 9634–9640. https://doi.org/10.1021/es2023626

Seitzinger, S., Harrison, J.A., Böhlke, J.K., Bouwman, A.F., Lowrance, R., Peterson, B., Tobias, C., Drecht, G. Van, 2006. Denitrification Across Landscapes and Waterscapes: a Synthesis. Ecol. Appl. 16, 2064–2090.

Spang, A., Offre, P., Zumbrägel, S., Haider, S., Rychlik, N., Nowka, B., Schmeisser, C., Lebedeva, E. V., Rattei, T., Böhm, C., Schmid, M., Galushko, A., Hatzenpichler, R., Weinmaier, T., Daniel, R., Schleper, C., Spieck, E., Streit, W., Wagner, M., 2012. The genome of the ammonia-oxidizing candidatus nitrososphaera gargensis: Insights into metabolic versatility and environmental adaptations. Environ. Microbiol. 14, 3122–3145. https://doi.org/10.1111/j.1462-2920.2012.02893.x

Takeuchi, M., Hamana, K., Hiraishi, A., 2001. Proposal of the genus Sphingomonas sensu stricto and three new genera. Int. J. Syst. Evol. Microbiol. 51, 1405–17. https://doi.org/10.1099/00207713-51-4-1405

Tedoldi, D., Chebbo, G., Pierlot, D., Kovacs, Y., Gromaire, M.C., 2016. Impact of

runoff infiltration on contaminant accumulation and transport in the soil/filter media of Sustainable Urban Drainage Systems: A literature review. Sci. Total Environ. 569–570, 904–926. https://doi.org/10.1016/j.scitotenv.2016.04.215

Vitousek, P.M., Aber, J.D., Howarth, R.W., Likens, G.E., Matson, A., Schindler, D.W., Schlesinger, W.H., Tilman, D.G., 1996. Human alteration of the global nitrogen cycle: sources and consequences. Ecol. Appl. 7, 737–750.

Vogel, J.C., Talma, A.S., Heaton, T.H.E., 1981. Gaseous nitrogen as evidence for denitrification in groundwater. J. Hydrol. 50, 191–200. https://doi.org/10.1016/0022-1694(81)90069-X

Wada, Y., Van Beek, L.P.H., Van Kempen, C.M., Reckman, J.W.T.M., Vasak, S., Bierkens, M.F.P., 2010. Global depletion of groundwater resources. Geophys. Res. Lett. 37, 1–5. https://doi.org/10.1029/2010GL044571

Xu, H., Wang, X., Yao, H., Su, J., Li, H., Zhu, Y.-G., 2014. Biochar impacts soil microbial community composition and nitrogen cycling in an acidified soil. Environ. Sci. Technol. 17, 9391–9399. https://doi.org/10.1021/es5021058

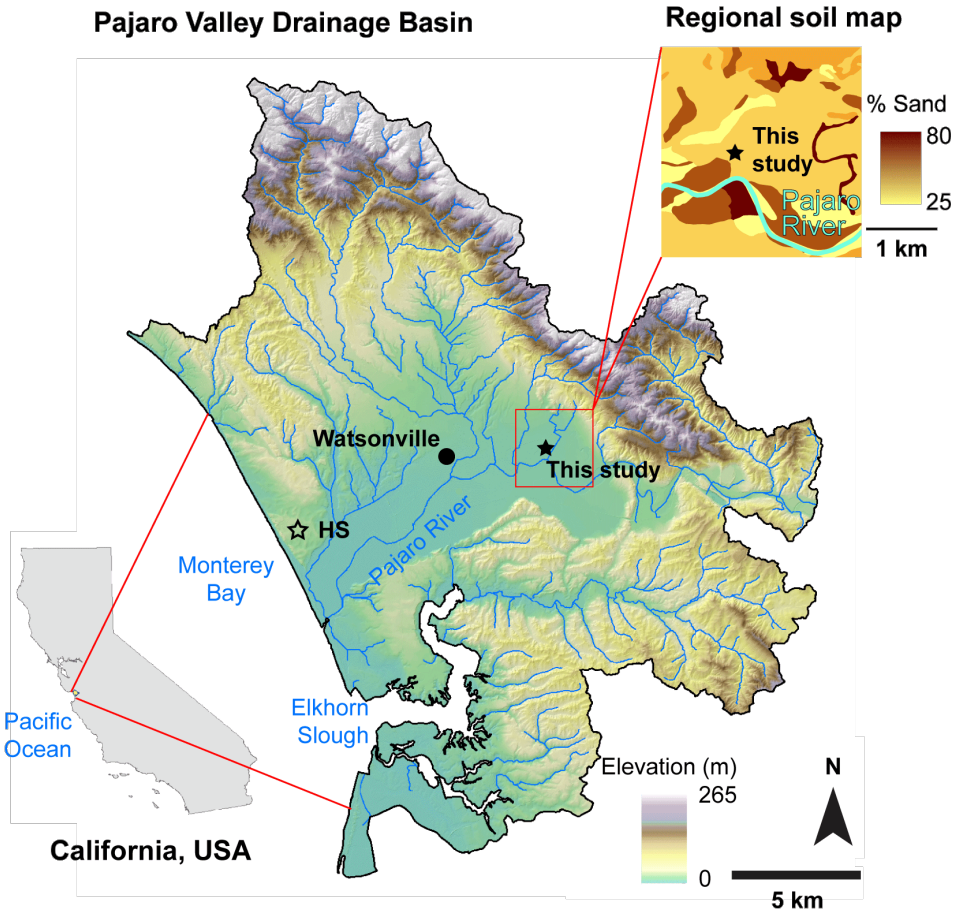

Figure 1-S1 Map of the Pajaro Valley Drainage Basin in central coastal California, USA. Solid black star indicates the location of the current study site. Open star labeled "HS" indicates location of the Harkins Slough managed recharge system, location of an earlier PRB study completed in coarser soil. Red box shows a regional soil map near the current study site. Soils in the region are generally loam to sandy loam, being flood plain, alluvial, and fluvial deposits, and vary considerably in texture and composition over short distances.

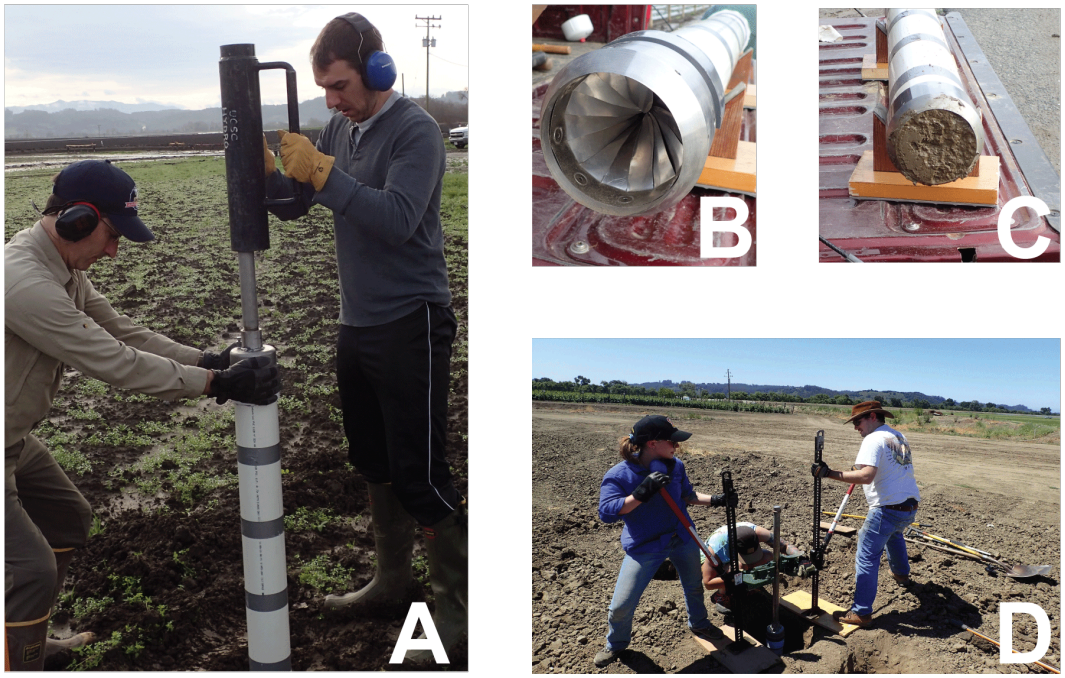

Figure 1-S2 Photos of soil core collection method Soil cores used for laboratory column studies were collected using a custom-built coring apparatus consisting of **A** a stainless-steel drive shaft mountable on a schedule 40, PVC tube for hammering to depth with a slide hammer, and **B** a coring shoe with a core catcher, which secures the core during extraction. **C** shows the core catcher after extraction and **D** shows the core extraction method; using truck jacks and a "pipe dog" to pull the core upward using the drive shaft. The intact core is extracted from the ground, then brought back to the laboratory for testing.

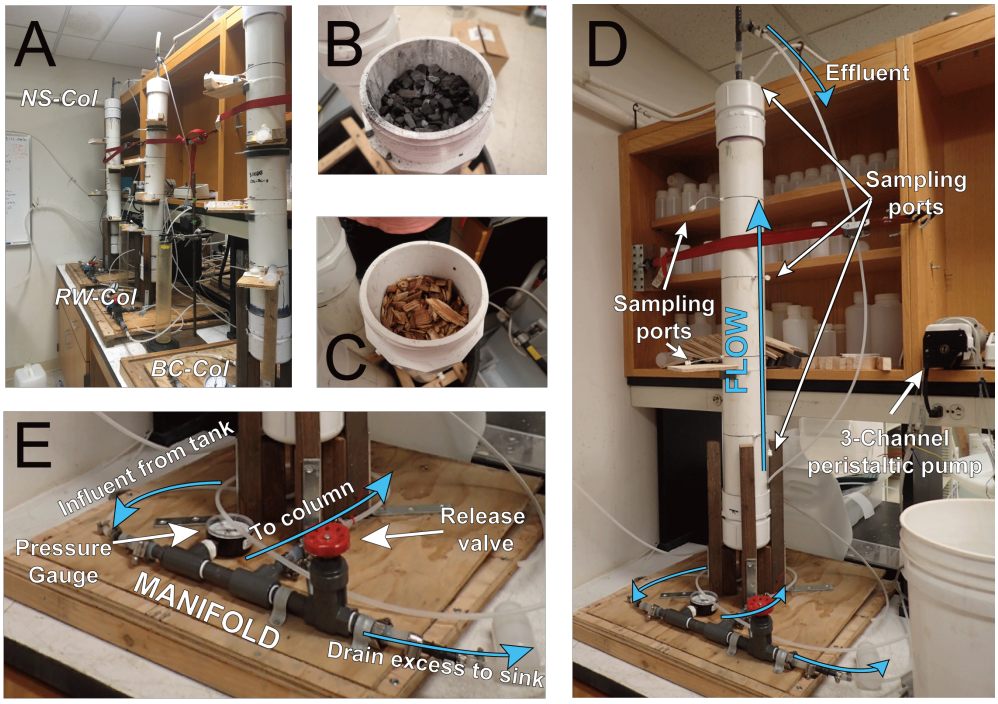

Figure 1-S3 Laboratory column experimental configuration. **A** All three columns running simultaneously driven by the same peristaltic pump**.** Installation of biochar **B** and woodchips **C** as PRB materials at the bottom of the columns before they were sealed and inverted. **D** Single column showing valves, water flow direction (blue arrows), and sampling ports. **E** Detail showing column manifold. Release valve and pressure gauge were used to maintain and monitor stable flow throughout the tests.

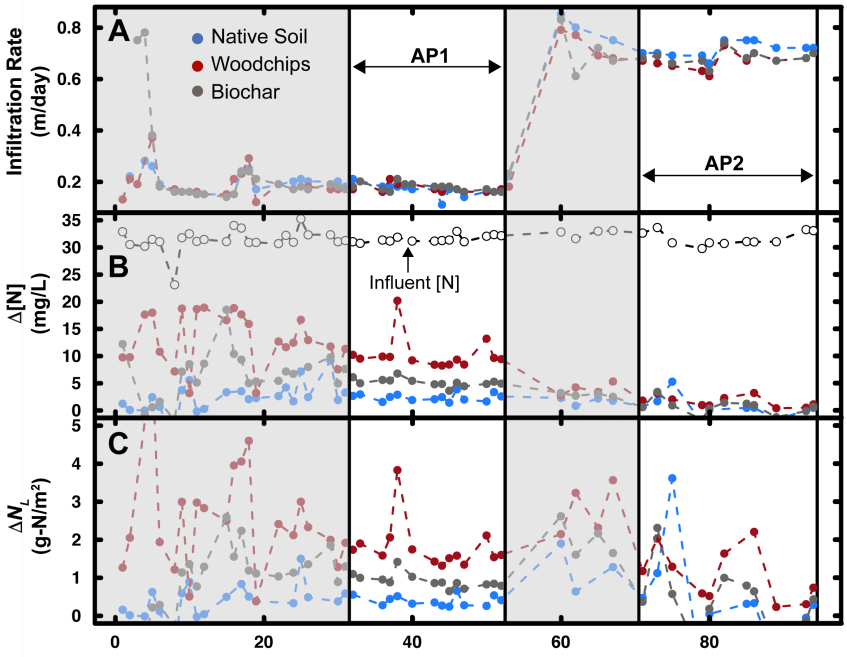

Figure 1-S4 Laboratory column studies experimental conditions and analysis periods. Two analysis periods were chosen for comparison to field studies, AP1 and AP2, based on relatively stable flow and pressure conditions. **A** Infiltration rate (m/day) controlled by a peristaltic pump and measured daily for each treatment. **B** Δ[N] for each treatment, with the [N] of influent water shown in open circles. **C** ΔN_L for each treatment.

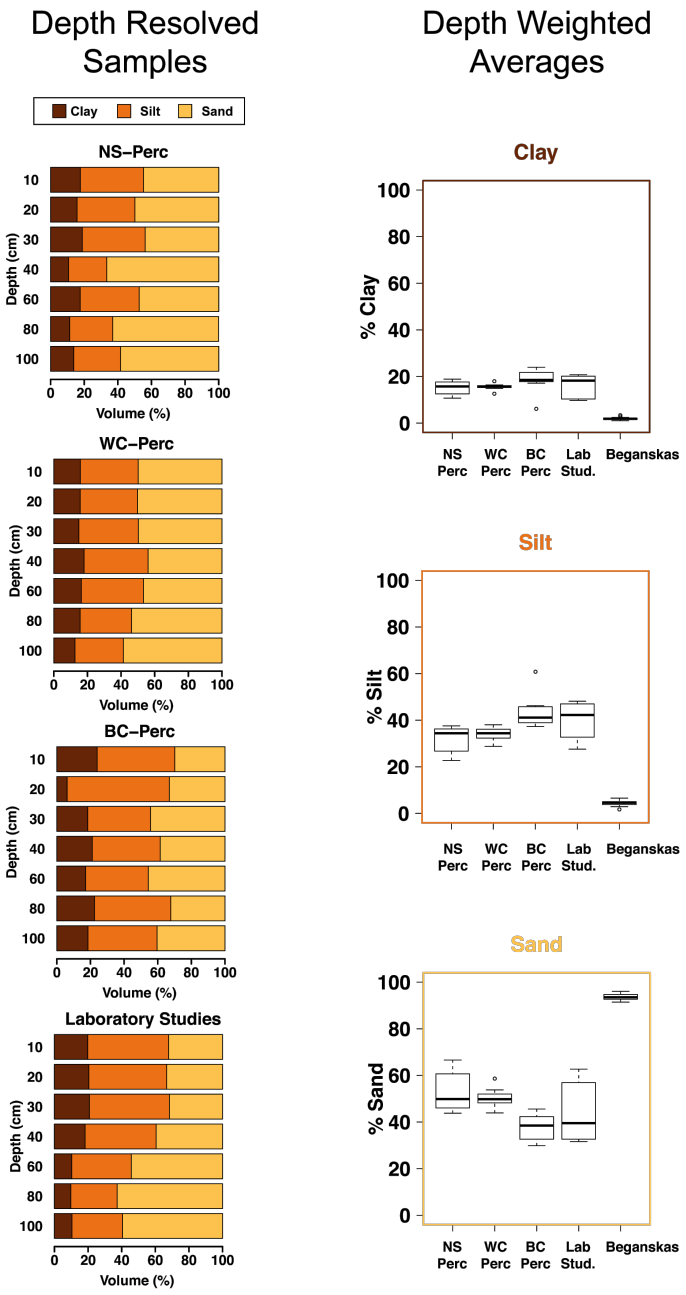

Figure 1-S5 Grainsize data from experiments Left panel Grain size analyses from field and laboratory studies showing samples from 10-100 cm at 10 cm intervals binned into clay (<4µm), silt (4-63µm) and sand (>63µm) and **Right panel** Box and whisker diagrams showing the percentage distribution of clay, silt and sand size particles for field and laboratory experiments, and for similar experiments done at the Harkins Slough MAR site(Beganskas et al., 2018) in very coarse sandy soil. Grainsize samples for laboratory studies were collected adjacent from within 10 cm of the location of all three columns.

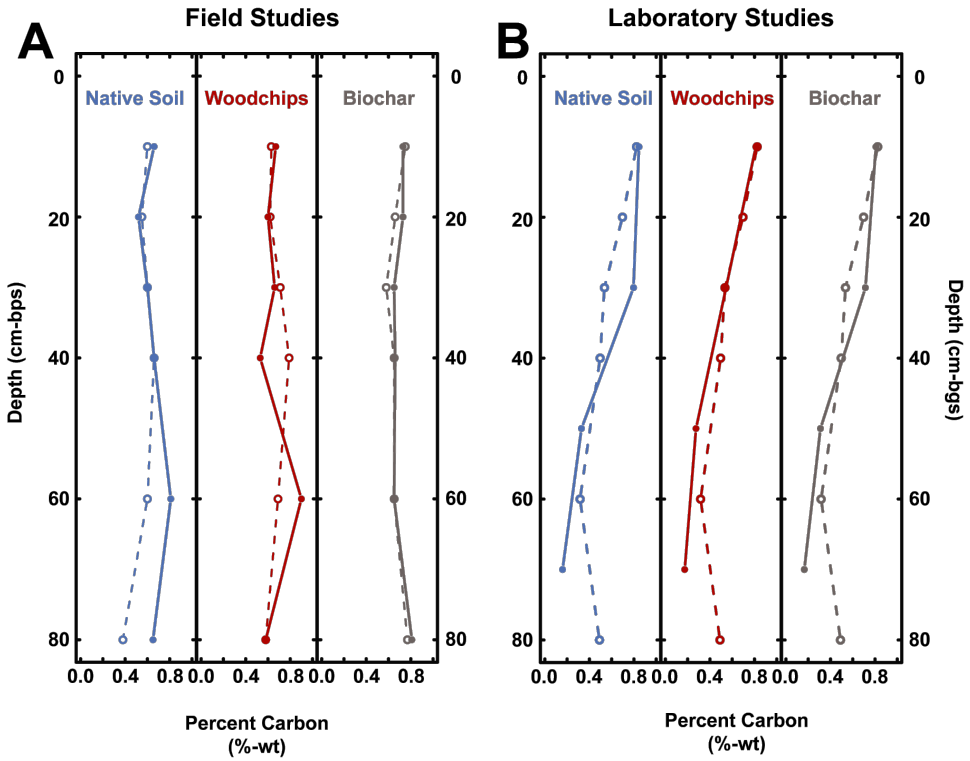

Figure 1-S6 Soil total organic carbon content (**A)** and laboratory studies (**B)** collected before (open circles, dotted lines) and after (closed circles, solid lines) each experiment.

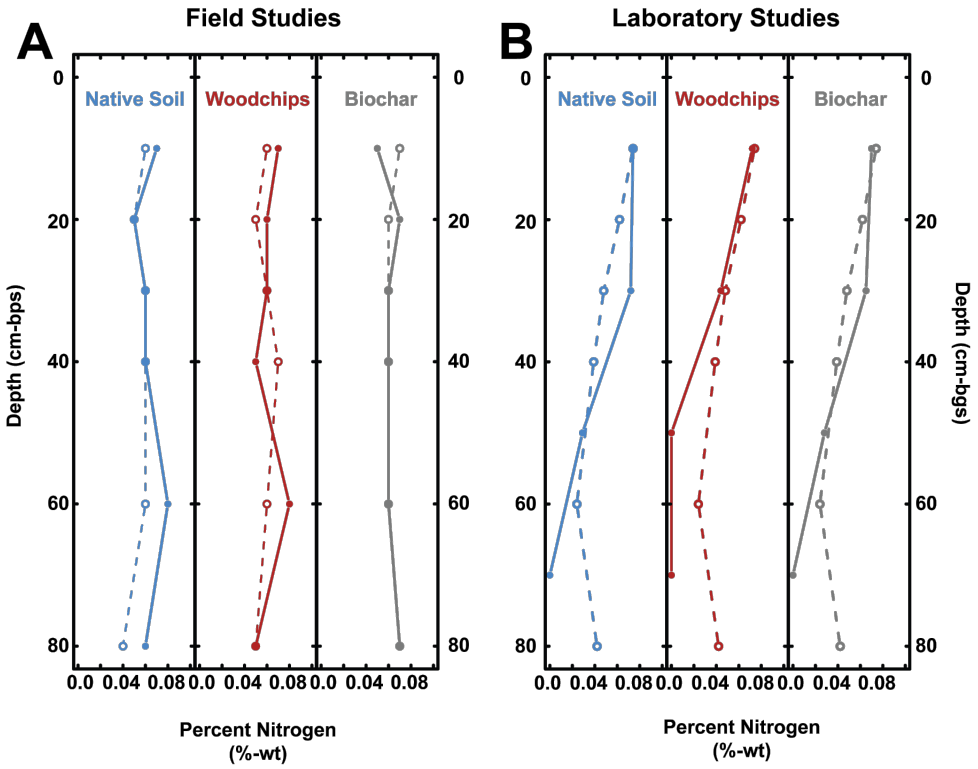

Figure 1-S7 Soil total nitrogen content (**A**) and laboratory studies (**B**) collected before (open circles, dotted lines) and after (closed circles, solid lines) each experiment.

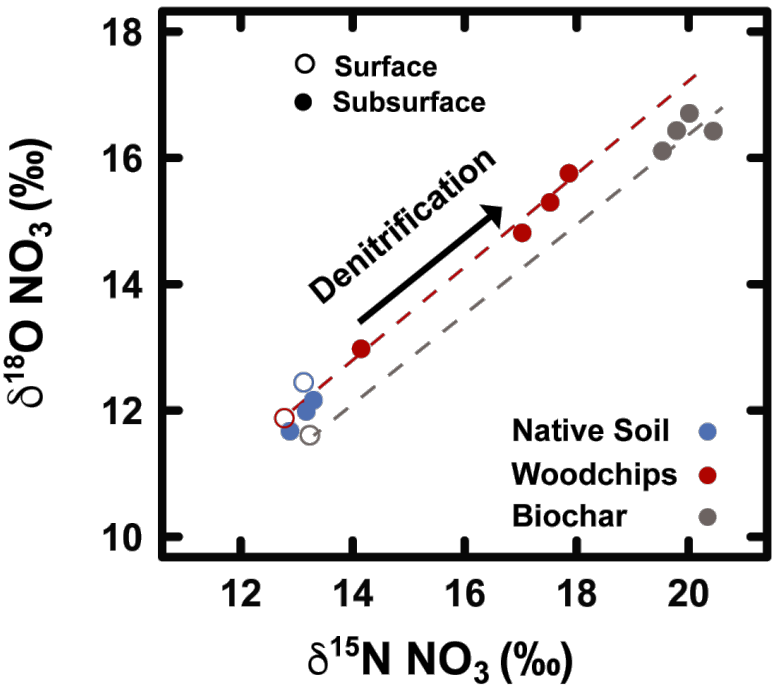

Figure 1-S8 Double isotope plot of residual pore water NO_3 during field percolation tests for different treatments. Surface samples are shown with open circles and subsurface samples are shown with closed circles. For each treatment, the average of multiple samples is shown (NS, n = 2; WC, n = 6; BC, n = 3). Dotted lines show linear regression for *WC-Perc* and *BC-Perc* treatments, *WC-Perc* had a slope of 0.72 and *BC-Perc* had a slope of 0.71.

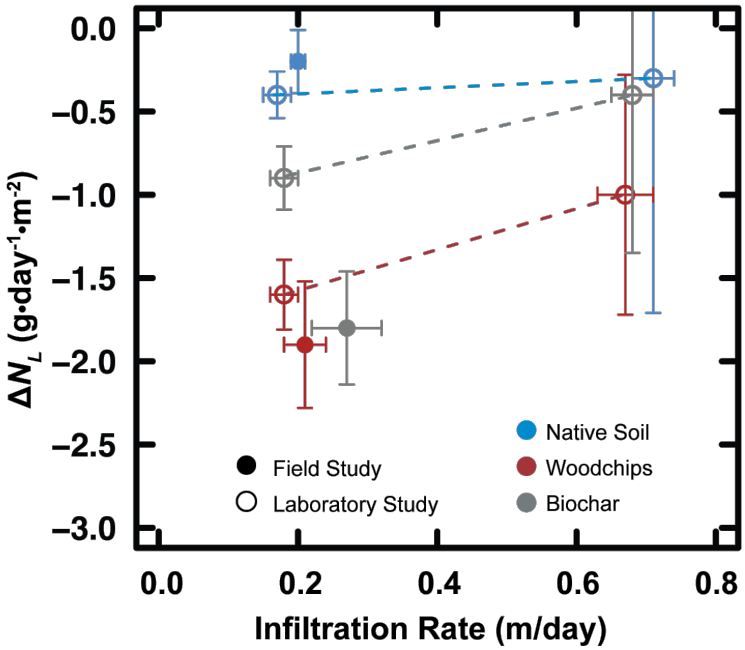

Figure 1-S9 Comparison of ΔN_L for field percolation tests to laboratory column studies across a range of infiltration rates measured for all soil treatments with percolation tests shown with closed circles and column experiments shown with open circles. Bars show standard deviation of values measured for each test during each analysis period. In general, ΔN_L shows a stronger dependence on infiltration rate for the PRB treatments than for the native soil treatment (Table S2). Dashed lines show hypothesized relationships between infiltration rate and ΔN_L.

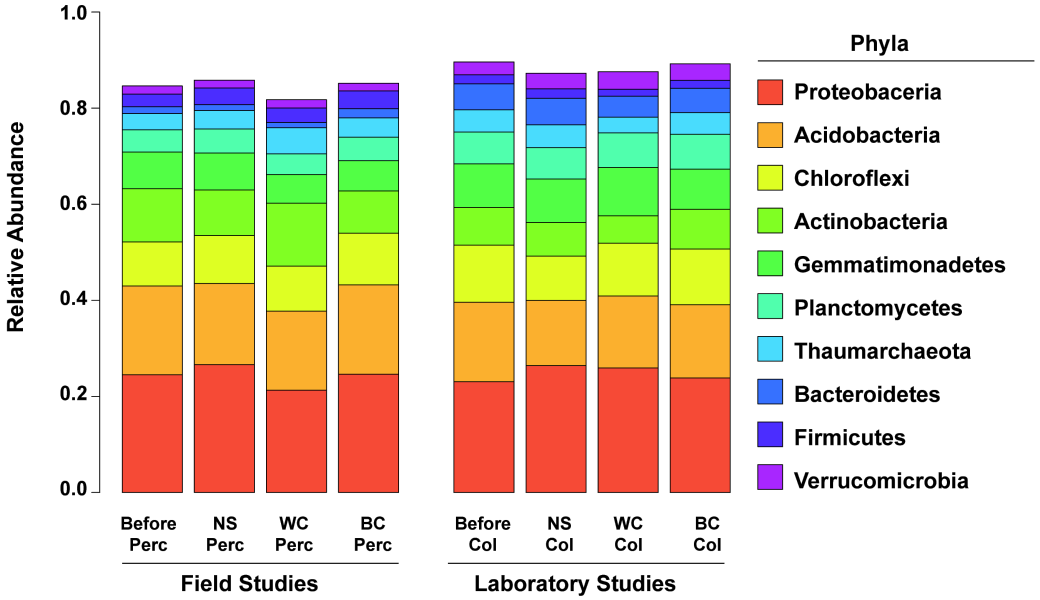

Figure 1-S10 Relative abundance of the 10 most frequently found phyla for all study groups for each experiment. The 10 most abundant phyla represented ≥80% of total reads for all sample

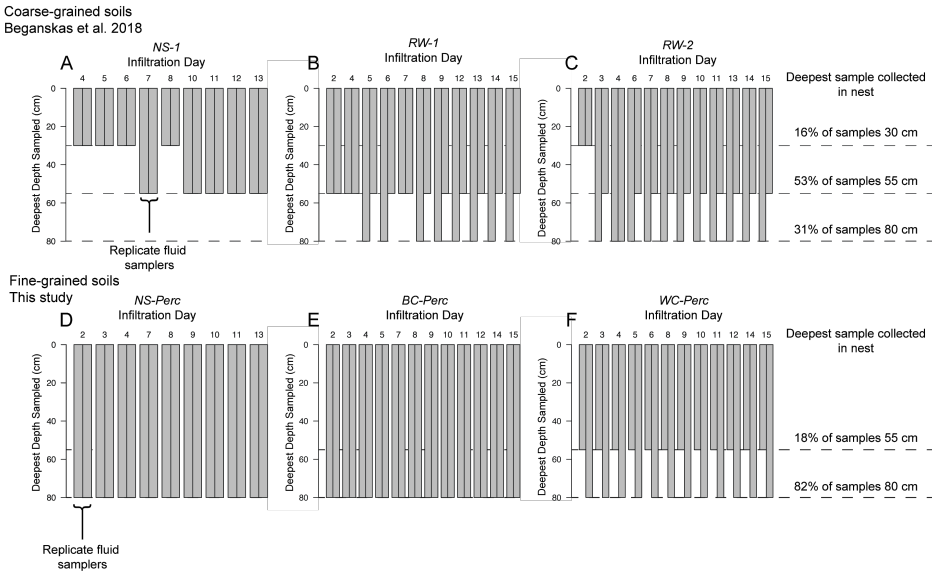

Figure 1-S11 The deepest depths at which samples could be collected from three infiltration tests in coarse-grained soil (Beganskas et al. 2018) (A-C) and in finer-grained soil (this study) (D-F). Plot construction in both studies consisted of two replicate nests with fluid samplers at multiple depths, and paired bars show the deepest depth of sample collected for each replicate. Coarse-grained sites showed more variability in depth within the range sampled, while the finer-grained soils consistently produced from 80 cm depth

Table 1-S1 Effect of soil treatments: T-tests to compare Δ[N] and ΔN_L values for each soil treatment within each experiment

				Δ[N]		ΔN_L	
Experiment	Signif. Compar.	Type	Tails	p.value	sig @0.05[a] ?	p.value	sig @0.05 [a] ?
Perc	WC vs NS	3	1	6.0E-07	1	9.5E-07	1
	BC vs NS	3	1	4.7E-05	1	8.6E-04	1
	WC vs BC	3	1	7.8E-02	0	3.3E-01	0
AP1	WC vs NS	3	1	8.0E-17	1	9.0E-13	1
	BC vs NS	3	1	4.6E-09	1	8.5E-08	1
	WC vs BC	3	1	1.7E-12	1	2.0E-08	1
AP2	WC vs NS	3	1	8.9E-02	0	9.6E-02	0
	BC vs NS	3	1	4.5E-01	0	4.5E-01	0
	WC vs BC	3	1	4.8E-02	1	5.4E-02	0

[a]where 1 indicates a statistically significant difference and 0 indicates that none was detected

Table 1-S2 Effect of infiltration rates: T-tests to compare Δ[N] and ΔN_L values for each soil treatment between experiments

				Δ[N]		ΔN_L	
Treatment	Signif. Compar.	Type	Tails	p.value	sig @0.05 [a] ?	p.value	sig @0.05 [a] ?
NS	Perc vs AP1	3	1	9.4E-03	1	3.7E-02	1
	Perc vs AP2	3	1	2.4E-01	0	4.2E-01	0
	AP1 vs AP2	3	1	9.4E-03	1	4.2E-01	0
WC	Perc vs AP1	3	1	4.8E-01	0	2.3E-02	1
	Perc vs AP2	3	1	1.2E-06	1	1.8E-03	1
	AP1 vs AP2	3	1	2.8E-12	1	1.7E-02	1
BC	Perc vs AP1	3	1	2.2E-02	1	7.8E-03	1
	Perc vs AP2	3	1	2.2E-05	1	6.4E-04	1
	AP1 vs AP2	3	1	4.5E-08	1	5.0E-02	1

[a]where 1 indicates a statistically significant difference and 0 indicates that none was detected

Table 1-S3 Effect of depth during field experiments: Single factor ANOVA, Factor: depth

		[N]		[DOC]	
Treatment	Signif. Compar.	p.value	sig @0.05[a] ?	p.value	sig @0.05 [a] ?
NS	All depths	3.9E-01	0	2.3E-01	0
WC	All depths	7.3E-11	1	1.8E-09	1
BC	All depths	5.6E-10	1	3.2E-10	1

[a]where 1 indicates a statistically significant difference and 0 indicates that none was detected

Chapter Two

DENITRIFICATION DURING INFILTRATION FOR MANAGED AQUIFER RECHARGE: INFILTRATION RATE CONTROLS AND MICROBIAL RESPONSE

Published: Gorski G., Dailey H., Fisher A. T., Schrad N., Saltikov C., (2020) Denitrification during infiltration for managed aquifer recharge: Infiltration rate controls and microbial response. *Science of the Total Environment.* 727, 138642. doi: https://doi.org/10.1016/j.scitotenv.2020.138642

Abstract

Managed aquifer recharge (MAR) systems can be designed and operated to improve water supply and quality simultaneously by creating favorable conditions for contaminant removal during infiltration through shallow soils. We present results from laboratory flow-through column experiments, using intact soil cores from two MAR sites, elucidating conditions that are favorable to nitrate (NO_3) removal via microbial denitrification during infiltration. Experiments focused on quantitative relations between infiltration rate and the presence or absence of a carbon-rich permeable reactive barrier (PRB) on both amounts and rates of nitrate removal during infiltration and associated shifts in microbial ecology. Experiments were conducted using a range of infiltration rates relevant to MAR (0.3-1.4 m/day), with PRBs made of native soil *(NS)*, woodchips (*WC*) and a 50:50 mixture of woodchips and native soil (*MIX*). The latter two (carbon-rich) PRB treatments led to statistically significant increases in the amount of nitrate removed by increasing zero-order denitrification rates, both within the PRB materials and in the underlying soil. The highest fraction of nitrate removal occurred at the lowest infiltration rates for all treatments. However, the highest nitrogen mass removal (ΔN_L) was observed at 0.4-0.7 m/day for both the *WC* and *MIX* treatments. In contrast, the maximum ΔN_L for the *NS* treatment was observed at the lowest infiltration rates measured (~0.3 m/day). Further, both carbon-rich PRBs had a substantial impact on the soil microbial ecology in the underlying soil, with lower overall diversity and a greater relative abundance of groups known to degrade carbon and metabolize nitrogen. These results demonstrate that infiltration rates and carbon

availability can combine to create favorable conditions for denitrification during infiltration for MAR and show how these factors shape and sustain the microbial community structures responsible for nutrient cycling in associated soils.

2.1 Introduction

Managed aquifer recharge (MAR) is a suite of techniques that increase groundwater storage through the collection and infiltration of excess surface water (Bouwer, 2002). Infiltration can be achieved through dedicated basins, canals or wells, and source water can be derived from rivers, streams, and wetlands (Grau-Martínez et al., 2018; Valhondo et al., 2018), treated wastewater (Bekele et al., 2011), stormwater runoff (Page et al., 2017), desalinized seawater (Ganot et al., 2018), or other sources. During passage through the soil, nutrients (and other contaminants) can be removed, leading to improved groundwater quality (Grau-Martínez et al., 2018; Tzoraki et al., 2018; Valhondo et al., 2015; F. Wang et al., 2018).

There is considerable interest in the conditions under which nitrate (NO_3) can be removed from infiltrating water via microbially mediated denitrification. Nitrate is a pervasive contaminant in groundwater and surface water with detrimental effects on human and ecological health (Burri et al., 2019; van Drecht et al., 2003). In both managed and natural environments, denitrification is influenced by hydrologic and geochemical controls. For example, several studies have noted an inverse relationship between infiltration rate and denitrification (Hampton et al., 2019; Nordström et al., 2017; Schmidt et al., 2011b). Lower infiltration rates allow higher hydraulic retention

time (HRT), allowing more geochemical processing. Geochemical conditions can also have a strong influence on nitrate removal as increased carbon availability is often associated with denitrification (Seitzinger et al., 2006). Abundant electron donors, including organic carbon, accelerate oxygen consumption leading to more favorable conditions for denitrification. Relatively little is known about how soil microbial communities respond to changes in carbon availability and hydrologic conditions, although earlier field studies suggest connections (Beganskas et al., 2018; Valhondo et al., 2018).

MAR sites offer a unique window into linked hydrologic, geochemical, and microbiological processes and how they interact to influence denitrification during infiltration. Many MAR sites are located in areas that infiltrate water rapidly; rapid infiltration and thus short HRTs may result in suboptimal conditions for denitrification. In an effort to enhance denitrification, a carbon amendment can be added to the soil, often in the form of woodchips or other carbon-rich materials. A layer of one or more of these materials, collectively known as a permeable reactive barriers (PRB), can promote denitrification even at low HRTs, $\leq$ 1 hr, and can increase nutrient cycling and microbial activity during infiltration (Beganskas et al., 2018; Grau-Martínez et al., 2018).

Field-based observations at MAR sites are critical for constraining the key factors that control denitrification during infiltration and help to generate testable hypotheses. For example, denitrification rates measured during active infiltration for MAR showed a positive relationship with infiltration rate up to 0.6-0.8 m/day, above

which denitrification rates apparently ceased (Schmidt et al., 2011b). It is unclear if this is a common phenomenon as many MAR site operators do not measure infiltration rates and pore water fluid chemistry simultaneously across the range of relevant infiltration rates. Recent studies have found evidence for enhanced denitrification in pore fluid samples collected from soils beneath an infiltration basin installed with a PRB made of vegetal compost (Grau-Martínez et al., 2018; Valhondo et al., 2014). While samples collected beneath a carbon-rich PRB showed more evidence of nitrate removal than those beneath unamended soil, the extent of spatial and temporal variability in denitrification is unclear.

Quantifying controls on denitrification during infiltration is inherently difficult in a field setting due to challenges in contemporaneous and co-located sample and data collection, dynamic processes that change on multiple timescales, and spatial heterogeneity in soil and fluid properties across multiple scales. One useful approach is to conduct laboratory studies that are carefully linked to field conditions, allowing strong control on system parameters that is not feasible in a field setting (Bertelkamp et al., 2016; Park and Lee, 2018; Ronen-eliraz et al., 2017). Previous work demonstrated a method for conducting flow-through experiments on intact sediment cores collected from MAR sites to test the effect of infiltration rate on denitrification (Gorski et al., 2019a). Laboratory experiments in that study included assessment of nitrate removal after passage through sediment columns, showing results that were similar to those measured at the field site using equivalent soils.

In the present study, we collected intact soil cores from two other MAR sites to quantify the relationship between infiltration rates and nitrate removal in the presence or absence of a carbon-rich PRB. The close coupling between field and laboratory techniques allowed controlled testing across a range of parameters that are relevant to operating MAR systems, including infiltration rates up to ~1.4 m/day. The objectives of this study were to: (a) quantify relationships in multiple soils between infiltration rates and the extent/occurrence of denitrification during infiltration for MAR; (b) determine how those relationships change in the presence of PRBs made of woodchips and a 50:50 mixture of woodchips and native soil; and (c) compare the influence of infiltration on microbial community ecology in the presence and absence of the carbon-rich amendment, with an emphasis on microbes that are involved in carbon and nitrogen cycling. Results of this work elucidate chemical and microbiological responses to integrated hydrologic and geochemical controls on denitrification during infiltration for MAR. Additionally, the results can be tested in the field, and used in design and operation of MAR systems to simultaneously improve water supplies and quality.

2.2 Methods

2.2.1 Column collection and sediment sampling

Three intact soil cores were collected from each of two sites in the Pajaro Valley Drainage Basin (PVDB) in central coastal California, USA (Figure 2-1). Cores from Site A were collected from an active MAR site in the northwestern part of the PVDB

and cores from Site B were collected from a proposed site near the coast (Section S1 for details).

Intact soil cores were collected in 10 cm internal diameter (ID) polyvinylchloride (PVC) tubes, 100 cm in length. The cores were tested in the same tubes, in order to maintain the layering, structure, and microbial habitat of the soil. Detailed description of the coring procedure can be found in an earlier study (Gorski et al., 2019a). Three cores were collected from adjacent locations at each site, in an effort to minimize variability. After collection, cores were capped and transported back to the laboratory for testing.

At each site, sediment samples were collected by hand auger ≤10 cm laterally from the core locations, and after each experiment from within the columns used for testing. Soil samples were collected at 10 cm depth intervals to 60 cm below ground surface, and sample splits were analyzed for soil texture, total organic carbon (TOC), total nitrogen (TN), and microbial 16S rRNA genes. Microbial sequencing has been completed to date only for soils from Site A. Detailed sampling and analytical techniques are described elsewhere (Gorski et al., 2019a).

2.2.3 Experimental configuration

Soil cores were excavated to a standardized length of 50 cm, approximately the thickness of the saturated zone that develops in the shallow subsurface during infiltration for MAR at regional field sites (Beganskas et al., 2018; Gorski et al., 2019a; Schmidt et al., 2011b). At 10, 30, 50 and 60 cm along the column length, micro-

sampling ports using ceramic 0.15 μm pore size rhizon samplers (Rhizosphere, Wageningen, Netherlands) were installed for pore water collection during experiments.

PRB capsules were constructed for each treatment and placed in line with the columns (Figure 2- 2 and S2). Capsules were built from the same stock material used for coring, 30 cm in length, and filled with native soil from the sites (*NS*), local redwood woodchips (*WC*), or a 1:1 by weight mixture of woodchips and topsoil (*MIX*). Untreated redwood chips were purchased from Aptos Landscape Supply (Aptos, CA) and averaged 3-5 cm in length. An additional fluid sampler was placed in the PRB capsule to collect pore fluid during the experiments.

For each soil site, three treatments were run in parallel with the same influent water pumped in an upward flow direction; first through the PRB capsule and then through an inverted soil core using a peristaltic pump. Cores were inverted prior to starting the flow experiments so that water would flow in the same direction as it would flow in the field, and a range of flow rates could be tested under saturated conditions, without core drainage (Figure 2-2). Influent water was local tap water mixed with KNO_3 (~3 mg/L NO_3-N for most tests, and up to ~12 mg/L for a selection of additional tests), similar to measured concentrations of stormwater collected for MAR projects in the region. Core hydraulic properties were determined using Darcy experiments and breakthrough tracer tests (with an inert tracer) for each core.

Average hydraulic retention times (HRT) were calculated by dividing the effective pore volume of the soil column and the PRB capsule by the volumetric flow rate. The effective pore volume of the soil columns was determined from solute

breakthrough tests (Supporting Information Section S4, Figure 2- S3, and Table S1). Effective pore volumes of the PRB capsules were calculated based on an effective porosity of 0.7 for the woodchip PRBs (Addy et al., 2016; Nordström et al., 2017; NRCS, 2016; van Driel et al., 2006), 0.3 for the native soil PRBs (average value from soil breakthrough curves), and 0.5 for the mixed PRBs (average of native soil and woodchips). The average infiltration during the breakthrough tests was 0.74±0.13 m/day and the average HRT was 9.6±3.9 hours.

2.2.4 Experimental procedures

Tests ran continuously and lasted 68-74 days for each set of columns, and temporal results are reported in terms of infiltration days since test start. Infiltration rates tested during experiments were 0.30 to 1.44 m/day (volume/area/time), covering a range that is commonly observed in MAR settings (Beganskas and Fisher, 2017; Bouwer, 2002), equivalent to volumetric flow rates of 1.7 to 8.0 ml/min. Every 1-2 days, the infiltration rate was measured, and pore fluid samples were collected from the influent, three sampling points along the column, PRB capsule, and the effluent (Figure 2-2).

At each new infiltration rate, the system was allowed to equilibrate for ≥24 hours before sampling and a minimum of two sets of daily samples were collected for each rate. Samples were analyzed for nitrogen species (NO_3, NO_2 and NH_4), dissolved organic carbon (DOC), and for $\delta^{15}N$ and $\delta^{18}O$ of NO_3. Sample collection and analysis procedures are described in Supporting Information (Section 2-S5). Isotopic enrichment factors were calculated using a simplified version of the Rayleigh equation.

The influence of initial NO_3 concentration was tested with samples from Site B. Three initial nitrate concentrations (3.2, 5.9 and 11.6 mg/L NO_3-N) were used, each at two infiltration rates (0.45 and 0.64 m/day). Each new initial NO_3 concentration equilibrated for ≥24 hours before sampling, and each combination of infiltration rate and initial nitrate concentration was sampled twice for each treatment.

We use [NO_3-N] to refer to the sum of [NO_3-N] + [NO_2-N] unless explicitly stated otherwise. Nitrate removal was calculated in two ways. The mass removal rate of nitrate (ΔN_L) was calculated as:

$$\boxed{\Delta N_L = \Delta[NO_3 - N] \times IR} \quad [2.1]$$

where ΔN_L has units of g N/m^2/day, IR is the infiltration rate (m/day), and

$$\boxed{\Delta[NO_3 - N] = ([NO_3 - N] + [NO_2 - N])_{Influent} - ([NO_3 - N] + [NO_2 - N])_{Effluent}}$$

[2.2]

Zero order NO_3-N removal rates were calculated as:

$$\boxed{R_N = \frac{\Delta[NO_3 - N]}{HRT}} \quad [2.3]$$

where R_N is reported in units of mg-N/L/day and HRT is the hydraulic residence time. R_N for soil columns and PRB capsules were calculated using their respective effective pore volumes.

To compare R_N between treatments and soils, we analyzed flow periods in which nitrate was not fully consumed along the length of the column, and therefore was not considered limiting (infiltration rate ≥0.68 m/day for *WC* and *MIX*, and ≥0.44 m/day for *NS*). Under these conditions, denitrification is often modeled as a zero order reaction (e.g., Ghane et al., 2015; Halaburka et al., 2017). Statistical methods were applied to determine the significance of observed differences between treatment and depths (Tables 2-S7 and 2-S8).

2.2.5 DNA Extraction, sequencing, and data processing

DNA was extracted from soil samples using the PowerSoil DNA Isolation Kit (QIAGEN). The normalized and pooled sequences were quantified using a Qubit 4 Fluorometer (Invitrogen). The pooled library was sequenced on the Illumina MiSeq (600 cycles v3 PE300 flow cell kit) at the University of California, Davis Genome Center. Primer specifications and PCR set up were identical to those in an earlier study (Beganskas et al., 2018).

Resulting 16S rRNA Illumina paired end sequences were filtered, trimmed, and merged using the Divisive Amplicon Denoising Algorithm version 1.7.7 (DADA2) (Callahan et al., 2016). Sequences were assigned to Operational Taxonomic Units (OTUs) using an RDP naïve Bayes classifier (Wang et al., 2007) and the Greengenes reference database (DeSantis et al., 2006) version 13.8 with a 97% similarity threshold. The phyloseq package (McMurdie and Holmes, 2013) was used with R (v.3.6.0) to perform data analysis. More details are provided in Supporting Information (Sections S7-8).

2.3 Results

2.3.1 Net nitrogen transformations

For all treatments, more nitrate was removed from the columns at lower infiltration rates (Figure 2-3). For *WC* and *MIX* treatments, greater increases in [DOC] were observed at lower infiltration rates. This is likely due to a combination of higher hydraulic retention times within the PRB capsule and the most soluble carbon leaching from the woodchips during the early part of the experiments (Figure 2- 3). Despite clear differences in [DOC] between *WC* and *MIX* in both soils near the beginning of the experiments, [NO_3-N] and [NO_2-N] patterns are similar within each soil.

At infiltration day 39 (for Soil A) and 30 (for Soil B), both *WC* and *MIX* treatments showed elevated [NO_2-N], but [NO_2-N] never exceeded 1.0 mg/L, the USEPA drinking water contaminant level (USEPA, 2011) and decreased near the end of the tests. Similar to previous studies, elevated [NO_2-N] appeared to be associated with the onset of incomplete denitrification and decreased HRT (Christianson et al., 2017; Hua et al., 2016). [NO_2-N] decreased after infiltration day 60 in both soils, even at higher infiltration rates, suggesting that microbial populations may have responded to increased nutrient fluxes (Betlach and Tiedje, 1981). Additionally, NH_4 was observed in Soil B in all treatments at low concentrations (≤0.5 mg/L [NH_4-N]) with generally less NH_4 at the end of the experiments however, this pattern was not observed in Soil A. Alternative pathways for nitrogen cycling, such as the generation of NH_4 via dissimilatory nitrate reduction to ammonia (DNRA) or ammonification of organic N and subsequent conversion to N_2 by anaerobic ammonium oxidation (annamox) are

possible under these suboxic conditions (Bernard et al., 2015; Zhao et al., 2013). However, while these pathways may have been active during these experiments, we see no evidence that they accounted for major N-cycling; we do not observe concomitant changes in the standing stock of [NO_2-N] or [NH_4-N] nor did we observe large changes in the relative abundance of the phylum *Planctomycetes*, which are primarily responsible for annamox (Strous et al., 1999).

$\delta^{15}N$ values of NO_3 during days in which [NO_3-N] removal was observed show enrichment consistent with denitrification (Figure 2-S4 and Table 2-S3). Enrichment factor values for $\delta^{15}N$ ($\varepsilon^{15}N$) ranged from -6.92 to -18.18‰ (median -11.83‰), overlapping ranges reported in column flow-through denitrification experiments using aquifer materials (Carrey et al., 2013), and field experiments using a soil carbon amendment to enhance denitrification (Beganskas et al., 2018).

2.3.2 Effect of infiltration rate on amount and rate of nitrate removal

For all treatments in both soils, the fraction of initial nitrate removed decreased as infiltration rates increased (Figure 2-4A-C). The *WC* and *MIX* treatments produced similar patterns ($p > 0.1$) of decreasing nitrate removal with increasing infiltration rate, ranging from near total removal at ≤0.5 m/day to approximately ~15% removal at the highest infiltration rates measured, 1.24-1.44 m/day (Figure 2-3B-C).

ΔN_L decreased monotonically with increasing infiltration rates in *NS* treatments (Figure 2-4D), whereas in *WC* and *MIX* treatments the relationship was more complex (Figure 2-4E-F). At lower infiltration rates (≤0.5 m/day), in *WC* and *MIX* treatments, virtually all nitrate was removed, suggesting that the systems were nitrate limited at

these lower infiltration rates. As infiltration rates increased, ΔN_L increased until it reached a peak between IR = 0.45 to 0.70 m/day, before decreasing at higher infiltration rates. For Soil A, maximum ΔN_L values of 1.31±0.10 and 1.42±0.07 g-N/m^2/day were observed at 0.64 and 0.69 m/day for *WC* and *MIX*, respectively. Soil B showed higher maximum ΔN_L values of 1.75±0.06 and 1.80±0.12 g-N/m^2/day for *WC* and *MIX* at infiltration rates of 0.46 and 0.58 m/day, respectively. In comparison, for *NS* columns, the largest ΔN_L values were observed at the lowest infiltration rates and were only 32-51% of those measured for amended soils (Figure 2-4). Maximum ΔN_L values for *NS* were 0.46±0.14 and 0.90±0.07 g-N/m^2/day for Soil A and Soil B, respectively. These ΔN_L values compare favorably to a survey of nitrate removal rates calculated from flow through experiments of undisturbed sediment cores collected from shallow water environments, 0.06 – 0.76 g-N/m^2/day (Laverman et al., 2012).

2.3.3 Depth of nitrogen transformations

Infiltration rates impacted both the amounts and locations of nitrogen transformations along the length of the columns (Figure 2-5). For all experiments, a lower infiltration rate resulted in more NO_3 removal within the PRB and at shallower column depths. At infiltration rates ≤0.68 m/day during the *MIX* and *WC* experiments, ≥50% of the initial [NO_3-N] was removed within the PRB and the first 10 cm of the soil columns in both soils. In contrast, in the *NS* experiments, >50% [NO_3-N] removal along the whole length of the column was observed only at the lowest infiltration rate in Soil A (0.32 m/day) and the two slowest rates in Soil B (0.31 and 0.45 m/day).

At higher infiltration rates in all treatments, unprocessed NO_3 flowed farther along the length of the columns to depths that became active in cycling as they were exposed to increased NO_3 fluxes. At higher infiltration rates in both *MIX* and *WC* experiments (≥1.04 m/day), there was ≤60% NO_3 removal in both soils. In Soil B, at higher infiltration rates (≥1.04 m/day), there was a consistent and progressive removal of NO_3 with depth, continuous between PRB and column in both *MIX* and *WC* experiments (Figure 2-5E-F). In Soil A, at higher infiltration rates (≥1.05 m/day), the patterns were less consistent, but persistent removal was observed both within and below the PRB in both *MIX* and *WC* experiments (Figure 2-5C-D).

In the *WC* treatment in Soil A at 10 cm depth, [NO_3-N] values deviated from the trend at high infiltration rates (≥1.05 m/day). We hypothesize that these samples might have originated from occluded pore space that, under lower infiltration rates, was in better communication with primary flow paths. The potential for development of biogeochemical microzones or processing hotspots has been observed in natural and modeled soils in multiple settings (e.g., Briggs et al., 2015; McClain et al., 2003).

For each treatment, zero-order nitrate removal rates (R_N) generally decreased with greater infiltration rates, a trend that was more pronounced in the PRB capsules than in the soils (Figure 2-6). The *WC* and *MIX* soil columns exhibited generally higher R_N values than the *NS* soil columns at all infiltration rates (Figure 2-6C-D), a difference that is more clearly demonstrated in Soil B, where the differences are statistically significant ($p < 0.05$). This observation is consistent with earlier results that have demonstrated that a woodchip PRB increases denitrification rates both within and

below the woodchip layer likely due to the transport of DOC from the PRB layer into the underlying soil (Beganskas et al., 2018). However, as the infiltration rate increased, the difference between treated soils and non-treated soils diminished.

In general, R_N values measured within the PRB capsules of the *WC* and *MIX* treatments were higher than those measured in the *NS* treatment (where the PRB capsule was filled with native soil) (Figure 2-6A-B). Those differences are statistically significant ($p < 0.05$) at infiltration rates ≤0.68 m/day in Soil A and ≤0.79 m/day in Soil B (Table 2-S6). At the highest infiltration rates measured (1.24 m/day in Soil A and 1.44 m/day in Soil B), R_N values in the PRB capsules for all treatments began to converge, although the *MIX* treatment in Soil A maintained an elevated R_N value of 3.18±0.92 mg-N/L/day. R_N values within the PRB capsules with *WC* and *MIX* PRB treatments showed a strong dependence on infiltration rate ($p < 0.05$), perhaps indicating a limitation imposed by the short hydraulic residence time within the PRB. In contrast, in the *NS* treatments, the PRB capsules and the soil showed less dependence on infiltration rate, likely because carbon availability limited R_N.

2.3.4 Effect of initial nitrate concentration

Variations in the initial [NO_3-N] in Soil B, tested at two intermediate infiltration rates (0.45 and 0.64 m/day), showed that higher initial [NO_3-N] resulted in a smaller fraction of [NO_3-N] reduction in all treatments (Figure 2-7A and B). The highest initial [NO_3-N] measured (11.6 mg N/L) at higher infiltration rates of 0.64 m/day led to a similar fraction of nitrate removal for all treatments (Figure 2-7B). However, the response of ΔN_L showed a marked difference between the two infiltration rates (Figure

2-s 7C and 7D). At 0.45 m/day, a higher initial [NO_3-N] led to more load reduction with *WC* and *MIX* treatments, but slightly less with *NS* treatments (Figure 2-7C); in contrast, at 0.65 m/day, a higher initial [NO_3-N] led to no difference in ΔN_L in *WC* and *MIX* and a decrease in removal in *NS* (Figure 2-7D). This pattern suggests that with low initial [NO_3-N] values, ΔN_L values were limited by nitrate availability at 0.45 m/day, but limited by HRT at 0.65 m/day, consistent with observations from the main flow-through experiments (Figure 2-4).

Combined results from all initial [NO_3-N] concentrations show that the fractional removal of [NO_3-N] decreased exponentially with the product of [NO_3-N] and infiltration rate, equivalent to the incoming nitrate load (mass/area/time) (Figure 2-7E). Data from *WC* and *MIX* experiments follow a similar pattern, approximated by the function $F_{NO3} = A\exp(-BL_i)$, where F_{NO3} = fraction [NO_3-N] removed, L_i = incoming nitrate load and A and B are fitted parameters (Figure 2-7E). The data from the *NS* treatments can be approximated with a similar function, but with a much less [NO_3-N] removal. The difference between these two functional relations can be conceptualized as the benefit provided by the PRB material in terms of the fractional removal of [NO_3-N] (blue shading Figure 2-7E).

Similarly, these data show that ΔN_L varies with incoming [NO_3-N] load in distinct ways for columns tested with (*WC* and *MIX*) and without (*NS*) the use of a carbon-rich PRB (Figure 2-7F). Note that for both fractional [NO_3-N] removal and ΔN_L (Figure 2-7E-F), the benefit is maximized at intermediate values of incoming [NO_3-N] load. This occurs because low incoming loads are marked by low initial [NO_3-N] and/or

infiltration rates (and thus there is relatively little NO_3 to remove). In contrast, at higher incoming loads, the influence of the PRB is limited mainly by short hydraulic retention times. In addition, the intermediate incoming [NO_3-N] loads that lead to the largest calculated benefit are different for the two metrics: fraction removed versus mass removed.

2.3.5 Differences and changes in microbial ecology

Soil samples collected after each treatment from Soil A cluster independently and form a gradient of beta (between sample) diversity, with *NS* samples showing the most similarity to samples collected before the experiments, and *MIX* and *WC* showing more dissimilarity (Figure 2-8A). Within the samples collected before the experiments, the three most abundant phyla were Proteobacteria (26.0%), Acidobacteria (18.8%) and Actinobacteria (14.2%) (Figure 2-8B). Soil samples collected after the *NS* experiments showed an increase in Proteobacteria (37.2%), and a decrease in Actinobacteria (6.7%), and smaller changes among the other phyla. Soil samples collected after the *WC* and *MIX* experiments showed a marked decrease in diversity, with the three most abundant phyla accounting for ≥79.1% of all sequences. Proteobacteria (54.6% in *MIX* and 54.0% in *WC* treatments) and Bacteroidetes (21.4% in *WC* and 13.2% in *MIX* treatments) showed the biggest increases in both relative abundance and raw sequence reads compared to before samples. Increases in Proteobacteria relative abundance after infiltration are consistent with other MAR studies (Li et al., 2012). PRB samples showed similar but more extreme trends, with Proteobacteria alone accounting for 82.0% and 66.2% in the *WC* and *MIX* PRBs respectively.

Changes in select groups of microorganisms shown to be capable of carrying out key steps in the denitrification process account for many of the aforementioned shifts in microbial community structure (Figure 2-9). While denitrification is a common microbial function generally carried out by consortia of inter-reliant species, the families listed in Figure 2-9 have been identified previously as having members associated with denitrification, and as such, we refer to them as "denitrifiers" even though their mechanistic role in the denitrification process may not be fully understood.

In comparison to samples collected before infiltration, all samples collected after the experiments show increases in the relative abundance of denitrifiers and concomitant decreases in the total number of unique OTUs (Figure 2- 9). For samples collected after the flow experiments within in each treatment, the PRB showed the lowest number of unique OTUs identified and the highest relative abundance of denitrifiers.

The *WC* PRB showed the lowest number of unique OTUs identified, only 42 compared to an average of 355 from before the experiments. The two most abundant families in the *WC* PRB were *Spingomonadaceae* (28.7%) and *Comamonadaceae* (12.5%). Within *Spingomonadaceae*, the most abundant genera were *Sphingobium* (21.0%), *Novospingobium* (4.2%) and *Sphingomonas* (3.2%); species within each are capable of nitrate reduction and degradation of complex organic molecules (Glaeser and Kampfer, 2014). Within the family *Comamonadaceae*, the genera *Limnohabitans* (5.8%) and *Methylibium* (3.2%) were the most abundant; both genera contain facultative organotrophs that could play important roles in breaking down wood-

derived carbon (Hahn et al., 2010; Nakatsu et al., 2006). Within the *MIX* PRB, the most common denitrifying families were *Comamonadaceae* (12.8%), *Rhodocyclaceae* (6.5%), *Rhodobacteraceae* (5.9%), *Methylophilaceae* (5.2%), and *Spingomonadaceae* (5.0%), accounting in aggregate for 35.4% of the total sequences. The *NS* PRB showed more overall diversity than the other PRBs, with *Rhodospirillaceae* (7.5%), *Oxalobacteraceae* (5.8%), *Comamonadaceae* (5.4%), and *Spingomonadaceae* (4.8%) being the most common denitrifiers.

In the soil below each PRB, microbial communities were more diverse than their respective PRB materials, and showed large changes compared to soil collected from the same depths before the experiments (Figure 2-S7). At all depths for all treatments there was an increase in the *Rhodocyclaceae* family ($p < 0.01$ for all depths except *WC* 10 cm where $p < 0.05$), most of which can be attributed to the genera *Dechloromonas, Zoogloea, Azoarcus* and to a lesser extent *Methyloversatilis* and *Propionivibrio*. *Dechloromonas, Zoogloea,* and *Azoarcus* have been identified as acetate and methanol metabolizers important in denitrification of wastewater treatment (Ginige et al., 2005; Hagman et al., 2008). Significant increases in the *Comamonadaceae* family were identified at 30 and 50 cm below the *MIX* and *WC* PRBs ($p < 0.01$ for all depths except *MIX* 50 cm where $p < 0.05$), but not below the *NS* PRB. Members of the *Comamonadaceae* family were also enriched in studies of enhanced denitrification in nitrate impacted aquifer sediments (Calderer et al., 2014).

2.4 Discussion

2.4.1 Both PRB materials enhance denitrification

The two carbon-rich PRB treatments (*WC* and *MIX*) enhanced denitrification compared to the native soil treatment in both soils. There appears to be little systematic difference in denitrification when comparing a PRB made of woodchips and one made of a 50:50 mixture of woodchips and native soil. While effluent [DOC] values were consistently higher in the *WC* treatment than in the *MIX* treatment, nitrate removal at high infiltration rates appeared to be limited by hydraulic retention time and not [DOC], as the two treatments showed similar nitrate removal within each soil (Figure 2-3 and 2-7E-F). At lower infiltration rates, where hydraulic retention time was not limiting, both *WC* and *MIX* showed effluent [DOC] ≥ 4.2 mg/L, concentrations in excess of the required carbon for complete consumption of initial nitrate, assuming a 5:4 stoichiometric C:N ratio of consumption (Korom, 1992). Thus, both materials released sufficient carbon to consume the available nitrate.

Interestingly, for all treatments, Soil B showed higher ΔN_L values than Soil A at similar infiltration rates, up to ~1 m/day (Figure 2-4). Soil B had a higher initial soil carbon content (Figure 2-1), and perhaps the "native" soil carbon influenced the maximum amount and rate of nitrate removal between different soils. This could have resulted from the molecular makeup and bioavailability of the carbon, or perhaps associated differences in native soil microbial ecology. Additionally, Soil B had a larger average grain size and a greater fraction of sand, which could contribute to greater biofilm production and function (Perujo et al., 2017). Finally, experiments on

Soil A were started on infiltration day 20, due to leakage issues, whereas Soil B experiments were started on infiltration day 10. This may have resulted in a higher fraction of the soluble carbon leaching off the woodchips in Soil A before the experiments began.

While the geochemical results show little difference between *WC* and *MIX* treatments, microbiological analysis shows that changes in the community structure in the *WC* treatment were more extreme than that for the *MIX* treatment (Figure 2-8 and 2-9). The *WC* PRB and the soil directly below were marked by a lack of microbial diversity compared to that from the *MIX* treatment. However, deeper in the soil (30 and 50 cm), the diversity beneath the *WC* and *MIX* PRBs were comparable. These differences in microbial community structure appeared to have little to no effect on the nitrate removal as the *WC* and *MIX* treatments showed comparable depth-resolved nitrate removal (Figure 2-5). The *MIX* PRB and soil showed higher relative abundances of the family *Rhodobacteraceae*, whereas the *WC* PRB and soil showed higher relative abundances of the family *Sphingomonaceae*. Both families contain carbon degraders and groups with the ability to carry out key steps in the denitrification pathway. The differential abundances between the treatments are striking and additional work is underway to resolve genomic relations. The similar geochemical response coupled with differences in microbial community structure between *WC* and *MIX* treatments may not be surprising, as many diverse groups of microbes are capable of carrying out carbon degradation and denitrification. A PRB comprised of pure woodchips may be a more extreme and selective environment than that within native soils used for the 50:50

mixture PRB, and this could result in fewer groups of microorganisms thriving and becoming relatively more abundant.

2.4.2 Integrated controls on denitrification during infiltration

The incoming load of nitrate exhibits primary control on denitrification during infiltration for a given soil and treatment. The fraction of nitrate removed decreases exponentially with increasing initial nitrate load (Figure 2-7E). This is consistent with the expectation that higher infiltration rates lead to deeper penetration of oxygen and thus less favorable conditions for denitrification (e.g., Greenan et al., 2009; Lepine et al., 2016). In the initial flow through experiments, the influent nitrate concentration was held constant, making differences in the incoming nitrate load dependent entirely on the infiltration rate (Figure 2-4A-C). In the later experiments in which the influent nitrate concentration was varied and different infiltration rates were tested, the initial nitrate load was a function of both variables, but a similar pattern emerged (Figure 2-7E). This suggests that, under some conditions, nitrate load may be a fundamental controlling factor, rather than concentration or infiltration rate *per se*.

The nitrate load reduction (ΔN_L) in the *NS* treatments exhibited a decreasing, monotonic trend as a function of the initial nitrate load (Figure 2- 4D and 7F). However, ΔN_L for the carbon amended treatments, *WC* and *MIX*, showed a more complicated pattern, with maximum values at intermediate initial nitrate loads (Figure 2-4E-F and 2-7F). This may be a function of the carrying capacity of the denitrifying microbial community within the PRB and underlying soils. At low infiltration rates, load reduction is limited by the delivery of nitrate, whereas at high infiltration rates it is

limited by hydraulic retention time. As such, higher infiltration rates result in the breakthrough of more unprocessed nitrate, leading to lower ΔN_L. As a consequence, for these tests and associated experimental configurations, the peak in load reduction occurs with input of ~5 g-N/m^2/day (Figure 2- 7F).

The addition of a carbon-rich PRB stimulates denitrification by creating favorable conditions within the PRB that are subsequently translated into the underlying soil. The addition of carbon leads to quantitative shifts in the microbial community structure, including a reduction of microbial diversity and an increase in groups known to degrade carbon and/or metabolize nitrate. The enriched microbial taxa in these studies are a combination of some taxa that were detected in the soil before the experiments and some that were not, perhaps because they were below detection limits. In addition to providing organic carbon for metabolic processes, the woodchips may also provide habitat and substrate for microbial communities to colonize and for the growth and formation of biofilms, which have been linked to denitrification in wastewater bioreactors (Chu and Wang, 2013).

2.4.3 Implications for MAR design and field operations

These results demonstrate the complexity in assessing the performance and water quality benefits that accrue during infiltration for MAR. Benefit can be measured by nutrient load reduction (ΔN_L), lowering of nutrient concentrations ($\Delta[NO_3\text{-}N]$), and/or the rate of nutrient removal (R_N), and each metric has a unique relationship with infiltration rate in the presence or absence of a PRB. Based on results from the present study, there does not appear to be a universal optimum where all metrics are maximized

(e.g., low infiltration rates lead to large reductions in nutrient concentrations, but low load reduction), as has been proposed in other settings (e.g., Lepine et al., 2016). This suggests that designing and operating MAR systems to improve water quality will require making a choice of metrics and benefits to prioritize.

The addition of a PRB does not fundamentally change these considerations, but it does allow for a greater range in infiltration rates to deliver water quality benefits and increase the extent of benefits achieved with native soils, thus making operational considerations less restrictive and potentially improving the ability of MAR systems to achieve multiple goals. Soils whose infiltration rate is too high to improve water quality (>~1m/day) in native soil could potentially deliver quantitative supply and quality benefits if a PRB were installed.

The determination that *WC* and *MIX* treatments produced similar patterns of nitrate removal has significant implications for MAR operations. First, half of the carbon amendment produced the same water quality benefit, which could have significant cost and time implications for installation in large basins or fields. Second, the installation of a pure PRB layer within an infiltration basin or an active agricultural field or other open space is difficult to maintain due to the fragility of such a layer and the buoyancy of many carbon sources. Mixing a PRB material into the shallow subsurface of an infiltration basin or field (by disking, tilling, or other methods) presents easier management over the long term, more readily allowing removal of fine sediments that are deposited as inflowing waters slow and drop their suspended load (Beganskas and Fisher, 2017; Racz et al., 2012). New results suggest that, at high

infiltration rates, nitrate removal was limited mainly by short hydraulic retention times. For a given infiltration rate, the hydraulic retention time within the PRB could be increased by increasing the thickness of the PRB layer, simply mixing the same amount of material deeper into the native soil. As we learn more about linked hydrologic, biogeochemical, and microbial processes that occur during infiltration for MAR, we are likely to find additional opportunities to design and operate these systems for more extensive and diverse benefits.

2.5 Conclusions

Laboratory flow-through experiments that were tightly coupled to field conditions demonstrated that the addition of a carbon-rich permeable reactive barrier made of woodchips or a mixture of woodchips and soil increased the nitrate concentration reduction, nitrate mass removal, and denitrification rate both within the carbon-rich layer and within the underlying soil. Infiltration rate, and more precisely, the incoming load of nitrate, exhibits a primary control on the amount of nitrate removed during infiltration. We found no evidence for a systematic difference between a layer of pure woodchips and a layer of 50:50 woodchips and soil in terms of nitrogen cycling during infiltration. Both carbon-rich layers had a profound impact on the microbial community structure of the soil below the layer. The changes in community structure were more extreme in the case of the pure woodchips compared to the 50:50 mixture of woodchips and soil. For both materials, the changes could be broadly characterized as a reduction in microbial diversity and an increase in the abundance of groups capable of degrading

carbon and metabolizing nitrogen.

These results highlight the coupled hydrologic and geochemical controls on denitrification and demonstrate that water quality benefits can be achieved across a wider range of infiltration rates by adding a carbon-rich amendment to soils used for infiltration during managed aquifer recharge. This means water quantity and quality can be improved in a wider range of settings.

ACKNOWLEDGEMENTS

The authors thank Paige Borges, Molly Cribari, Sarah Faraola, Jennifer Pensky, Araceli Serrano, and Walker Weir for their help with laboratory and field sampling efforts. We would also like to thank Kelli Camara and Brian Lockwood for their guidance and cooperation on with field work, and project land-owners for permission to access sites and collet cores and other samples.

FUNDING

This work was supported by the Gordon and Betty Moore Foundation (Grant GBMF5595), UC Water Security and Sustainability Research Initiative (UCOP Grant #13941), the USDA/NIFA (Award #2017-67026-26315), the Water Foundation (Award #10069), the National Science Foundation Graduate Research Fellowship Program, and the Recharge Initiative (http://www.rechargeinitiative.org/).

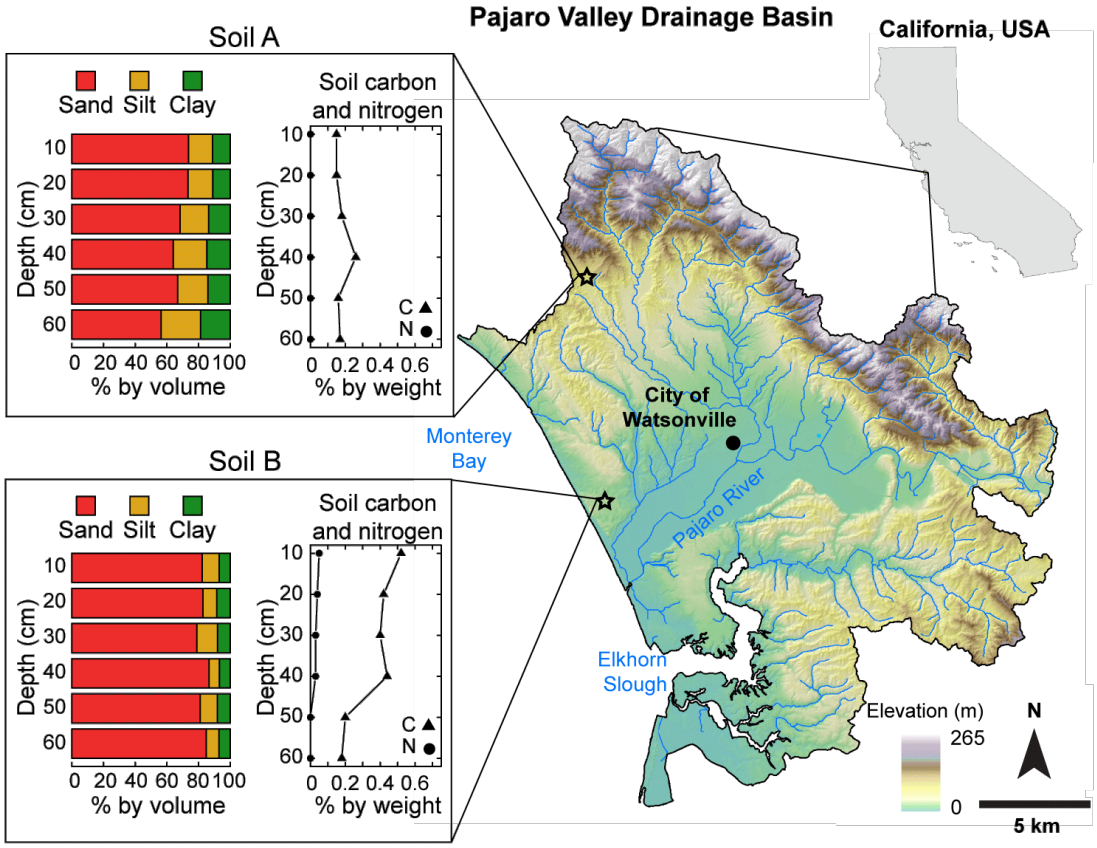

Figure 2-1 Map of site locations where soil columns were collected Insets show the grain size distribution and soil carbon and nitrogen for each site as a function of depth.

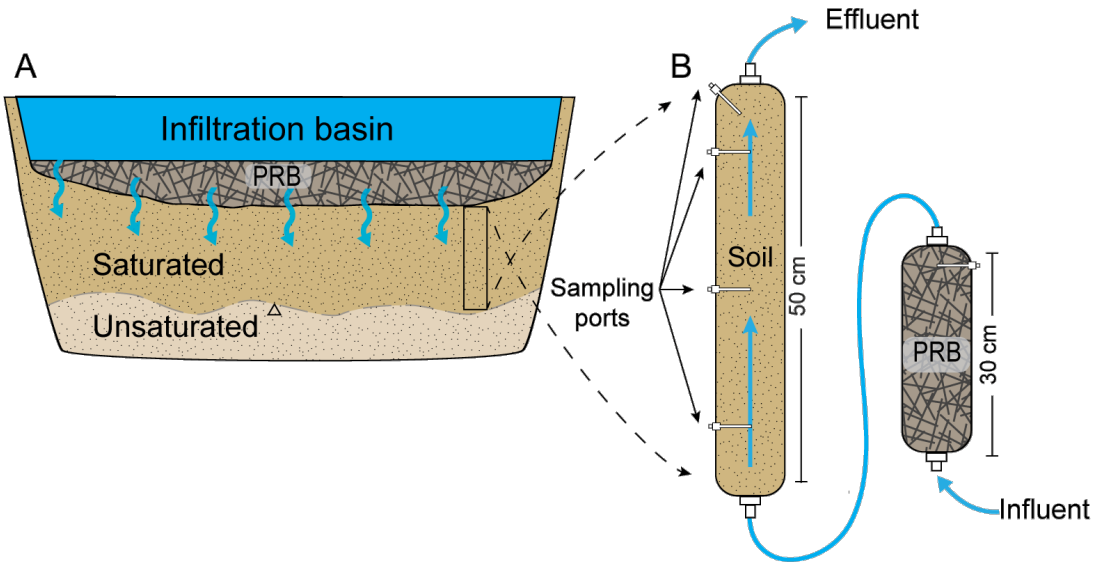

Figure 2-2 Experimental configuration Columns were constructed as direct analogs to sediments from the saturated zone beneath an infiltration basin during MAR operation (A), but they were collected from beside the infiltration basins so as not to disturb operations. The columns were inverted, and flow was in an upward direction (B) and the PRB capsule was filled with woodchips (*WC*), a 50:50 mixture of native soil and woodchips (*MIX*) or native soil (*NS*).

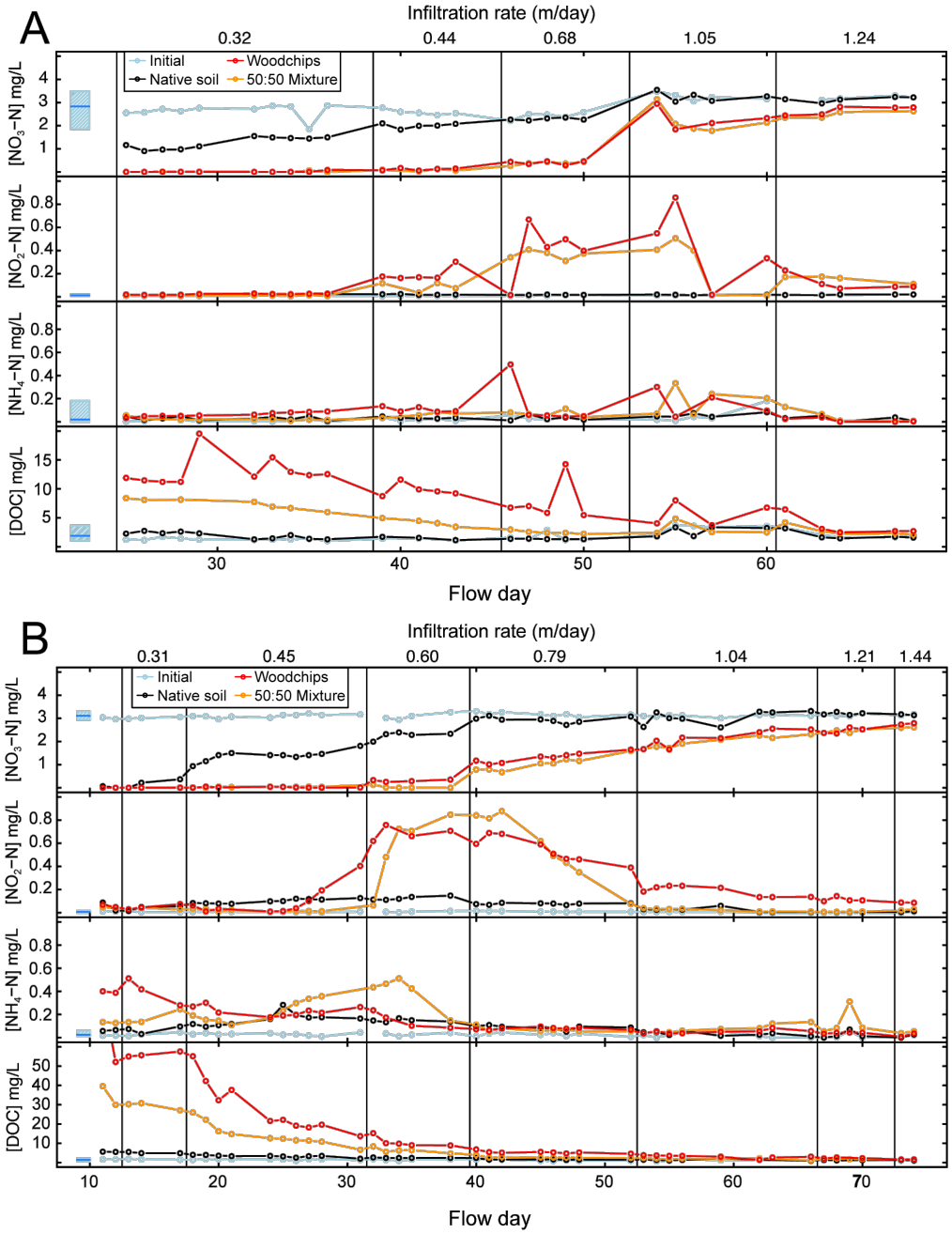

Figure 2-3 N-species and DOC influent and effluent Soil A (A) and Soil B (B) [NO_3-N], [NO_2-N], [NH_4-N], and [DOC] for 3 different soil treatments. The light blue rectangles indicate the range and mean (solid line) of the initial concentration of the influent water before introduction into the columns. Black, yellow, and red indicate the effluent concentrations for *NS*, *MIX*, and *WC*, respectively. Plots are divided by vertical lines that delineate analysis periods for different infiltration rates, which are tabulated above each section. Infiltration rate standard deviation within each flow period were always ≤10% (Supporting Information Table 2-S4).

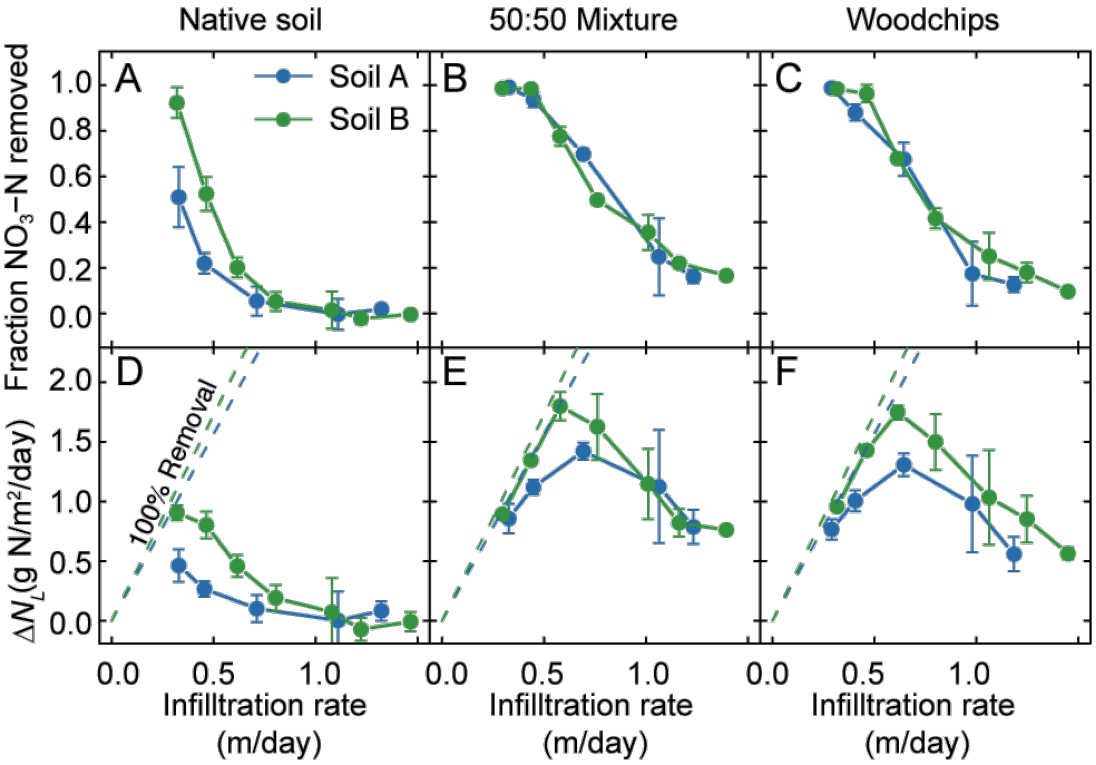

Figure 2-4 Results averaged by flow period Fraction of NO_3-N removed in *NS* (A), *MIX* (B), and *WC* (C) treatments and nitrogen mass removal ΔN_L in *NS* (D), *MIX* (E), and *WC* (F) treatments across a range of infiltration rates relevant to MAR for two soils. Both were measured as net changes between the influent and the effluent fluid from the columns. 100% removal is shown for reference in D and F.

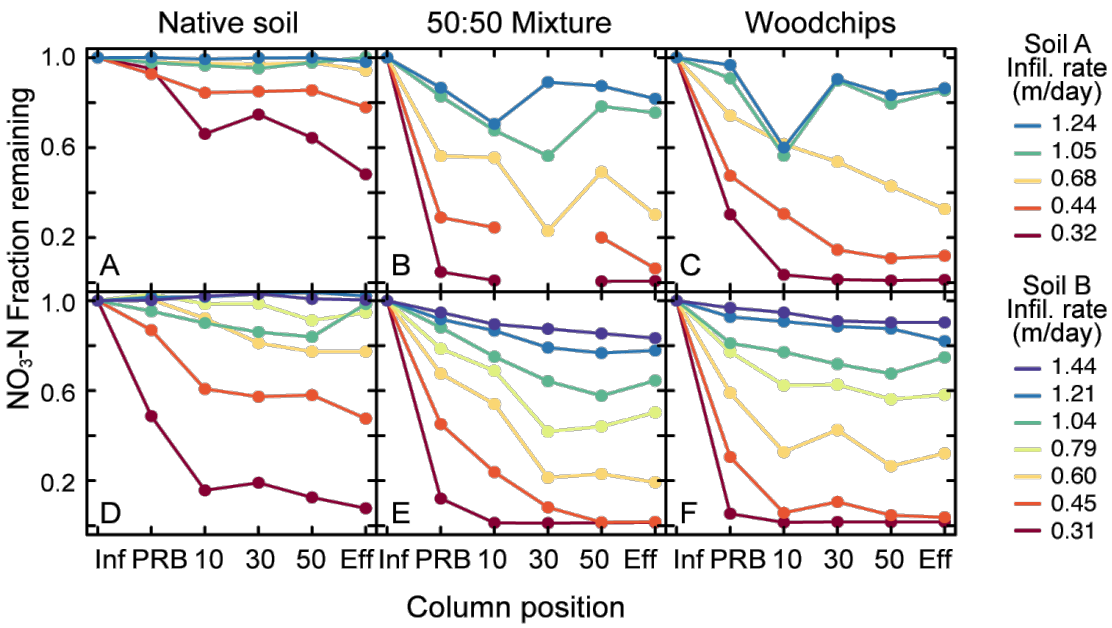

Figure 2-5 Nitrogen removal by depth Fraction of NO_3-N remaining along the length of the columns for Soil A (A-C) and Soil B (D-F) coded for each flow period by color. Fraction of NO_3-N is calculated as [NO_3-N] at each sampling point divided by initial [NO_3-N]. Column positions are Influent, PRB, 10 cm, 30 cm, 50 cm, and Effluent along the fluid flow path, as water flows from left to right, schematically.

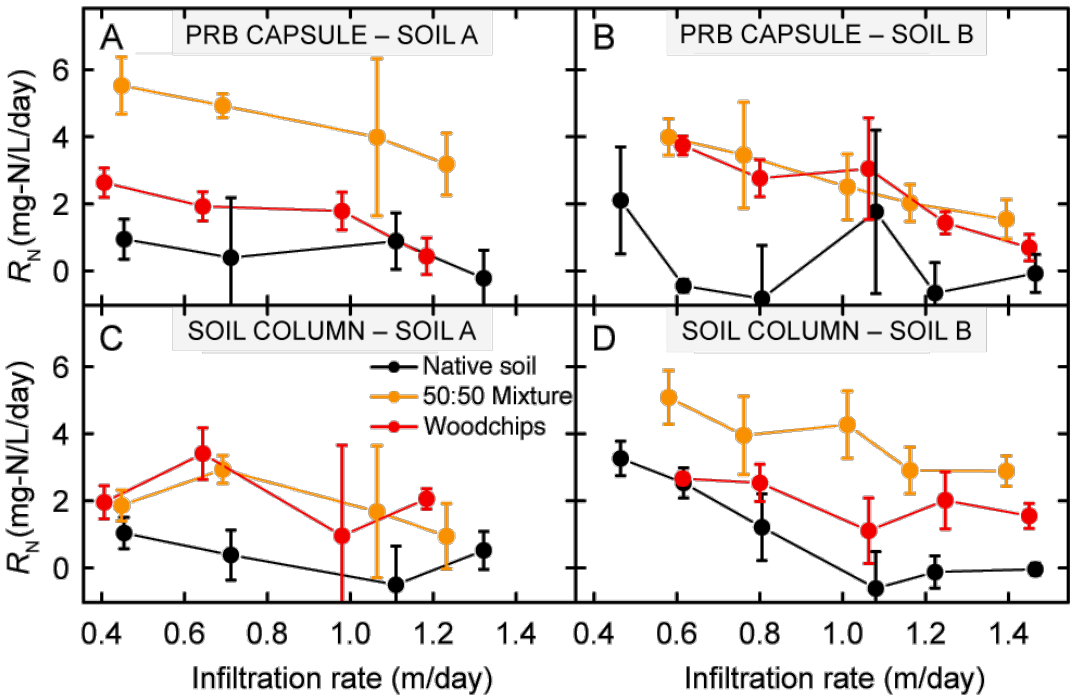

Figure 2-6 Zero-order NO_3-N removal rates (R_N) reported in mg-N/L/day calculated separately for the PRB capsule (A and B) and the soil column (C and D) across a range of infiltration rates in which [NO_3-N] were not limiting. Rates are shown for Soil A (A and C) and Soil B (B and D) for each treatment. Error bars represent one standard deviation during each flow period.

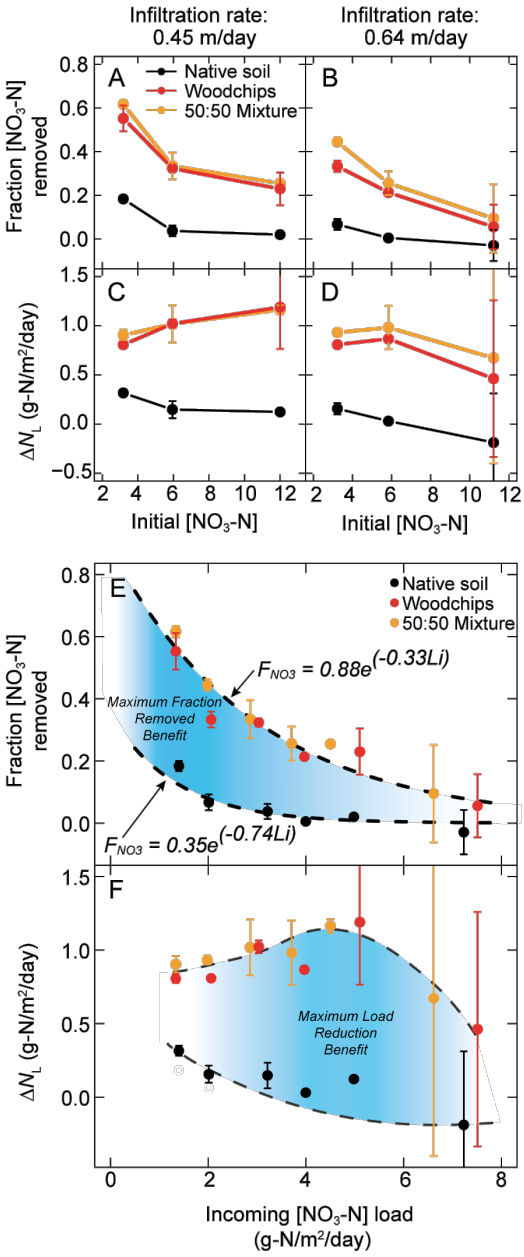

Figure 2-7 Variable initial nitrate concentration Experiments done on Soil B to determine the effect of varying the initial nitrate concentration on the fraction of [NO_3-N] removed (A and B), and ΔN_L (B and C) at two flow rates (0.45 m/day, A and C and 0.65 m/day, B and D). E shows the fraction of initial [NO_3-N] removed and F shows the change in ΔN_L as a function of the incoming load in g-N/m^2/day for each different soil treatment. Curves were developed by varying infiltration rate (0.45 and 0.65 m/day) and initial [NO_3-N] (3.2, 5.9, and 11.6 mg/L). Dashed lines in E show exponential fits with fitted constants shown, where F_{NO3} is the fraction of NO_3-N removed and Li is the incoming nitrate load. Dashed lines in F are schematic.

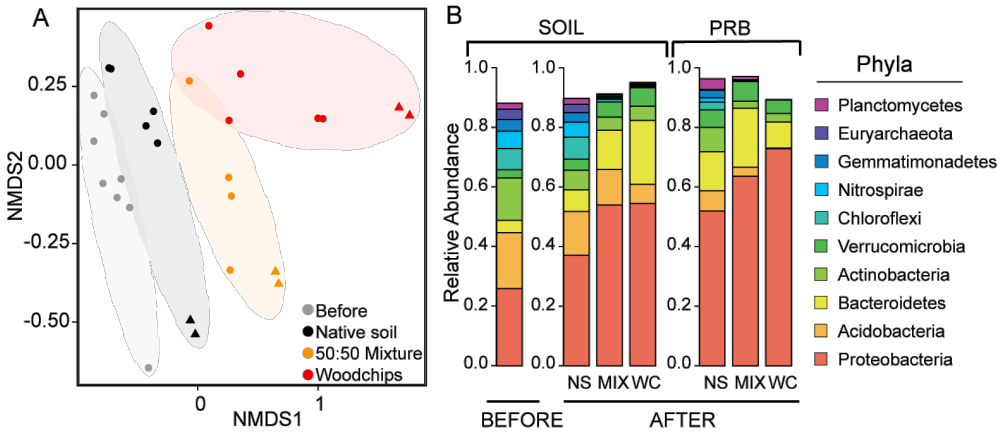

Figure 2-8 Microbial communities' response to PRB materials A) NMDS of 16S rRNA shows grouping of soil samples collected after each treatment from Soil B (coded by color). PRB samples (triangles) show the greatest differences, while soil samples (circles) cluster closer together, highlighted by shaded areas which are schematic. B) Proportions of the ten most abundant phyla averaged by depth within each treatment, these phyla comprise ≥88% of the total sequences. The largest changes were seen in the Proteobacteria and Bacteriodetes phyla.

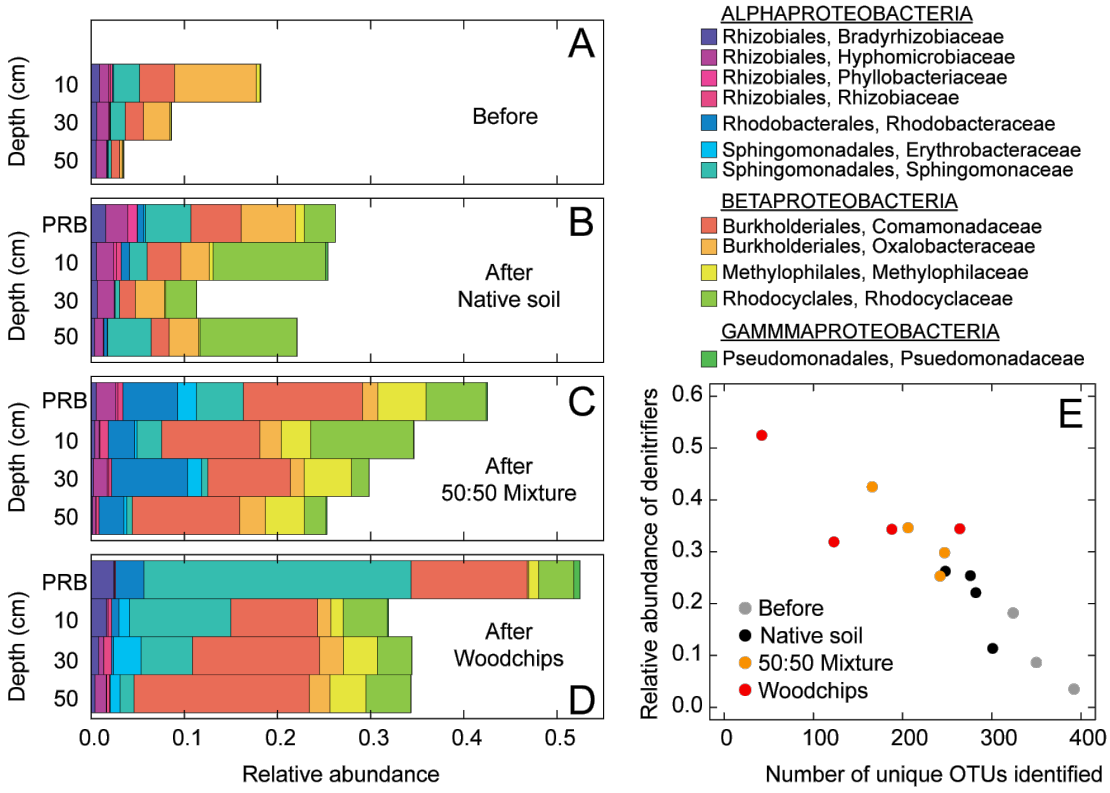

Figure 2-9 Changes in denitrifying community structure Relative abundance of families capable of carrying out key steps in the denitrification process averaged by depth for samples collected before experiments (A), and after *NS* (B), *MIX* (C), and *WC* (D). Panel E shows the relationship between the number of unique OTUs identified and the relative abundance of denitrifiers grouped by treatment, where each point represents an individual soil or PRB sample.

References

Addy, K., Gold, A.J., Christianson, L.E., David, M.B., Schipper, L.A., Ratigan, N.A., 2016. Denitrifying Bioreactors for Nitrate Removal: A Meta-Analysis. J. Environ. Qual. 45, 873. https://doi.org/10.2134/jeq2015.07.0399

Beganskas, S., Fisher, A.T., 2017. Coupling distributed stormwater collection and managed aquifer recharge: Field application and implications. J. Environ. Manage. 200, 366–379. https://doi.org/10.1016/j.jenvman.2017.05.058

Beganskas, S., Gorski, G., Weathers, T., Fisher, A.T., Schmidt, C., Saltikov, C., Redford, K., Stoneburner, B., Harmon, R., Weir, W., 2018. A horizontal permeable reactive barrier stimulates nitrate removal and shifts microbial ecology during rapid infiltration for managed recharge. Water Res. 144, 274–284. https://doi.org/10.1016/j.watres.2018.07.039

Bekele, E., Toze, S., Patterson, B., Higginson, S., 2011. Managed aquifer recharge of treated wastewater: Water quality changes resulting from infiltration through the vadose zone. Water Res. 45, 5764–5772. https://doi.org/10.1016/j.watres.2011.08.058

Bernard, R.J., Mortazavi, B., Kleinhuizen, A.A., Biogeochemistry, S., August, N., Bernard, R.J., Mortazavi, B., 2015. Dissimilatory nitrate reduction to ammonium (DNR) seasonally dominates N03 reduction pathways in an anthropogenically impacted sub-tropical coastal lagoon. Biogeochemistry 125, 47–64. https://doi.org/10.1007/s

Bertelkamp, C., Verliefde, A.R.D., Schoutteten, K., Vanhaecke, L., Bussche, J.

Vanden, Singhal, N., Hoek, J.P. Van Der, 2016. Science of the Total Environment The effect of redox conditions and adaptation time on organic micropollutant removal during river bank fi ltration : A laboratory-scale column study. Sci. Total Environ. 544, 309–318. https://doi.org/10.1016/j.scitotenv.2015.11.035

Betlach, M.R., Tiedje, J.M., 1981. Kinetic explanation for accumulation of nitrite, nitric oxide, and nitrous oxide during bacterial denitrification. Appl. Environ. Microbiol. 42, 1074–1084. https://doi.org/Article

Bouwer, H., 2002. Artificial recharge of groundwater: Hydrogeology and engineering. Hydrogeol. J. 10, 121–142. https://doi.org/10.1007/s10040-001-0182-4

Briggs, M.A., Day-Lewis, F.D., Zarnetske, J.P., Harvey, J.W., 2015. A physical explanation for the development of redox microzones in hyporheic flow. Geophys. Res. Lett. 42, 4402–4410. https://doi.org/10.1002/2015GL064200

Burri, N.M., Weatherl, R., Moeck, C., Schirmer, M., 2019. A review of threats to groundwater quality in the anthropocene. Sci. Total Environ. 684, 136–154. https://doi.org/10.1016/j.scitotenv.2019.05.236

Calderer, M., Martí, V., Pablo, J. De, Guivernau, M., Prenafeta-boldú, F.X., Viñas, M., 2014. Effects of enhanced denitrification on hydrodynamics and microbial community structure in a soil column system. Chemosphere 111, 112–119. https://doi.org/10.1016/j.chemosphere.2014.03.033

Callahan, B.J., Mcmurdie, P.J., Rosen, M.J., Han, A.W., A, A.J., 2016. DADA2:

High resolution sample inference from Illumina amplicon data. Nat Methods 13, 581–583. https://doi.org/10.1038/nmeth.3869.DADA2

Carrey, R., Otero, N., Soler, A., Gómez-Alday, J.J., Ayora, C., 2013. The role of Lower Cretaceous sediments in groundwater nitrate attenuation in central Spain: Column experiments. Appl. Geochemistry 32, 142–152. https://doi.org/10.1016/j.apgeochem.2012.10.009

Christianson, L.E., Lepine, C., Sibrell, P.L., Penn, C., Summerfelt, S.T., 2017. Denitrifying woodchip bioreactor and phosphorus filter pairing to minimize pollution swapping. Water Res. 121, 129–139. https://doi.org/10.1016/j.watres.2017.05.026

Chu, L., Wang, J., 2013. Chemosph ere Denitrification performance and biofilm characteristics using biodegradable polymers PCL as carriers and carbon source. Chemosphere 91, 1310–1316. https://doi.org/10.1016/j.chemosphere.2013.02.064

DeSantis, T.Z., Hugenholtz, P., Larsen, N., Rojas, M., Brodie, E.L., Keller, K., Huber, T., Dalevi, D., Hugenholtz, P., Dalevi, D., Hu, P., Andersen, G.L., 2006. Greengenes, a Chimera-Checked 16S rRNA Gene Database and Workbench Compatible with ARB. Appl. Environ. Microbiol. 72, 5069–5072. https://doi.org/10.1128/aem.03006-05

Ganot, Y., Holtzman, R., Weisbrod, N., Russak, A., Katz, Y., Kurtzman, D., 2018. Geochemical Processes During Managed Aquifer Recharge With Desalinated Seawater. Water Resour. Res. 54, 978–994.

https://doi.org/10.1002/2017WR021798

Ghane, E., Fausey, N.R., Brown, L.C., 2015. Modeling nitrate removal in a denitrification bed. Water Res. 71, 294–305. https://doi.org/10.1016/j.watres.2014.10.039

Ginige, M.P., Keller, J., Blackall, L.L., 2005. Investigation of an acetate-fed denitrifying microbial community by stable isotope probing, full-cycle rRNA analysis, and fluorescent in situ hybridization-microautoradiography. Appl. Environ. Microbiol. 71, 8683–8691. https://doi.org/10.1128/AEM.71.12.8683-8691.2005

Glaeser, S.P., Kampfer, P., 2014. The Family Sphingomonadaceae, in: Rosenberg, E., DeLong, E.F., Lory, S., Stackebrandt, E., Thompson, F. (Eds.), The Prokaryotes: Alphaproteobacteria and Betaproteobacteria. Springer, pp. 641–707. https://doi.org/10.1007/978-3-642-30197-1

Gorski, G., Fisher, A.T., Beganskas, S., Weir, W., Redford, K., Schmidt, C., Saltikov, C., 2019. Field and laboratory studies linking hydrologic, geochemical, and microbiological processes and enhanced denitrification during infiltration for managed recharge. Environ. Sci. Technol. 53, acs.est.9b01191. https://doi.org/10.1021/acs.est.9b01191

Grau-Martínez, A., Folch, A., Torrentó, C., Valhondo, C., Barba, C., Domènech, C., Soler, A., Otero, N., 2018. Monitoring induced denitrification during managed aquifer recharge in an infiltration pond. J. Hydrol. 561, 123–135. https://doi.org/10.1016/j.jhydrol.2018.03.044

Greenan, C.M., Moorman, T.B., Parkin, T.B., Kaspar, T.C., Jaynes, D.B., 2009. Denitrification in wood chip bioreactors at different water flows. J. Environ. Qual. 38, 1664–1671. https://doi.org/10.2134/jeq2008.0413

Hagman, M., Nielsen, J.L., Nielsen, P.H., Jansen, J.C., 2008. Mixed carbon sources for nitrate reduction in activated sludge-identification of bacteria and process activity studies. Water Res. 42, 1539–1546. https://doi.org/10.1016/j.watres.2007.10.034

Hahn, M.W., Kasalický, V., Jezbera, J., Brandt, U., Šimek, K., 2010. Limnohabitans australis sp. nov., isolated from a freshwater pond, and emended description of the genus Limnohabitans. Int. J. Syst. Evol. Microbiol. 60, 2946–2950. https://doi.org/10.1099/ijs.0.022384-0

Halaburka, B.J., Lefevre, G.H., Luthy, R.G., 2017. Evaluation of Mechanistic Models for Nitrate Removal in Woodchip Bioreactors. Environ. Sci. Technol. 51, 5156–5164. https://doi.org/10.1021/acs.est.7b01025

Hampton, T.B., Zarnetske, J.P., Briggs, M.A., Singha, K., Harvey, J.W., Day-Lewis, F.D., MahmoodPoor Dehkordy, F., Lane, J.W., 2019. Residence Time Controls on the Fate of Nitrogen in Flow-Through Lakebed Sediments. J. Geophys. Res. Biogeosciences 124, 689–707. https://doi.org/10.1029/2018JG004741

Hua, G., Salo, M.W., Schmit, C.G., Hay, C.H., 2016. Nitrate and phosphate removal from agricultural subsurface drainage using laboratory woodchip bioreactors and recycled steel byproduct fi lters. Water Res. 102, 180–189. https://doi.org/10.1016/j.watres.2016.06.022

Korom, S.F., 1992. Natural denitrification in the saturated zone: A review. Water Resour. Res. 28, 1657–1668. https://doi.org/10.1029/92WR00252

Laverman, A.M., Pallud, C., Abell, J., Cappellen, P. Van, 2012. Comparative survey of potential nitrate and sulfate reduction rates in aquatic sediments. Geochim. Cosmochim. Acta 77, 474–488. https://doi.org/10.1016/j.gca.2011.10.033

Lepine, C., Christianson, L., Sharrer, K., Summerfelt, S., 2016. Optimizing Hydraulic Retention Times in Denitrifying Woodchip Bioreactors Treating Recirculating Aquaculture System Wastewater 813–821. https://doi.org/10.2134/jeq2015.05.0242

Li, D., Sharp, J.O., Saikaly, P.E., Ali, S., Alidina, M., Alarawi, M.S., Keller, S., 2012. Composition and Diversity in Managed Aquifer Recharge Systems. Appl. Environ. Microbiol. 78, 6819–6828. https://doi.org/10.1128/AEM.01223-12

McClain, M.E., Boyer, E.W., Dent, C.L., Gergel, S.E., Grimm, N.B., Groffman, P.M., Hart, S.C., Harvey, J.W., Johnston, C. a., Mayorga, E., McDowell, W.H., Pinay, G., 2003. Biogeochemical Hot Spots and Hot Moments at the Interface of Terrestrial and Aquatic Ecosystems. Ecosystems 6, 301–312. https://doi.org/10.1007/s10021-003-0161-9

McMurdie, P.J., Holmes, S., 2013. Phyloseq: An R Package for Reproducible Interactive Analysis and Graphics of Microbiome Census Data. PLoS One 8. https://doi.org/10.1371/journal.pone.0061217

Nakatsu, C.H., Hristova, K., Hanada, S., Meng, X.Y., Hanson, J.R., Scow, K.M., Kamagata, Y., 2006. Methylibium petroleiphilum gen. nov., sp. nov., a novel

methyl tert-butyl ether-degrading methylotroph of the Betaproteobacteria. Int. J. Syst. Evol. Microbiol. 56, 983–989. https://doi.org/10.1099/ijs.0.63524-0

Nordström, A., Herbert, R.B., Herbert, R.B., 2017. Denitrification in a low-temperature bioreactor system at two different hydraulic residence times : laboratory column studies. Environ. Technol. 3330, 1362–1375. https://doi.org/10.1080/09593330.2016.1228699

NRCS, 2016. Iowa Amendment to the Engineering Field Handbook. NEH Part 650 Amendment IA68.

Page, D.W., Peeters, L., Vanderzalm, J., Barry, K., Gonzalez, D., 2017. Effect of aquifer storage and recovery (ASR) on recovered stormwater quality variability. Water Res. 117, 1–8. https://doi.org/10.1016/j.watres.2017.03.049

Park, S., Lee, W., 2018. Science of the Total Environment Removal of selected pharmaceuticals and personal care products in reclaimed water during simulated managed aquifer recharge. Sci. Total Environ. 640–641, 671–677. https://doi.org/10.1016/j.scitotenv.2018.05.221

Perujo, N., Sanchez-Vila, X., Proia, L., Romaní, A.M., 2017. Interaction between Physical Heterogeneity and Microbial Processes in Subsurface Sediments: A Laboratory-Scale Column Experiment. Environ. Sci. Technol. 51, 6110–6119. https://doi.org/10.1021/acs.est.6b06506

Racz, A.J., Fisher, A.T., Schmidt, C.M., Lockwood, B.S., Huertos, M.L., 2012. Spatial and Temporal Infiltration Dynamics During Managed Aquifer Recharge. Ground Water 50, 562–570. https://doi.org/10.1111/j.1745-6584.2011.00875.x

Ronen-eliraz, G., Russak, A., Nitzan, I., Guttman, J., Kurtzman, D., 2017. Investigating geochemical aspects of managed aquifer recharge by column experiments with alternating desalinated water and groundwater. Sci. Total Environ. 574, 1174–1181. https://doi.org/10.1016/j.scitotenv.2016.09.075

Schmidt, C.M., Fisher, A.T., Racz, A.J., Lockwood, B.S., Huertos, M.L., 2011. Linking denitrification and infiltration rates during managed groundwater recharge. Environ. Sci. Technol. 45, 9634–9640. https://doi.org/10.1021/es2023626

Seitzinger, S., Harrison, J.A., Böhlke, J.K., Bouwman, A.F., Lowrance, R., Peterson, B., Tobias, C., Drecht, G. Van, 2006. Denitrification Across Landscapes and Waterscapes: a Synthesis. Ecol. Appl. 16, 2064–2090.

Strous, M., Fuerst, J.A., Kramer, E.H.M., Logemann, S., Muyzer, G., van de Pas-Schoonen, K.T., Webb, R., Kuenen, J.G., Jetten, M.S.M., 1999. Missing lithotroph identified as new planctomycete 400.

Tzoraki, O., Dokou, Z., Christodoulou, G., Gaganis, P., Karatzas, G., 2018. Assessing the efficiency of a coastal Managed Aquifer Recharge (MAR) system in Cyprus. Sci. Total Environ. 626, 875–886. https://doi.org/10.1016/j.scitotenv.2018.01.160

USEPA, 2011. Drinking Water Contaminants: List of Contaminants & their MCLs. U.S. Environmental Protection Agency, Office of Water Program Operations.

Valhondo, C., Carrera, J., Ayora, C., Barbieri, M., Nodler, K., Licha, T., Huerta, M., 2014. Behavior of nine selected emerging trace organic contaminants in an

artificial recharge system supplemented with a reactive barrier. Environ. Sci. Pollut. Res. 2. https://doi.org/10.1007/s11356-014-2834-7

Valhondo, C., Carrera, J., Ayora, C., Tubau, I., Martinez-Landa, L., Nodler, K., Licha, T., 2015. Characterizing redox conditions and monitoring attenuation of selected pharmaceuticals during artificial recharge through a reactive layer. Sci. Total Environ. 512–513, 240–250. https://doi.org/10.1016/j.scitotenv.2015.01.030

Valhondo, C., Martinez-Landa, L., Carrera, J., Ayora, C., Nödler, K., Licha, T., 2018. Evaluation of EOC removal processes during artificial recharge through a reactive barrier. Sci. Total Environ. 612, 985–994. https://doi.org/10.1016/j.scitotenv.2017.08.054

van Drecht, G., Bouwman, A.F., Knoop, J.M., Beusen, A.H.W., Meinardi, C.R., 2003. Global modeling of the fate of nitrogen from point and nonpoint sources in soils, groundwater, and surface water. Glob. Biogeochem. Cycles 17, 1115. https://doi.org/10.1029/2003gb002060

van Driel, P.W., Robertson, W.D., Merkley, L.C., 2006. Denitrification Of Agricultural Drainage Using Wood-Based Reactors. Trans. ASABE 49, 565–574. https://doi.org/http://dx.doi.org/10.13031/2013.20391

Wang, F., van Halem, D., Ding, L., Bai, Y., Lekkerkerker-Teunissen, K., van der Hoek, J.P., 2018. Effective removal of bromate in nitrate-reducing anoxic zones during managed aquifer recharge for drinking water treatment: Laboratory-scale simulations. Water Res. 130, 88–97.

https://doi.org/10.1016/j.watres.2017.11.052

Wang, Q., Garrity, G.M., Tiedje, J.M., Cole, J.R., 2007. Naïve Bayesian classifier for rapid assignment of rRNA sequences into the new bacterial taxonomy. Appl. Environ. Microbiol. 73, 5261–5267. https://doi.org/10.1128/AEM.00062-07

Zhao, Y., Xia, Y., Kana, T.M., Wu, Y., Li, X., Yan, X., 2013. Seasonal variation and controlling factors of anaerobic ammonium oxidation in freshwater river sediments in the Taihu Lake region of China. Chemosphere 93, 2124–2131. https://doi.org/10.1016/j.chemosphere.2013.07.063

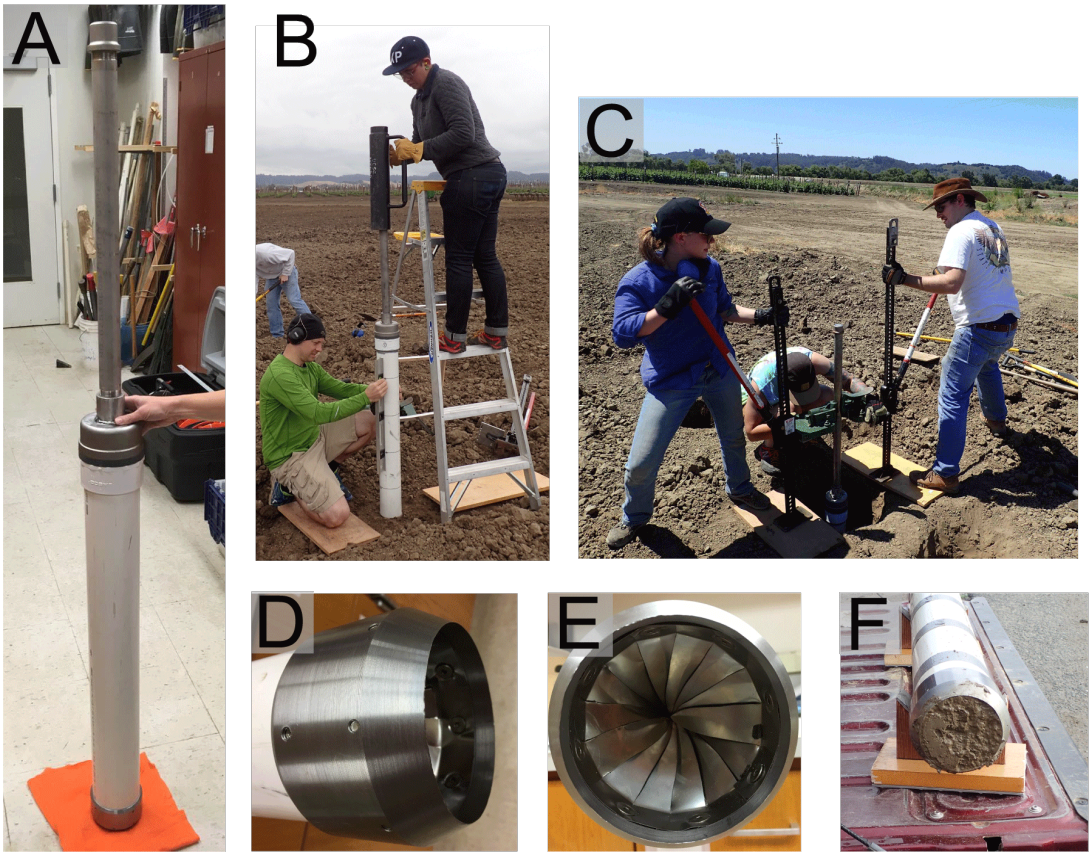

Figure 2-S1. Field collection of cores involved a custom-built coring device that used 10-cm inner diameter PVC as the coring tube (A). The coring device consisted of a drive shaft (A) and a coring shoe (D) fit with a core catcher (E) for securing the core during extraction. Cores were collected by driving the core into the ground using a slide hammer (B) and extracted using truck jacks and a pipe dog to hold the drive shaft (C). F shows an end on view of the coring shoe after core extraction.

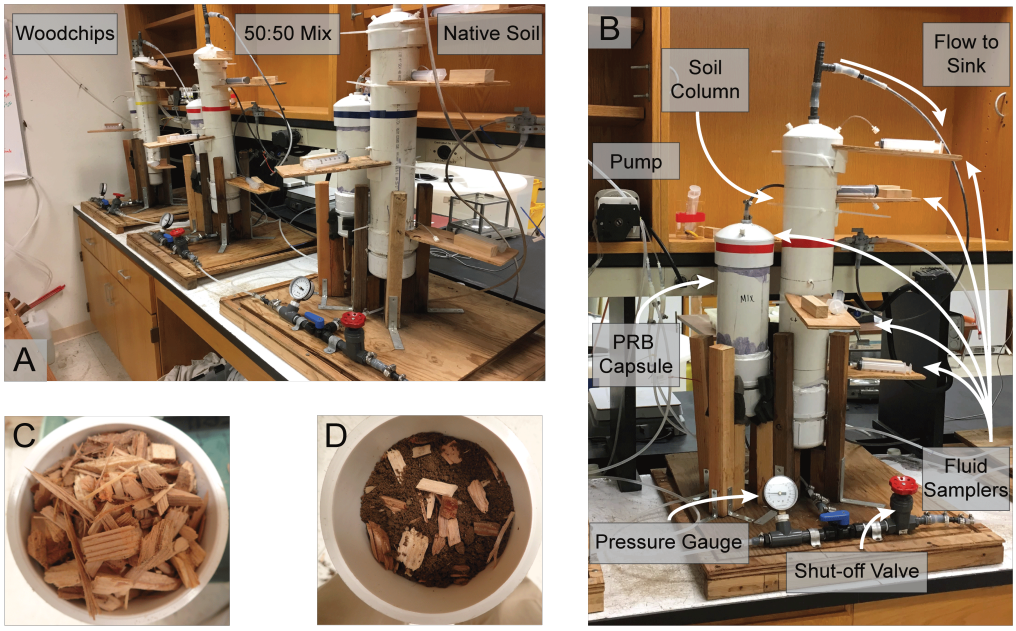

Figure 2-S2 Laboratory configuration For each soil, treatments were run in parallel (A), drawing influent water from the same reservoir. B shows the experimental operation for each treatment; water is drawn from the reservoir using a peristaltic pump, first through a manifold where pressure is monitored, then through the PRB capsule and finally through the soil column. Pore water samplers were installed along the length of the column and within the PRB capsule. *WC* and *MIX* PRB capsules are shown in C and D respectively, whereas the *NS* PRB capsule consisted of 100% native soil from each of the two sites.

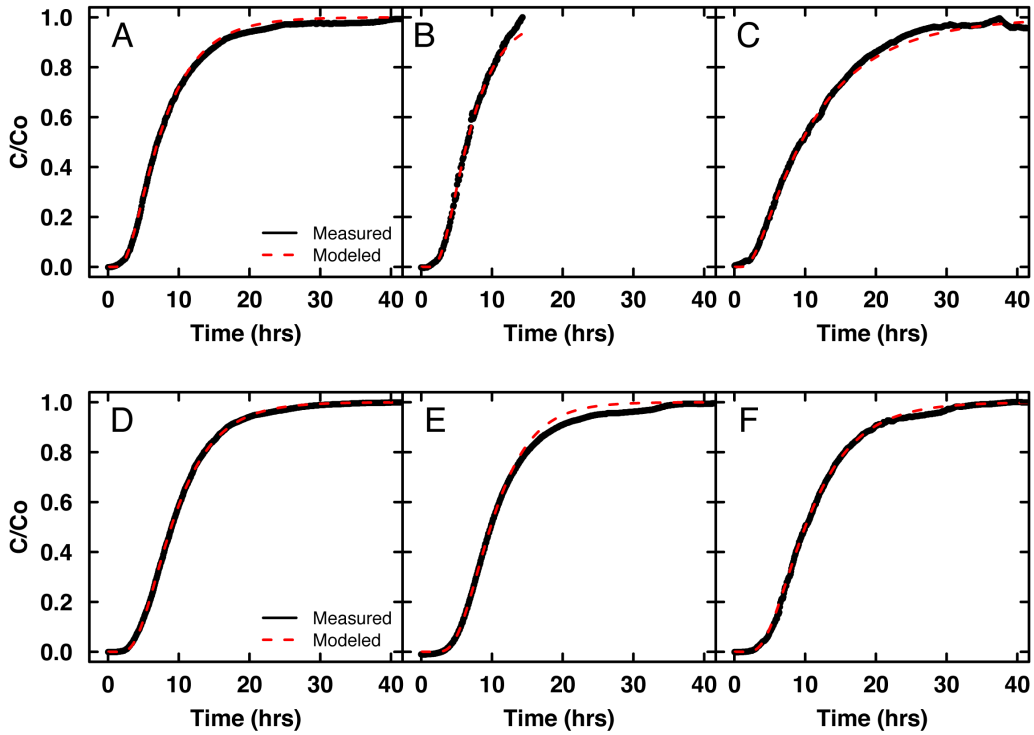

Figure 2-S3. **NaCl tracer breakthrough curves for column experiments** in Soil A (A, B, and C) and Soil B (D, E, and F) for *NS* (A and D), *MIX* (B and E) and *WC* (C and F). The ratio C/Co is a measure of the effluent electrical conductivity and the tracer solution normalized to the maximum electrical conductivity measured. The measured C/Co (black) was modeled (red) using a simplified solution of the advection-dispersion equation to determine the hydraulic properties of the columns (i.e. average linear velocity, longitudinal dispersion coefficient, and effective porosity). The tracer test for Soil A *MIX* (B) had to be terminated early due to tubing failure, however fitting procedure focused on the portion of the record surrounding C/Co = 0.5 so the record was determined to be adequate.

Table 2-S1 Hydraulic Properties determined by solute breakthrough curves

Soil	Treatment	Infiltration Rate (m/day)	V_L[a] (m/day)	n_e[c] -	a_L[b] (cm)	PV_e[d] (L)
A	NS	0.87	3.11	0.28	17	2.04
A	MIX	0.83	3.33	0.25	13	1.82
A	WC	0.74	2.29	0.32	27	2.36
Average A:				*0.28*	*19*	*2.07*
B	NS	0.69	2.42	0.29	12	2.08
B	MIX	0.64	2.20	0.29	9	2.12
B	WC	0.68	2.16	0.32	13	2.30
Average B				*0.30*	*7*	*2.17*

[a] linear velocity
[b] longitudinal dispersion
[c] effective porosity
[d] effective pore volume

Table 2-S2 16S DNA soil sample groupings and median read counts

Treatment Group	n	Depth (cm)	Median number of sequences
BEFORE	8	10*,20,30*,40,50*	106,683
AFTER-SOIL-NS	5	10*,30*,50	86,058
AFTER-PRB-NS	2	PRB*	59,912
AFTER-SOIL-MIX	5	10*,30*,50	116,078
AFTER-PRB-MIX	2	PRB*	127,240
AFTER-SOIL-RW	5	10*,30*,50	123,558
AFTER-PRB-RW	2	PRB*	94,139

*indicates that biological replicates were analyzed

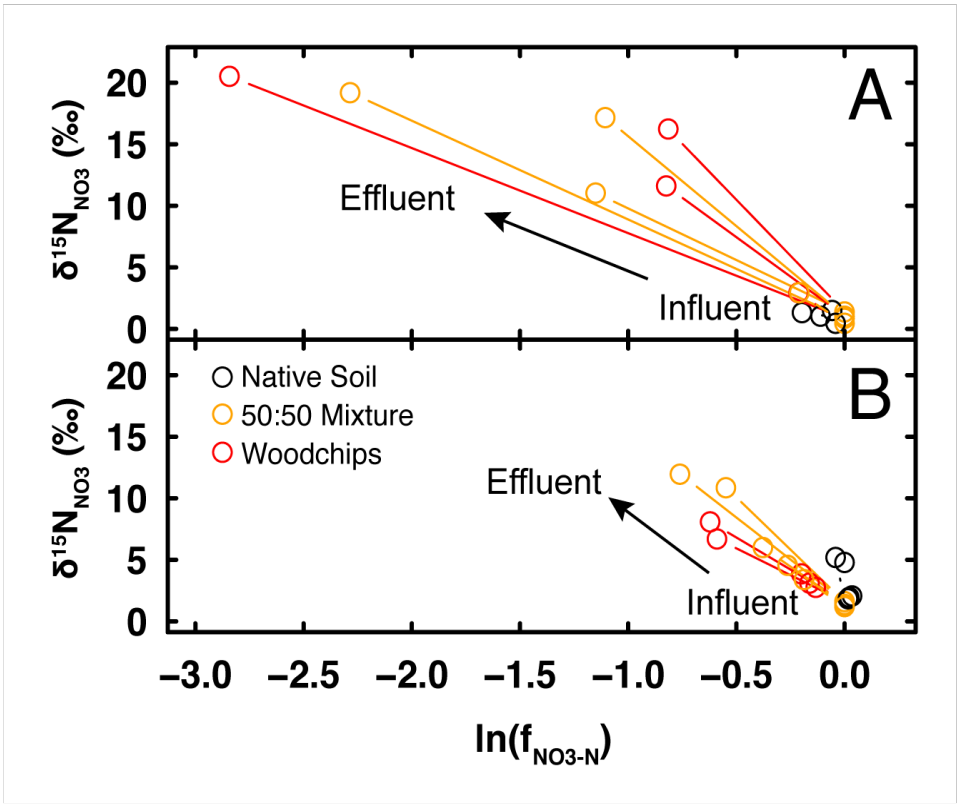

Figure 2-S4. Stable isotopes of residual nitrate Influent and effluent samples were used to plot of $\delta^{15}N$ (‰ vs. Air) of residual NO_3 against the natural log of the fraction of NO3 remaining, yielding a slope corresponding to the ε_{15N} enrichment factor. ε15N values are tabulated in Table 2-S2. Arrows indicate that the effluent nitrate was heavier (more enriched in ^{15}N).

Table 2-S3 Isotope values of NO_3 for selected days

Soil	Treatment	Flow Day	Infiltration Rate (m/day)	Influent (mg-N/L)	Effluent (mg-N/L)	Influent $\delta^{15}N$ (‰ vs. Air)	Effluent $\delta^{15}N$ (‰ vs. Air)	$\varepsilon^{15}N$[a,b]
A	NS	42	0.46	2.46	2.02	0.86	1.31	-2.27
A	NS	47	0.72	2.50	2.24	1.40	1.03	3.31
A	NS	48	0.71	2.48	2.35	10.50	1.51	-7.95
A	NS	63	1.34	3.11	2.98	0.44	0.48	-0.97
A	MIX	42	0.47	2.46	0.25	0.86	19.21	-8.03
A	MIX	47	0.74	2.50	0.79	1.40	11.06	-8.39
A	MIX	48	0.66	2.48	0.82	10.50	17.19	-14.60
A	MIX	63	1.24	3.11	2.53	0.44	2.92	-11.90
A	WC	42	0.41	2.46	0.14	0.86	20.51	-6.92
A	WC	47	0.66	2.50	1.11	1.40	16.23	-18.18
A	WC	48	0.63	2.48	1.09	10.50	11.62	-12.80
A	WC	63	1.21	3.11	2.51	0.44	2.95	-11.73
B	NS	48	0.76	3.05	2.93	1.61	5.17	-88.09
B	NS	52	0.83	3.16	3.16	1.58	4.77	-
B	NS	63	1.10	3.15	3.26	1.40	2.07	-
B	NS	69	1.21	3.09	3.15	1.31	1.97	-
B	NS	73	1.50	3.13	3.18	1.22	1.81	-
B	MIX	48	0.72	3.05	1.43	1.61	11.98	-13.65
B	MIX	52	0.84	3.16	1.83	1.58	10.88	-16.99
B	MIX	63	0.99	3.15	2.16	1.40	5.99	-12.20
B	MIX	69	1.13	3.09	2.37	1.31	4.56	-12.33
B	MIX	73	1.43	3.13	2.60	1.22	3.41	-11.76
B	WC	48	0.75	3.05	1.64	1.61	8.08	-10.41
B	WC	52	0.84	3.16	1.75	1.58	6.71	-8.71
B	WC	63	1.05	3.15	2.58	1.40	3.88	-12.49
B	WC	69	1.22	3.09	2.62	1.31	3.13	-11.14
B	WC	73	1.50	3.13	2.74	1.22	2.77	-11.64

[a] Calculated using an approximation of the Rayleigh equation
[b] Only calculated for days in which [NO_3-N] removal was detected

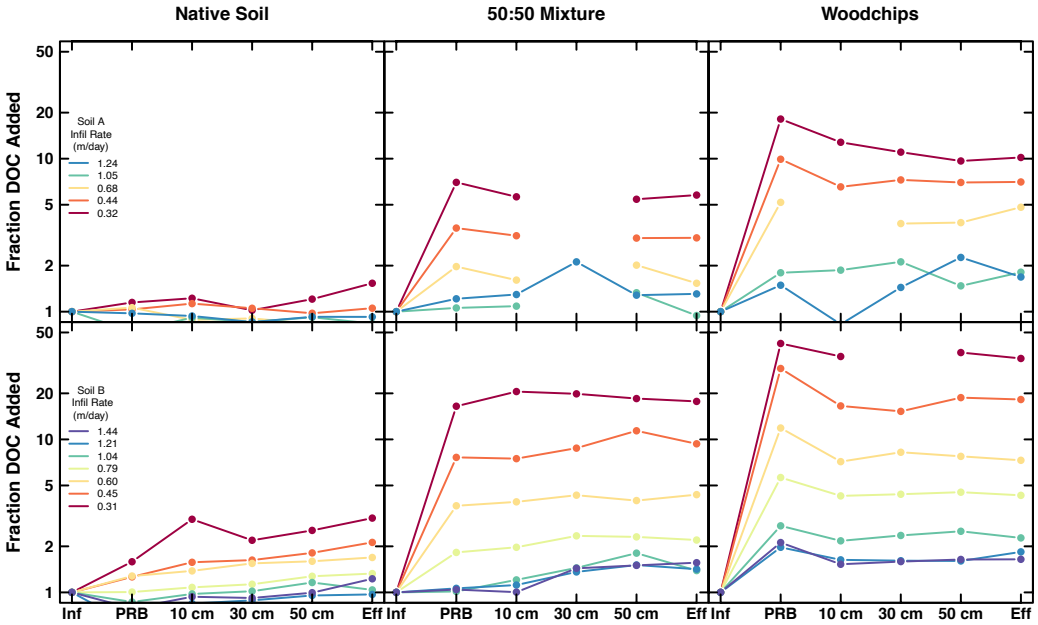

Figure 2-S5. Changes in DOC added along the length of columns for Soil A (top row) and Soil B (bottom row) coded for each flow period by color. Fraction DOC is calculated as the [DOC] at each sampling point divided by the initial [DOC]. Average initial [DOC] was 1.9±1.3 mg/L for Soil A and 1.4±0.4 mg/L for Soil B.

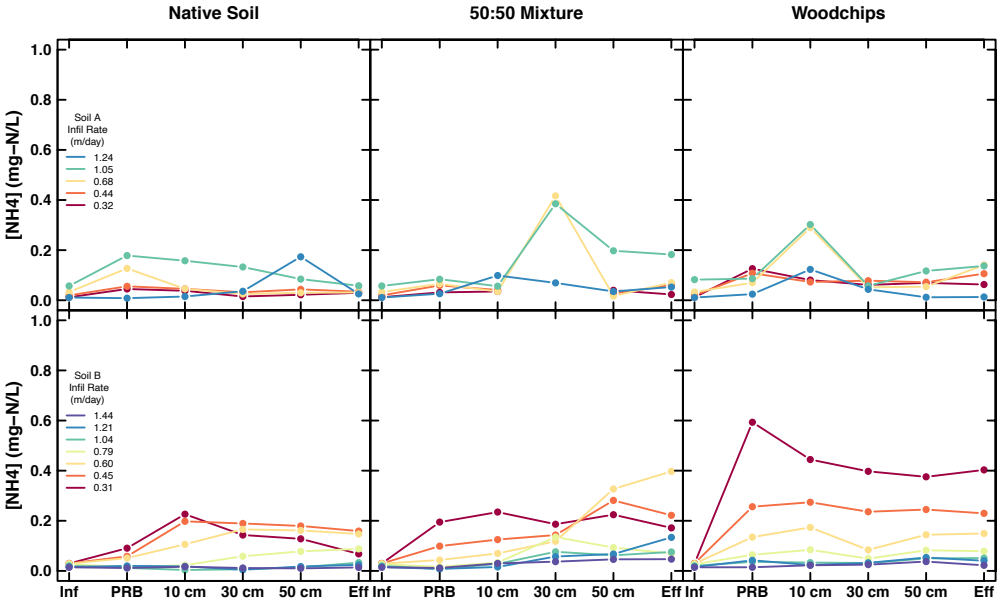

Figure 2-S6. Changes in [NH_4-N] along the length of columns for Soil A (top row) and Soil B (bottom row) coded for each flow period by color. Average initial [NH_4-N] was ≤0.06 mg/L NH_4-N for both Soils.

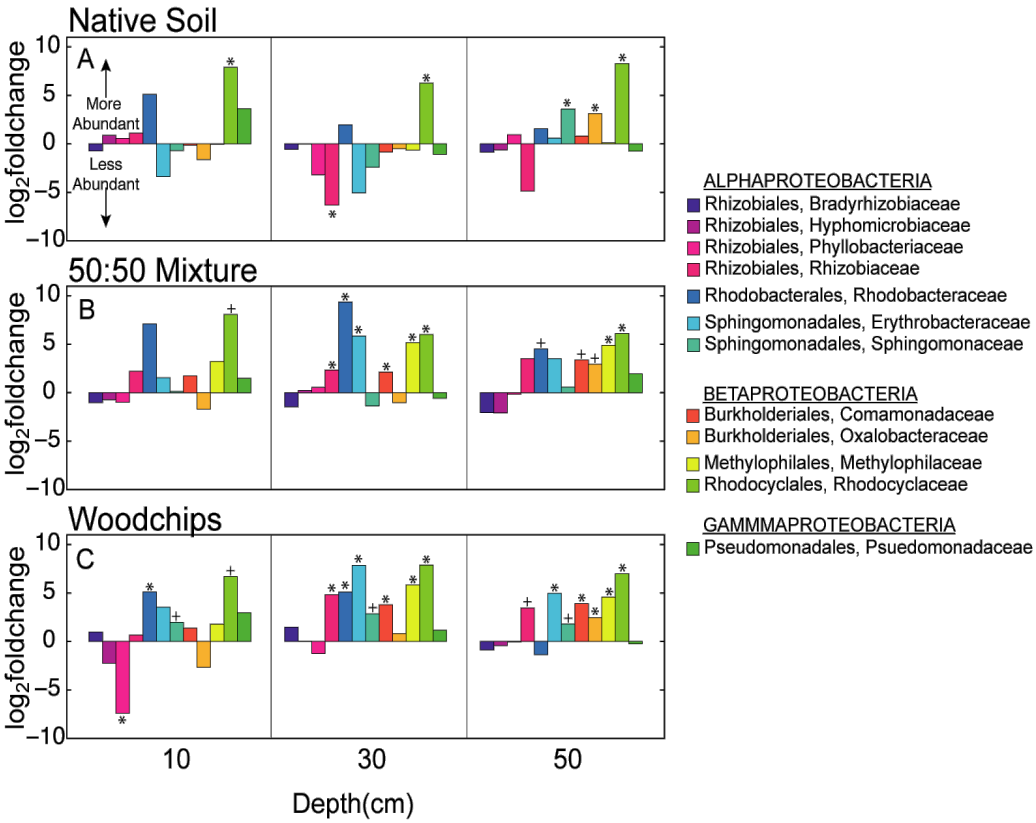

Figure 2-S7. log_2fold change in the counts of denitrifying OTUs. Comparisons were made on a depth-wise basis, comparing each treatment to the before samples at the respective depths. A positive log2fold change indicates an increase in the number of counts after the experiment at that depth. The DeSeq2 algorithm was used to estimate significance, with a (*) above the bar indicating a $p < 0.01$ and a (+) indicating a $p < 0.05$.

Table 2-S4 Summary of nitrate and DOC concentration data

Soil	Treatment	Infiltration Rate	Influent [N-NO3]	Effluent [N-NO3]	Influent [DOC]	Effluent [DOC]
		m/day	mg/L	mg/L	mg/L	mg/L
A	NS	0.33 (0.01)	2.64 (0.03)	1.26 (0.36)	1.28 (0.19)	1.97 (0.57)
A	NS	0.45 (0.01	2.58 (0.12)	2.00 (0.10)	1.39 (0.19)	1.47 (0.30)
A	NS	0.71 (0.03)	2.43 (0.14)	2.28 (0.05)	1.63 (0.70)	1.34 (0.03)
A	NS	1.11 (0.02)	3.25 (0.16)	3.25 (0.21)	3.25 (0.69)	2.72 (0.82)
A	NS	1.32 (0.07)	3.20 (0.08)	3.14 (0.11)	2.07 (0.68)	1.91 (0.71)
A	MIX	0.33 (0.02)	2.64 (0.3)	0.01 (0.02)	1.28 (0.19)	7.42 (0.91)
A	MIX	0.45 (0.01)	2.58 (0.12)	0.08 (0.05)	1.39 (0.19)	4.23 (0.65)
A	MIX	0.69 (0.04)	2.43 (0.14)	0.37 (0.07)	1.63 (0.70)	2.51 (0.28)
A	MIX	1.06 (0.04)	3.25 (0.16)	2.20 (0.55)	3.25 (0.69)	3.07 (1.18)
A	MIX	1.23 (0.07)	3.20 (0.08)	2.48 (0.15)	2.07 (0.68)	2.70 (0.86)
A	WC	0.29 (0.01)	2.64 (0.30)	0.01 (0.03)	1.28 (0.19)	13.07 (2.58)
A	WC	0.41 (0.02)	2.58 (0.12)	0.11 (0.05)	1.39 (0.19)	9.82 (1.10)
A	WC	0.64 (0.03)	2.43 (0.14)	0.40 (0.08)	1.63 (0.70)	7.88 (3.63)
A	WC	0.98 (0.20)	3.30 (0.14)	2.31 (0.47)	3.16 (0.76)	5.64 (2.10)
A	WC	1.18 (0.07)	3.20 (0.08)	2.66 (0.18)	2.07 (0.68)	3.48 (1.67)
B	NS	0.32 (0.01)	3.02 (0.04)	0.19 (0.18)	1.66 (0.24)	5.07 (0.35)

B	NS	0.46	3.11	1.38	1.54	3.28
		(0.01)	(0.07)	(0.23)	(0.23)	(0.60)
B	NS	0.62	3.08	2.27	1.45	2.45
		(0.02)	(0.14)	(0.16)	(0.35)	(0.12)
B	NS	0.81	3.18	2.94	1.23	1.63
		(0.03)	(0.08)	(0.13)	(0.34)	(0.30)
B	NS	1.08	3.11	3.04	1.35	1.40
		(0.03)	(0.05)	(0.29)	(0.49)	(0.39)
B	NS	1.22	3.14	3.20	1.28	1.24
		(0.04)	(0.06)	(0.06)	(-)	(0.18)
B	NS	1.47	3.15	3.16	1.00	1.23
		(0.05)	(0.03)	(0.03)	(0.03)	(0.13)
B	*NS*	*0.63*	*3.22*	*2.97*	*0.98*	*1.66*
		(0.01)	*(0.06)*	*(0.15)*	*(0.14)*	*(0.53)*
B	*NS*	*0.44*	*3.19*	*2.47*	*0.90*	*1.44*
		(0.001)	*(0.02)*	*(0.10)*	*(0.32)*	*(0.10)*
B	*NS*	*0.54*	*5.95*	*5.68*	*1.34*	*1.75*
		(0.03)	*(0.13)*	*(0.30)*	*(0.57)*	*(0.77)*
B	*NS*	*0.69*	*5.84*	*5.79*	*1.09*	*1.47*
		(0.01)	*(0.07)*	*(0.04)*	*(0.20)*	*(0.13)*
B	*NS*	*0.65*	*11.21*	*11.50*	*1.14*	*1.50*
		(0.01)	*(0.89)*	*(0.12)*	*(0.24)*	*(0.20)*
B	*NS*	*0.42*	*12.01*	*11.88*	*1.05*	*1.49*
		(0.01)	*(0.24)*	*(-)*	*(0.02)*	*(0.23)*

B	MIX	0.30	3.02	0.01	1.66	29.38
		(0.01)	(0.04)	(0.01)	(0.24)	(1.98)
B	MIX	0.44	3.11	0.03	1.54	14.45
		(0.02)	(0.07)	(0.02)	(0.23)	(5.72)
B	MIX	0.58	3.08	0.03	1.45	6.30
		(0.04)	(0.14)	(0.06)	(0.35)	(1.34)
B	MIX	0.76	3.18	1.04	1.23	2.71
		(0.04)	(0.08)	(0.30)	(0.34)	(0.55)
B	MIX	1.01	3.11	1.98	1.35	1.88
		(0.04)	(0.05)	(0.25)	(0.49)	(0.39)
B	MIX	1.16	3.14	2.44	1.28	1.82
		(0.05)	(0.06)	(0.08)	(-)	(0.15)
B	MIX	1.40	3.15	2.61	1.00	1.56
		(0.05)	(0.03)	(0.02)	(0.03)	(0.13)
B	*MIX*	*0.62*	*3.22*	*1.71*	*0.98*	*1.57*
		(0.04)	*(0.06)*	*(0.10)*	*(0.14)*	*(0.04)*
B	*MIX*	*0.42*	*3.19*	*1.04*	*0.90*	*1.66*
		(0.01)	*(0.02)*	*(0.04)*	*(0.32)*	*(0.13)*

B	*MIX*	*0.48*	*5.95*	*3.83*	*1.34*	*1.89*
		(0.001)	*(0.13)*	*(0.52)*	*(0.57)*	*(0.29)*
B	*MIX*	*0.64*	*5.84*	*4.29*	*1.09*	*1.77*
		(0.01)	*(0.07)*	*(0.26)*	*(0.20)*	*(0.26)*
B	*MIX*	*0.59*	*11.21*	*10.05*	*1.14*	*1.99*
		(0.01)	*(0.89)*	*(0.95)*	*(0.24)*	*(0.001)*
B	*MIX*	*0.38*	*12.01*	*8.91*	*1.05*	*2.05*
		(0.01)	*(0.24)*	*(0.17)*	*(0.02)*	*(0.34)*
B	WC	0.32	3.02	0.00	1.66	56.09
		(0.01)	(0.04)	(0.0001)	(0.24)	(1.32)
B	WC	0.46	3.11	0.02	1.54	28.17
		(0.02)	(0.07)	(0.02)	(0.23)	(13.24)
B	WC	0.61	3.08	0.31	1.45	10.56
		(0.02)	(0.14)	(0.04)	(0.35)	(2.62)
B	WC	0.80	3.18	1.31	1.23	5.30
		(0.03)	(0.08)	(0.21)	(0.34)	(0.67)
B	WC	1.06	3.11	2.14	1.35	3.06
		(0.04)	(0.05)	(0.35)	(0.49)	(0.82)
B	WC	1.25	3.14	2.46	1.28	2.36
		(0.05)	(0.06)	(0.13)	(-)	(0.25)
B	WC	1.45	3.15	2.76	1.00	1.65
		(0.07)	(0.03)	(0.04)	(0.03)	(0.001)
B	*WC*	*0.64*	*3.22*	*1.96*	*0.98*	*1.71*
		(0.03)	*(0.06)*	*(0.08)*	*(0.14)*	*(-)*
B	*WC*	*0.42*	*3.19*	*1.27*	*0.90*	*2.17*
		(0.01)	*(0.02)*	*(0.16)*	*(0.32)*	*(0.04)*
B	*WC*	*0.51*	*5.95*	*3.95*	*1.34*	*2.29*
		(0.001)	*(0.13)*	*(0.21)*	*(0.57)*	*(0.07)*
B	*WC*	*0.68*	*5.84*	*4.56*	*1.09*	*2.17*
		(0.001)	*(0.07)*	*(0.03)*	*(0.20)*	*(0.05)*
B	*WC*	*0.67*	*11.21*	*10.52*	*1.14*	*2.30*
		(0.001)	*(0.89)*	*(0.30)*	*(0.24)*	*(0.03)*
B	*WC*	*0.43*	*12.01*	*9.22*	*1.05*	*2.20*
		(0.01)	*(0.24)*	*(0.71)*	*(0.02)*	*(0.10)*

Italics indicate that those measurements were used for the initial nitrate experiments, Section 2.3.4 main text

Table 2-S5 t-test results to determine significance of differences in R_N between soil and PRB

Soil	Treatment	Comparison	Infiltration Rate (m/day)	Flow Period	p-value
A	NS	PRB vs. Soil	0.45	2	0.77
A	NS	PRB vs. Soil	0.71	3	0.98
A	NS	PRB vs. Soil	1.11	4	0.07
A	NS	PRB vs. Soil	1.32	5	0.18
A	WC	PRB vs. Soil	0.41	2	0.07
A	WC	PRB vs. Soil	0.64	3	0.01
A	WC	PRB vs. Soil	0.98	4	0.59
A	WC	PRB vs. Soil	1.18	5	0.00
A	MIX	PRB vs. Soil	0.45	2	0.00
A	MIX	PRB vs. Soil	0.69	3	0.00
A	MIX	PRB vs. Soil	1.06	4	0.14
A	MIX	PRB vs. Soil	1.23	5	0.02
B	NS	PRB vs. Soil	0.46	2	0.05
B	NS	PRB vs. Soil	0.62	3	0.00
B	NS	PRB vs. Soil	0.81	4	0.01
B	NS	PRB vs. Soil	1.08	5	0.03
B	NS	PRB vs. Soil	1.22	6	0.33
B	NS	PRB vs. Soil	1.47	7	0.94
B	WC	PRB vs. Soil	0.61	3	0.01
B	WC	PRB vs. Soil	0.80	4	0.41
B	WC	PRB vs. Soil	1.06	5	0.02
B	WC	PRB vs. Soil	1.25	6	0.38
B	WC	PRB vs. Soil	1.45	7	0.17
B	MIX	PRB vs. Soil	0.58	3	0.09
B	MIX	PRB vs. Soil	0.76	4	0.54
B	MIX	PRB vs. Soil	1.01	5	0.01
B	MIX	PRB vs. Soil	1.16	6	0.11
B	MIX	PRB vs. Soil	1.40	7	0.13

Table 2-S6 t-test results to determine significance of differences in R_N between treatments

Soil	PRB/Soil	Comparison	Flow Period	p-value
A	PRB	NS vs. WC	2	0.001
A	PRB	NS vs. WC	3	0.123
A	PRB	NS vs. WC	4	0.011
A	PRB	NS vs. WC	5	0.242
A	Soil	NS vs. WC	2	0.024
A	Soil	NS vs. WC	3	0.000
A	Soil	NS vs. WC	4	0.374
A	Soil	NS vs. WC	5	0.002
A	PRB	NS vs. MIX	2	0.000
A	PRB	NS vs. MIX	3	0.003
A	PRB	NS vs. MIX	4	0.043
A	PRB	NS vs. MIX	5	0.002
A	Soil	NS vs. MIX	2	0.061
A	Soil	NS vs. MIX	3	0.001
A	Soil	NS vs. MIX	4	0.075
A	Soil	NS vs. MIX	5	0.483
A	PRB	WC vs. MIX	2	0.003
A	PRB	WC vs. MIX	3	0.000
A	PRB	WC vs. MIX	4	0.111
A	PRB	WC vs. MIX	5	0.007
A	Soil	WC vs. MIX	2	0.783
A	Soil	WC vs. MIX	3	0.246
A	Soil	WC vs. MIX	4	0.674
A	Soil	WC vs. MIX	5	0.086
B	PRB	NS vs. WC	3	0.000
B	PRB	NS vs. WC	4	0.000
B	PRB	NS vs. WC	5	0.228
B	PRB	NS vs. WC	6	0.014
B	PRB	NS vs. WC	7	0.260
B	Soil	NS vs. WC	3	0.510

B	Soil	NS vs. WC	4	0.008
B	Soil	NS vs. WC	5	0.008
B	Soil	NS vs. WC	6	0.036
B	Soil	NS vs. WC	7	0.037
B	PRB	NS vs. MIX	3	0.000
B	PRB	NS vs. MIX	4	0.000
B	PRB	NS vs. MIX	5	0.430
B	PRB	NS vs. MIX	6	0.004
B	PRB	NS vs. MIX	7	0.100
B	Soil	NS vs. MIX	3	0.006
B	Soil	NS vs. MIX	4	0.000
B	Soil	NS vs. MIX	5	0.000
B	Soil	NS vs. MIX	6	0.001
B	Soil	NS vs. MIX	7	0.062
B	PRB	WC vs. MIX	3	0.270
B	PRB	WC vs. MIX	4	0.310
B	PRB	WC vs. MIX	5	0.440
B	PRB	WC vs. MIX	6	0.120
B	PRB	WC vs. MIX	7	0.240
B	Soil	WC vs. MIX	3	0.011
B	Soil	WC vs. MIX	4	0.013
B	Soil	WC vs. MIX	5	0.000
B	Soil	WC vs. MIX	6	0.220
B	Soil	WC vs. MIX	7	0.128

Table 2-S7 Single factor ANOVA test with factor infiltration rate to determine significance of infiltration rate on R_N

Soil	Treatment	Soil/PRB	p-value
A	NS	PRB	0.251
A	NS	Soil	0.191
A	WC	PRB	0.000
A	WC	Soil	0.533
A	MIX	PRB	0.016
A	MIX	Soil	0.125
B	NS	PRB	0.497
B	NS	Soil	0.000
B	WC	PRB	0.002
B	WC	Soil	0.025
B	MIX	PRB	0.003
B	MIX	Soil	0.010

Table 2-S8 T-test for all infiltration rates to determine significance of differences in R_N within soil and PRBs

Soil	PRB/Soil	Comparison	p-value
A	PRB	NS vs. WC	0.077
A	Soil	NS vs. WC	0.033
A	PRB	NS vs. MIX	0.002
A	Soil	NS vs. MIX	0.030
A	PRB	WC vs. MIX	0.008
A	Soil	WC vs. MIX	0.720
B	PRB	NS vs. WC	0.027
B	Soil	NS vs. WC	0.229
B	PRB	NS vs. MIX	0.007
B	Soil	NS vs. MIX	0.006
B	PRB	WC vs. MIX	0.622
B	Soil	WC vs. MIX	0.008

Chapter Three

MAPPING THE POTENTIAL FOR DENITRIFICATION DURING INFILTRATION WITH MACHINE LEARNING INFORMED BY FIELD AND LABORATORY EXPERIMENTS

In prep: Gorski G., Fisher A.T., Dailey H., Beganskas S., Schmidt C., (2020) Mapping the potential for denitrification during infiltration with machine learning informed by field and laboratory experiments

Abstract

Managed aquifer recharge (MAR) can increase groundwater storage and, under some conditions, improve groundwater quality simultaneously. We synthesize observations from laboratory tests, field experiments and operational MAR facilities at four different MAR locations within the Pajaro Valley in central coastal California, USA to develop a predictive model of nitrate removal during infiltration. We combine data on soil and fluid properties and conditions during infiltration and compare three modeling approaches to assess nitrate removal potential during infiltration: multiple linear regression, random forests, and boosted regression trees. Our preferred model uses boosted regression trees based on four predictor variables: total soil organic carbon, soil clay fraction, fluid residence time, and initial nitrate concentration. Using this model, we simulate the spatial distribution of *potential nitrate removal* (NR_p) across a heterogeneous and mixed-use landscape. We find that areas of high NR_p are more common on floodplains and riparian areas, and urban areas tend to have higher NR_p than do forested or agriculturally developed areas. Combining maps of NR_p with simulated hillslope runoff (from independent stormwater routing calculations) links high nutrient loads to the nutrient cycling capacity of ambient soils, where simultaneous benefits may be achieved in meeting water supply and quality goals for nitrate reduction. We apply the NR_p model to agricultural areas across California to illustrate of the utility and flexibility of this approach, which could help guide decisions in resource management and identify promising MAR sites. NR_p simulations also show

where more and better experimental data might be especially useful and help to understand biogeochemical cycling capacity at large spatial scales.

3.1 Introduction

Groundwater is used to meet the freshwater demands of 2 billion people globally (Jasechko et al., 2017), yet increased reliance on groundwater resources, coupled with land use changes and increasing intensity and variability of precipitation, has put extreme pressure on groundwater supplies. In many parts of the world that rely on groundwater, issues of water supply and water quality are tightly coupled. Declining water tables are often accompanied by increasing concentrations of groundwater contaminants such as nitrate (NO_3), which has been linked to agricultural, residential and municipal activities (Kolbe et al., 2019; Sebilo et al., 2013).

Managed aquifer recharge (MAR) is a suite of techniques that is uniquely suited to address water supply and quality (Bouwer, 2002). MAR projects collect excess surface water from a variety of sources including excess river flows (Kocis and Dahlke, 2017), desalinated water (Ganot et al., 2018), treated wastewater (Schmidt et al., 2011b), stormwater (Kocis and Dahlke, 2017) and hillslope runoff (Beganskas and Fisher, 2017), and route it into underlying aquifers. In many cases, MAR can improve groundwater quality simply by dilution. Additionally, under certain conditions, MAR can remove contaminants through physical, biological, and chemical processes as water infiltrates through the soil, allowing for non-pristine water to be used for infiltration (Alidina et al., 2014; Bekele et al., 2011).

The removal of nitrate during infiltration has been shown to occur in many locations by denitrification, a microbially-mediated process that requires low oxygen conditions and abundant electron donors, often in the form of organic carbon (Seitzinger et al., 2006). Many factors affect the occurrence and extent of denitrification including the presence of common soil microbes, infiltration rate (Schmidt et al., 2011a), soil physical and chemical properties, fluid chemistry, and the availability of organic carbon (Boyer et al., 2006; DelGrosso et al., 2000; Šimek and Cooper, 2002).

Given excess nitrate in many surface water systems, there is possibility for denitrification to occur when such waters are used for MAR under the right biogeochemical conditions. Settings and conditions may include (but are not limited to): wetlands (Hansen et al., 2018), during hyporheic transport in streams (Liu et al., 2017), and during infiltration in shallow soils (Grau-Martínez et al., 2018). We focus on the latter, as collection and infiltration of stormwater is possible in many areas, and because it is beneficial to preventing nitrate from being exported to surface aquatic systems. Although denitrification is one important mechanism for nitrate removal during hydrologic transport, other nitrogen removal pathways may be active as well. In this study, we use the general terms *nitrate removal* (*NR*) and *potential nitrate removal* (NR_p) to refer to the measured or modeled (possible) reduction in dissolved nitrate concentration, respectively.

Previous studies have mapped patterns in physical and chemical soil properties that affect the spatial distribution of denitrification, particularly on flood plains, along riparian corridors, and in wetlands (Harms et al., 2009; Liu et al., 2016; Orr et al., 2014),

(Bruland et al., 2006). These hydrologic settings are characterized by conditions that are particularly favorable for nitrate removal via denitrification, including fine-textured soils, high organic carbon content, and high nitrate availability. In contrast, MAR sites are often located in areas with coarse-grained soils that promote rapid infiltration and low residence time, and often lack bioavailable carbon that can encourage nitrate removal. Nitrate removal during infiltration for MAR often exhibits considerable variability, both within and between measurement locations and times, making predictions beyond individual locations difficult (Grau-Martínez et al., 2018). A better understanding of the spatial distribution of conditions that are favorable for nitrate removal during infiltration would provide a powerful tool for identifying locations where MAR projects could improve groundwater supply and quality. More fundamentally, mapping the potential for nitrate removal during infiltration across landscapes links hydrologic flows and storage of the spatial organization of nitrate biogeochemical cycling, comprising a key component of coupled water, carbon and nutrient models.

This study leverages measurements of nitrate removal during infiltration from four sites within the Pajaro Valley Drainage Basin (PVDB) in central coastal California. Data from measurements were compiled from laboratory experiments, field infiltration studies (Beganskas et al., 2018; Gorski et al., 2019b), and observations from an operational MAR facility (Schmidt et al., 2011b). Data from the different sites and scales are synthesized to develop a generalized spatial model of potential nitrate removal: the potential for the landscape to promote nitrate removal during infiltration

for managed aquifer recharge. The model is used to generate predictions of potential nitrate removal across the PVDB using spatially mapped predictor variables and extended to broader regions.

To model NR_p, three modeling approaches are developed and compared; 1) multiple linear regression (MLR) 2) random forests (RF) and 3) boosted regression trees (BRT). The latter two approaches are machine learning methods which have been successfully adapted to environmental (Mcnicol et al., 2019a) and hydrologic applications (Koch et al., 2019; Nolan et al., 2014). These methods are particularly adept at developing relationships in non-linear systems with potentially missing data and have been shown to outperform more traditional approaches like linear regression (Knoll et al., 2019; Wheeler et al., 2015).

Two applications of this modeling effort and framework are highlighted. First, we combine maps of NR_p with modeled hillslope runoff for the PVDB to link nitrate removal during MAR with water supply. This results in estimates of the potential for nitrogen load reduction during MAR. Second, we expand the model of NR_p to make estimates across agricultural lands throughout California. These examples demonstrate how, detailed and site-specific data can be extended across spatial scales, helping to understand biogeochemical cycling more broadly and aiding efforts to sustain and improve water resources.

3.2 Methods

3.2.1 Data collection

Data and samples were collected from four existing or planned MAR sites within the Pajaro Valley Drainage Basin (PVDB) in central coastal California (Figure 3-1a). Each site consists of an infiltration basin that collects and infiltrates excess surface water during rainy periods.

Nitrate concentrations and other hydrologic and soils data were collected with three kinds and scales of experiments: managed aquifer recharge operations (*MAR*), percolation plot experiments (*Perc*), and column studies (*Col*). Experiments at all three scales measured nitrate removal during infiltration through saturated soil, focusing on the upper few meters below the ground surface (Beganskas et al., 2018; Gorski et al., 2019b, 2020; Schmidt et al., 2011b).

For *MAR* studies (Schmidt et al., 2011b) (site 1, Fig. 3-1A), synoptic sampling campaigns were conducted during infiltration operations. During infiltration, a saturated zone and inverted water table develop beneath the base of the infiltration basin, the thickness of which is determined by soil properties, driving head, and the balance between inflow from above and drainage from below. Subsurface samples were collected at multiple depths every 2 to 7 days over a period of weeks from within the saturated zone and compared to contemporaneous surface samples from the basin. At subsurface pore water nitrate sampling locations, vertical infiltration rates were measured using heat as a tracer (Hatch et al., 2006).

Perc experiments (Beganskas et al., 2018; Gorski et al., 2019b) (sites 1 and 3, Fig. 3-1A) were meter-scale field infiltration studies that emulated infiltration dynamics that occur during *MAR*. Plots were installed and instrumented with fluid

samplers, pressure piezometers, and thermal probes for measuring vertical infiltration rates using heat as a tracer. Individual percolation tests lasted 10-15 days, during which surface and subsurface samples were collected every 1 to 2 days.

Col studies (Gorski et al., 2019b, 2020) (sites 2, 3, and 4, Fig. 3-1A) were laboratory column experiments conducted on intact soil cores collected from MAR sites. Cores were collected using a custom-built coring device consisting of a stainless-steel drive shaft and coring cap that attached directly to the polyvinylchloride (PVC) tube (60 cm L x 10 cm ID) in which flow-through column experiments were conducted. After collection, cores were inverted and artificial groundwater was pumped through the cores in an upward flow direction (to maintain saturated conditions), allowing fine control over the flow rate. Daily samples were collected from the influent and effluent of the columns, and seepage rates were calculated from direct measurements of fluid discharge. Fluid flow in *Col* studies was controlled using a peristaltic pump across a range of infiltration rates relevant to field MAR operations.

For all studies at each scale, fluid samples were analyzed for primary nitrogen species, and stable isotopes of residual pore water nitrate were used to determine when denitrification was the primary mechanism of nitrate removal. While other nitrogen cycling pathways such as dissimilatory nitrate reduction to ammonia and anammox may also contribute to nitrogen transformation, in these studies, denitrification was found to be the primary mechanism of nitrate removal. Soil residence times (*SRT*) were calculated for each experimental/core location as: $SRT = IR_v/d$, where IR_v = vertical infiltration rate, and d = depth of sampling or measurement.

Each observation in the compiled dataset consisted of a surface (s) nitrate concentration, $[NO_3]_s$, one or more nitrate concentrations measured at depth (d) in the subsurface $[NO_3]_d$, and multiple covariates describing soil conditions and fluid chemistry. For each experiment, soil samples were collected along the fluid pathway at 10-20 cm resolution and analyzed for total organic carbon (TOC), total nitrogen (TN), and grain size distribution, with the latter classified as %Clay (≤ 5 μm), %Silt (> 5 μm and ≤ 50 μm) and %Sand (> 50 μm). Depth weighted averages were used to represent soil properties. At *MAR* and *Perc* sites, where several soil cores were collected for analysis, data from the soil core closest to the location of pore fluid measurements were used. In aggregate, each measurement of nitrate removal had eight covariates describing fluid and soil characteristics (Table 3-S1).

3.2.2 Model development and evaluation

The response variable for this study is the amount of nitrate removed during infiltration under saturated conditions. The simulation goal is to predict values of *potential nitrate removal* (NR_p) where: $NR_p = [NO_3]_s - [NO_3]_d$ in mg/L. We compared three approaches for predicting NR_p: multiple linear regression (LR), random forest (RF), and boosted regression trees (BRT). RF and BRT have been used for modeling regional groundwater and surface water solute concentrations (Erickson et al., 2018; B. Wang et al., 2018; Zarnetske et al., 2018), redox transition depths in groundwater (Tesoriero et al., 2015), and the regional distribution of soil types (Mcnicol et al., 2019b). Both RF and BRT are robust to non-linearity, missing values, and interactions and do not require assumptions about data distributions (Breiman, 2001) . Random

forest techniques have outperformed linear regression models, logistic regression models, and other machine learning techniques in recent studies of groundwater data (Knoll et al., 2019; Nolan et al., 2014; Wheeler et al., 2015).

The data were split into training (75%; n = 140) and testing (25%; n = 47) subsets, models were developed using the training data, and model performance was assessed using root mean squared error (RMSE) and R^2 of predictions for the testing subset. To develop and test for models with acceptable performance, we evaluated 33 combinations of 3 to 8 predictor variables. Due to the modest size of the observational dataset (n = 187), model performance varied somewhat due to the training/testing split. To quantify this sensitivity, 1,000 simulations were run for each candidate model by randomly splitting the full dataset into training and testing data. For model comparison, the median performer from each set of 1,000 was chosen as representative.

3.2.3 Spatial predictor variables

After model development and testing, models were applied to the PVDB using the *raster* package in R (v 3.6.1). Spatial coverages of predictor variables used in the final models were preprocessed and checked for gaps. Soil predictor variables (%Clay, SRT, and TOC) were derived from the SSURGO soils database (Soil Survey Staff, Natural Resource Conservation Service, 2016). For calculating SRT from the SSURGO database, the depth weighted harmonic mean of the saturated hydraulic conductivity (k_{sat}) was calculated for soil units that had depth resolved properties reported in the database. Soil residence time through the top meter of soil during infiltration was

approximated as $1/k_{sat}$, assuming a hydraulic gradient of 1 (a reasonable lower limit for conditions during infiltration for MAR).

Simulated potential nitrate removal was based on local runoff infiltrating into the ground, so initial nitrate concentrations, $[NO_3]_s$ were estimated using land cover data from the national landcover database (Dewitz, 2019). Land use types were binned into three categories of low, moderate, and high runoff nitrate concentration (Table S2). Cultivated crops were classified as high ($[NO_3]_s$ = 15 mg/L), pasture and developed spaces were classified as moderate ($[NO_3]_s$ = 5 mg/L), and all other categories were classified as low ($[NO_3]_s$ = 1 mg/L) (see Section S3 for details).

3.2.4 Runoff modeling and potential load reduction calculations

To link landscape denitrification potential during infiltration to the supply of water that might be available for infiltration across the modeled area, we incorporate results from a regional modeling study that generated spatially distributed estimates of hillslope runoff across the PVDB (Beganskas et al., 2019a). Annual runoff was simulated using the Precipitation Runoff Modeling Scenario (PRMS), a widely used, open-source surface water routing model. PRMS is a distributed-parameter watershed model that was run at a daily time step driven by daily precipitation and solar radiation. The model domain was divided into 1025 topographically defined hydrologic response units (HRUs), which ranged in size from 0.1-1.0 km^2 and were assigned static and time-varying parameters representing soil, vegetation, land use, meteorological conditions, and other properties.

Precipitation in the PVDB is strongly seasonal, with most rainfall occurring between November and April. Virtually no precipitation falls as snow. There is a spatial gradient in rainfall across the PVDB with > 130 cm/yr falling to the north in the Santa Cruz mountains near site 4, and < 50 cm/yr falling in the south. Meteorological data were drawn from historical records interpolated across the PVDB (water years 1982-2014, each starting on 1 October and ending on 30 September of the following calendar year), based on the Parameter-elevation Relationship on Independent Slopes Model (PRISM, spatial resolution of 800 m and daily temporal resolution) (Daly et al. 2008). Total annual precipitation in the PVDB was ranked for the 33-year period, and records were extracted to be representative of "dry," "normal," and "wet" conditions. Daily data from these years were assembled to generate rainfall-temperature scenarios for runoff simulation. For purposes of the present study, we focus on runoff generated within individual HRUs, with "casades off" to avoid double counting runoff that flows from one HRU into another (please see the earlier study for details concerning HRU formulation, property assignments, climate data categorization, and simulation settings (Beganskas et al., 2019a)).

Modeled runoff for each HRU was multiplied by the area weighted mean of potential nitrate removal within the HRU to yield a potential load reduction in kg-N/yr. This generates an estimate of the maximum potential nitrate load reduction if 100% of the runoff were collected and infiltrated within each HRU, during which saturated conditions were maintained in shallow soils. This is an upper limit from a management prospective, as not all runoff can be treated in this way but is helpful for identifying

differences in potential to improve water quality as a function of land use, precipitation patterns, soil nitrate reduction cycling capacity, and other factors.

3.3 Results and Discussion

3.3.1 Modeling results

For the 33 parameter sets tested, RF and BRT models outperformed LR models (Fig. 3-S1 and 3-S2). RF models tended to outperform BRT models during training, but comparison with known values during testing favored BRT models. This suggests that the RF approach may be subject to "overfitting". In general, models with more parameters performed better than models with fewer parameters. The preferred BRT model uses four covariates (TOC, %Clay, SRT, and $[NO_3]_s$) avoids overfitting while capturing much of the desired response behavior. For the preferred BRT model, RMSE = 0.93 mg/L and R^2 = 0.34 (Figure 1c, Figs S1, S2), values consistent with other statistical studies of nitrate cycling (Mcnicol et al., 2019a; Nolan et al., 2015; Wheeler et al., 2015).

The preferred BRT model showed the strongest predictive capacity for $NR_p \leq 2$ mg/L (Figure 3-1d). At higher values of nitrate removal, the model tended to underpredict removal, resulting in conservative estimates. This loss of model sensitivity for $NR_p > 2$ mg/L may result in part from uneven sample distribution across the range of nitrate removal measured (Figure 1b), with 24% of the full dataset having $NR_p \geq 1.5$ mg/L and 1.3% having $NR_p \geq 2$ mg/L.

3.3.2 Potential nitrate removal mapping

The preferred BRT model was applied to the full PVDB to delineate spatial differences in potential nitrate removal (Figure 3-2a). The model produced a range of NR_p values of -0.91 to 3.49 mg/L with a median value of 0.20 mg/L. While 75% of the area of the PVDB shows $NR_p < 1.0$ mg/L, areas of high NR_p (≥ 1.0 mg/L) are distributed throughout the basin. For example, portions of the floodplain of the Pajaro River, the major drainage of the basin, showed potential nitrate removal of ≥ 1.0 mg/L. The floodplain is made up of interbedded sands, silts and clays that can result in high SRTs, and is also a focus of agricultural activity, leading to elevated [NO_3] in runoff. The model also predicted elevated potential nitrate removal in association with former and current wetland and estuary-adjacent soils, and along the lower reaches of small drainages (Figure 3-2a). These results are consistent with findings that riparian zones, flood plains, and wetlands are often important for denitrification and other nutrient cycling processes due to episodic flooding and carbon rich soils (Arango and Tank, 2008; Hopfensperger et al., 2014a). High NR_p was often co-located with high soil organic carbon (Fig. 3-S5), consistent with other studies of denitrification potential (Hopfensperger et al., 2014b; Inwood et al., 2007; Newcomer et al., 2012).

The central portion of the PVDB showed several contiguous areas with potential nitrate removal ≥ 2.0 mg/L. These are largely urban and suburban areas around the City of Watsonville, which produce runoff with moderate to high [NO_3] commonly found in urban areas from sanitary sewer and septic systems and atmospheric deposition coupled with fast hydrologic flow paths that limit nitrogen

processing (Hopfensperger et al., 2014b; Kaushal and Belt, 2012). The highest potential nitrate removal was in urban areas, median NR_p = 0.58±0.98 mg/L (±standard deviation of values), compared to 0.20±0.65 and 0.44±0.66mg/L for forested and agricultural areas, respectively (Figure 3-2c). Additionally, the distribution of denitrification potential for urban areas show a longer tail, with the 90th percentile NR_p = 2.4 mg/L compared to 1.5 and 1.6 mg/L for forested and agricultural areas, respectively (Figure 3-2c). The relatively high potential nitrate removal in urban areas is likely a result of both higher $[NO_3]_S$ in associated waters, and the tendency for urbanization to occur on relatively flat landscapes and near aquatic systems, favoring occupation of flood plains, former wetlands, and riparian corridors in general. These latter characteristics tend to include soil properties with high organic carbon and long residence times (Figure 3-S5). Other studies have reported relatively high nitrogen retention and denitrification potential in urban watersheds in comparison to agricultural and forested areas (Groffman et al., 2004; Harrison et al., 2011).

Areas of low or negative potential nitrate removal tended to be co-located with low values of SRT, %Clay, and/or $[NO_3]_S$. Low SRT and low %Clay areas are prevalent in the southeastern and western portions of the model domain (Figure 3-S5), where soils commonly include aeolian (dune) deposits, often having coarse and well-rounded grains. Low NR_p areas in the north and northeast of the model domain are dominated by grasslands and forested areas with low runoff nitrate concentrations, despite having some areas of moderate to high organic carbon content and long soil

residence times. Thus in these areas, it is mainly the lack of excess [NO_3] in runoff that leads to low potential for removal (Gift et al., 2010).

In aggregate, trends relating predictors and response variables arising from these models are consistent with a conceptual understanding of nitrate removal during infiltration based on field and laboratory studies in multiple settings. As has been seen in earlier observational work, higher soil organic carbon, clay content, soil residence times, and initial nitrate concentrations tend to be associated with more nitrate removal via denitrification; these factors (and others) can combine in highly non-linear ways leading to complicated dependencies (Boyer et al., 2006; Gift et al., 2010; Hopfensperger et al., 2014b; Kaushal et al., 2011).

3.3.3 Potential nitrate load reduction under climate scenarios

As applied in this study, potential nitrate removal represents the capability of the landscape to reduce nitrate concentrations during infiltration, without consideration as to the availability of water. We combine spatial calculations of NR_p with modeled hillslope runoff for the PVDB, linking these independent quantities to assess the potential for NO_3 load reduction across the landscape (Figure 3-3). Within each hydrologic response unit, modeled runoff (from dry, normal, and wet climate scenarios) values were multiplied by the area-weighted denitrification potential to assess load reduction.

Modeled runoff across the PVDB followed an approximately log normal distribution with median values of 1.4, 0.66, and 5.46 cm/yr for normal, dry and wet climate scenarios, respectively (Beganskas et al., 2019b). Under all precipitation

scenarios, runoff was greatest in the northern part of the PVDB, consistent with the regional precipitation gradient, and in the urban and suburban areas near the basin center due to the high proportion of impervious surfaces (Figure 3-S7). Much less runoff was generated in the southern and western parts of the PVDB where sandy soils with high infiltration capacities dominate.

Urban areas showed the highest potential load reduction (Figure 3-3b), consistent with generally high denitrification potential (Figure 3-2c) and large volumes of runoff (Figures 3-S7a-c). These areas highlight an opportunity to manage storm flows in urban areas where high proportions of impervious surfaces, and rapid transport of sediment and nutrients create conditions where stormwater collection and infiltration could produce water quantity and quality benefits while mitigating urban flooding. Additionally, these areas showed consistent potential load reduction under dry, normal and wet precipitation scenarios (Figure 3b) indicating water quality improvements could be consistent through drought and extreme precipitation events that are likely to become increasingly common.

Areas in the southern and western portion of the basin, which have very sandy soils, produce little runoff except during extreme rain events. Because potential nitrate removal and surface runoff both have a negative relationship with soil infiltration capacity, there are many areas where high NR_p coincided with high surface runoff. Areas of moderate to high potential load reduction ($\geq$ 5.0 kg-N/yr) were spatially distributed and make up 46% of the model domain in normal precipitation years, compared to 78% and 28% in wet and dry years, respectively. This analysis provides

an upper limit for potential nitrate load reduction, if all runoff within each HRU were collected and infiltrated. That said, the analysis tends to underestimate NO_3 removal at higher rates (Figure 3-1d), so these factors may offset each other to a certain extent. More importantly, this analysis allows an assessment of spatial variability in the potential for load reduction on a regional basis, under different climate scenarios and land uses, which can help to identify locations where site-specific examination of soil and runoff conditions may be justified as part of MAR project development.

3.3.4 Potential nitrate removal on California agricultural lands

As a demonstration of broader application using this modeling framework, we extend the map of potential nitrate removal to agricultural regions across California (~71,000 km^2), identified by the Farmland Mapping and Monitoring Program (Figure 3-4a). These areas have previously been classified for groundwater recharge suitability using the Soil Agricultural Groundwater Banking Index (SAGBI) by considering soil physical and chemical properties and agricultural practices such as tillage and crop type (O'Geen et al., 2015). We recognize that spatial extrapolation of this kind is speculative, particularly because areas simulated contain soils and land use practices beyond the range of observations used to develop the model. However, extending modeling results to larger spatial areas can illustrate trends, and help identify potential regional hotspots.

We show calculations for the full SAGBI region and highlight the Sacramento Valley (Figure 3-4b), which makes up the northern one third of the Central Valley, and the Salinas Valley (Figure 3-4c), located in a coastal basin. Both of these are area are

highly productive agricultural regions. The Sacramento Valley shows higher nitrate removal potential than does the southern portion of the Central Valley, consistent with greater soil residence times in the Sacramento Valley in association with relatively fine soil textures (Faunt et al., 2009). The Sacramento Valley is marked by low nitrate removal potential to the west side and along alluvial fans associated with the Consumnes, American, Bear, Yuba, and Feather River drainage basins on the eastern side of the valley. Alluvial fan deposits are heterogeneous and, in some areas, contain coarse soils derived from weathering of the granitic Sierra Nevada Mountains. That said, areas of high nitrate removal potential are distributed throughout the Sacramento Valley, particularly along the axis of the valley and eastern areas on flood plains and other settings where soils are finer and more carbon rich.

The Salinas Valley (Figure 3-4b) is a coastal basin that suffers from declining groundwater levels, seawater intrusion, and elevated nitrate concentrations (Dubrovsky et al., 2010; Harter et al., 2012; Tomich et al., 2016). The areas of highest potential nitrate removal within the Salinas Valley surround the city of Salinas in the northern part of the valley (similar to results seen around Watsonville in the PVDB). Lower values of potential nitrate removal are seen on the edges of the Salinas Valley, and higher values are found along the central axis. Areas near the Salinas River, in the center of the valley show higher potential nitrate removal in association with flood plain and distal alluvial deposits derived from the Coast Ranges.

3.3.5 Model limitations and implications

Because the observational dataset was collected from active or planned managed aquifer recharge sites, the data coverage is naturally biased toward parameter sets that are most likely to occur in those settings. This may explain why model results are most robust where NR_p is moderate to low (≤ 1.5 mg/L); NR_p values for areas with higher nitrate removal potential are less constrained by field and laboratory data. Despite larger uncertainties for areas with NR_p > 2 mg/L, these areas may deserve focused studies specifically because recharge and water quality improvement goals might be met simultaneously, under appropriate conditions.

The preferred BRT model suggests that there is greater potential nitrate removal at moderate initial nitrate concentrations of $[NO_3]_s$ = 4-5 mg/L (Figure 3-S6), as seen in some urban areas. The availability of labile organic carbon also has a non-monotonic relationship with potential nitrate removal, with the greatest benefit being achieved in the range of 0.5-1.0% TOC (Figure 3-S6). Elevated initial nitrate concentrations (~10-15 mg/L) and low soil carbon were commonly associated in the PVDB with areas of intensive agricultural activity, especially where there are sandy, well-drained soils. This suggests that augmenting sandy soils with a bioavailable carbon source could help to reduce both nitrate concentrations and associated loads and export to underlying aquifers (Beganskas et al., 2018; Gorski et al., 2019b, 2020). Ongoing studies should help to resolve the nature of these emergent relationships and allow testing of carefully managed MAR operations at scale.

Some model misfit likely results from unmeasured parameters that influence nitrate removal and are not included in the model. For example, soil pH, temperature, and antecedent soil moisture have all been shown to influence rates and extent of denitrification (Boyer et al., 2006; Parton et al., 2001; Šimek and Cooper, 2002). Some of these parameters are highly variable in both space and time, making it difficult to extrapolate more broadly from limited observations. Still, these and other parameters that influence nitrate removal are readily measurable and can be added and tested on the basis of focused experiments and data collected from MAR field sites. Extrapolation of local data across larger regions introduces uncertainties, even what data are comprehensive and abundant, but with ongoing updating of both data and statistical relationships, models can be adapted for more accurate use in individual basins and regions, contributing to both greater understanding of nutrient cycling in general, and how MAR can improve water quality while increasing water supply.

3.4 Conclusions

Using observational data from three experimental scales and four managed aquifer recharge sites, we developed a model to predict nitrate removal during infiltration based on soil, fluid, and land use characteristics. The application of the model to the Pajaro Valley Drainage Basin shows that much of the area has $NR_p < 1.0$ mg/L, but areas of higher NR_p are spatially distributed and concentrated in floodplains and urban areas in association with soils that promote longer residence times and have higher organic carbon contents. We combined nitrate removal simulations with

hydrologic simulations of hillslope runoff to estimate potential load reductions. These calculations show that floodplains and urban areas may provide mostly undeveloped potential to link biogeochemical and hydrologic cycles, connected areas of rapid runoff to sites having a high capacity to cycle nutrients. Application of the statistical modeling approach to part of California's Central Valley and the Salinas Valley indicates that multiple areas have elevated potential for water quality improvement during infiltration, potential "hotspots" for biogeochemical cycling.

These models and analyses are useful for planning and informing decisions about project development to generate collocated water supply and quality benefits. A similar modeling framework can be applied to other regions, and additional parameters that are readily measured can be linked to desired goals in resource stewardship. Given the scope and nature of water resource challenges faced by many regions, especially in the arid and semi-arid western U.S., and the cost and time required to conduct detailed, process-based studies of small sites, this approach can help to leverage limited data, allowing extrapolation of local understanding to a landscape scale.

SUPPORTING MATERIAL

A more detailed description of experimental methods and design as well as supporting figures showing model development results.

ACKNOWLEDGEMENTS

The authors would like to acknowledge valuable contributions in collecting field and laboratory data from E. Adelstein, T. Weathers, P. Karim, M. Cribari, D. van den Dries, T. Stewart, A. Yoder, K. Young, J. Cox, P. Borges, S. Faraola, W. Weir, A. Serrano and J. Pensky. Additionally, A. Paytan, R. Franks, and D. Sampson provided key experimental, analytical and technical contributions. We would also like to thank E. and J. Kelly, S. Dobbler, T. Marg, K. Camara, C. Coburn, and B. Lockwood for their guidance and cooperation in accessing sites and conducting field studies.

FUNDING

This work was supported by the Gordon and Betty Moore Foundation (Grant GBMF5595), UC Water Security and Sustainability Research Initiative (UCOP Grant #13941), the USDA/NIFA (Award #2017-67026-26315), the Water Foundation (Award #10069), the National Science Foundation Graduate Research Fellowship Program, and the Recharge Initiative (http://www.rechargeinitiative.org/).

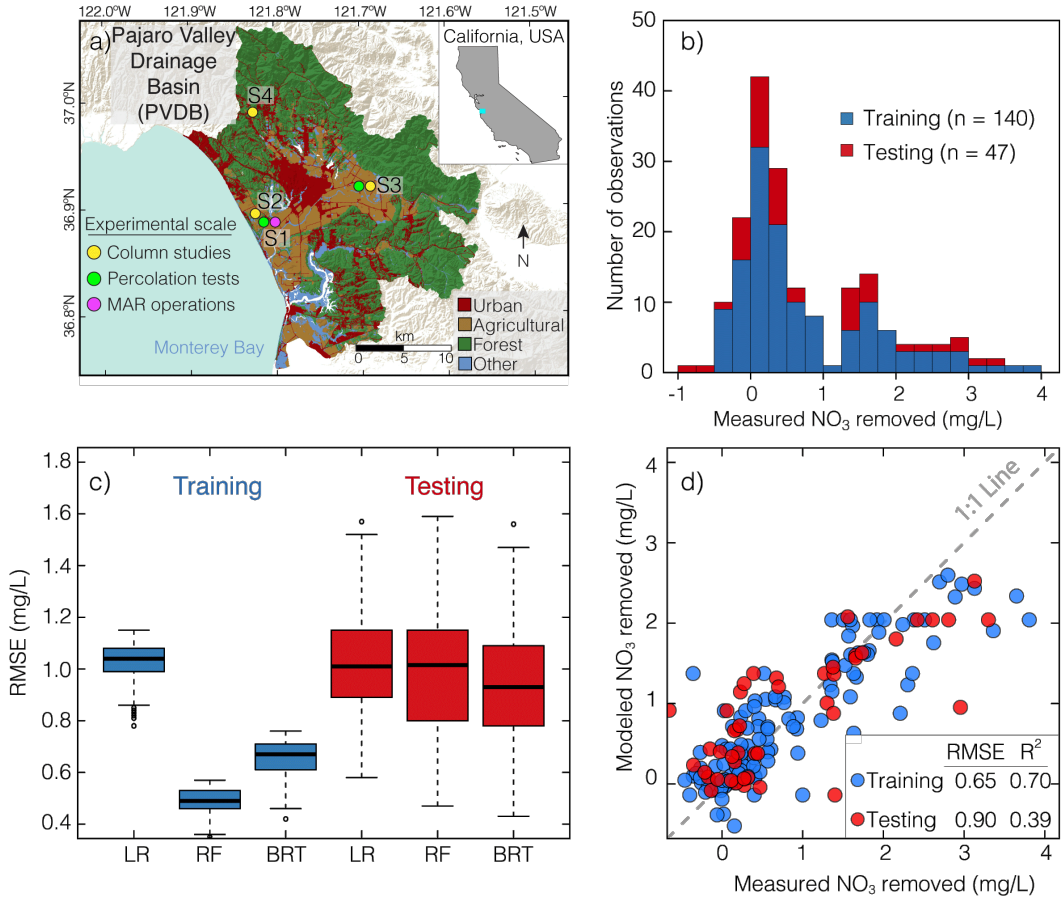

Figure 3-1 a) Map of Pajaro Valley Drainage Basin (PVDB) with land use and site locations (circles) colored by experimental scale. Note that at Site 1 (S1) percolation tests and MAR operations were conducted, at Site 3 (S3) percolation tests and column studies were conducted, while at Sites 2 and 4 (S2, S4) column studies were conducted. **b)** The distribution of the observations in the training (blue) and testing (red) sets across the range of measured NO_3 removal. **c)** The range of model performance using TOC, %Clay, $[NO_3]_s$, and SRT as predictors for training and testing data across 1,000 realizations for three modeling approaches; linear regression (LR), random forest (RF), and boosted regression trees (BRT). **d)** The BRT model performance in predicting the training and testing set.

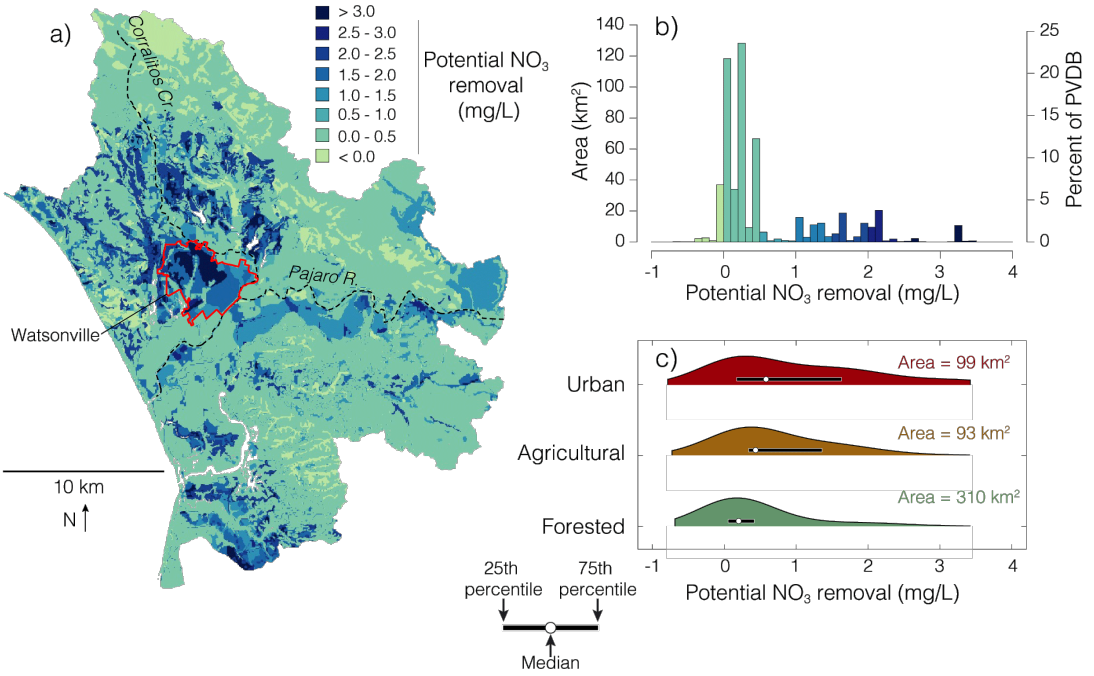

Figure 3-2 a) Spatial distribution of nitrate removal across the PVDB with the city of Watsonville outlined in red and the major drainages of the region shown in white and **b)** histogram of potential nitrate removal values across the PVDB. **c)** Distribution of potential nitrate removal by land use classes, using same color scheme as in land use map in Figure 1a.

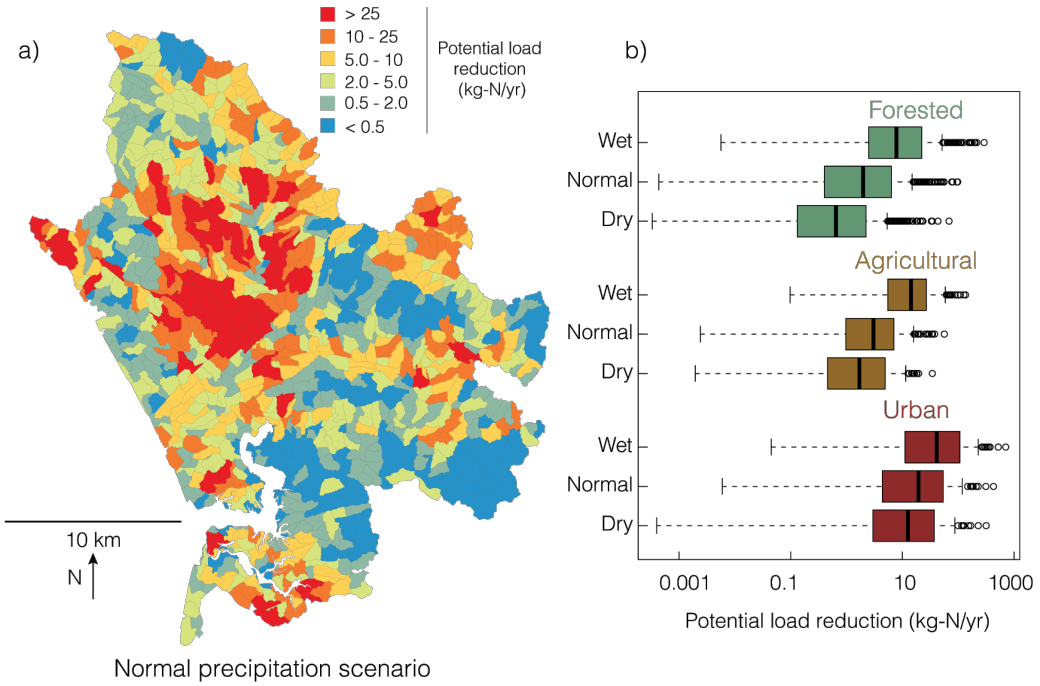

Figure 3-3 a) Spatial distribution of potential nitrate load reduction in normal precipitation scenario **b)** Boxplots showing the distribution of potential load reduction for HRUs of different land use under dry, normal, and wet precipitation scenarios.

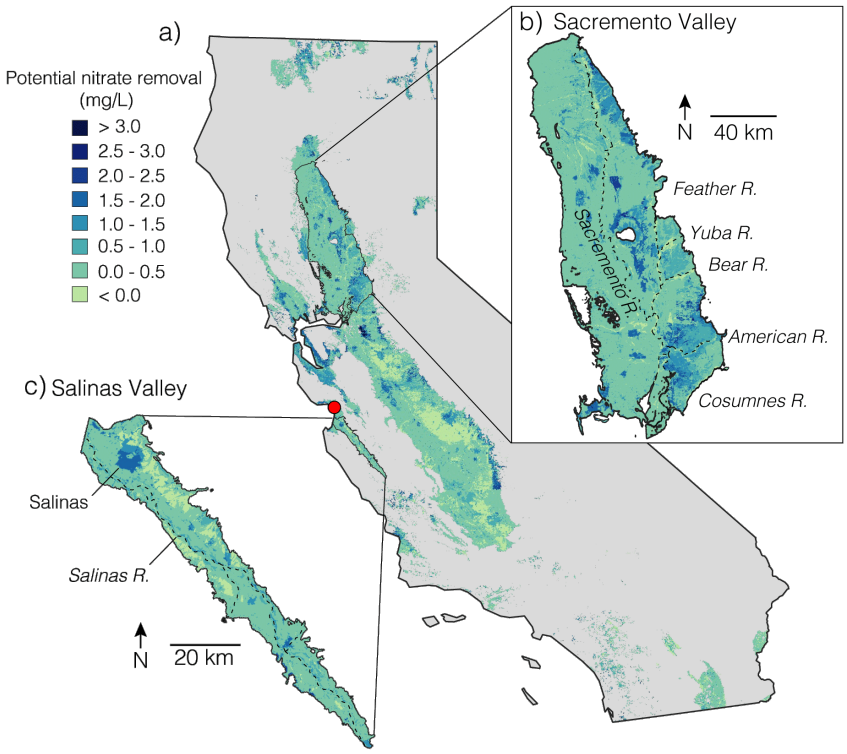

Figure 3-4 Potential nitrate removal in agricultural areas of California, highlighting two regions **b)** Sacramento Valley which constitutes the northern one third of California's Central Valley and **c)** the Salinas Valley in the central coastal region. Major rivers are shown with black dashed lines in the insets, and the PVDB is shown with a red dot.

REFERENCES

Alidina, M., Li, D., Ouf, M., Drewes, J.E., 2014. Role of primary substrate composition and concentration on attenuation of trace organic chemicals in managed aquifer recharge systems. J. Environ. Manage. 144, 58–66. https://doi.org/10.1016/j.jenvman.2014.04.032

Arango, C.P., Tank, J.L., 2008. Land use influences the spatiotemporal controls on nitrification and denitrification in headwater streams. J. North Am. Benthol. Soc. 27, 90–107. https://doi.org/10.1899/07-024.1

Beganskas, S., Fisher, A.T., 2017. Coupling distributed stormwater collection and managed aquifer recharge: Field application and implications. J. Environ. Manage. 200, 366–379. https://doi.org/10.1016/j.jenvman.2017.05.058

Beganskas, S., Gorski, G., Weathers, T., Fisher, A.T., Schmidt, C., Saltikov, C., Redford, K., Stoneburner, B., Harmon, R., Weir, W., 2018. A horizontal permeable reactive barrier stimulates nitrate removal and shifts microbial ecology during rapid infiltration for managed recharge. Water Res. 144, 274–284. https://doi.org/10.1016/j.watres.2018.07.039

Beganskas, S., Young, K.S., Fisher, A.T., Harmon, R., 2019. Runoff Modeling of a Coastal Basin to Assess Variations in Response to Shifting Climate and Land Use : Implications for Managed Recharge. Water Resour. Manag. https://doi.org/https://doi.org/10.1007/s11269-019-2197-4 Runoff

Bekele, E., Toze, S., Patterson, B., Higginson, S., 2011. Managed aquifer recharge of treated wastewater: Water quality changes resulting from infiltration through the vadose zone. Water Res. 45, 5764–5772. https://doi.org/10.1016/j.watres.2011.08.058

Bouwer, H., 2002. Artificial recharge of groundwater: Hydrogeology and engineering. Hydrogeol. J. 10, 121–142. https://doi.org/10.1007/s10040-001-0182-4

Boyer, E.W., Alexander, R.B., Parton, W.J., Li, C., Butterbach-Bahl, K., Donner,

S.D., Skaggs, R.W., Grosso, S.J. Del, 2006. Modeling Denitrification in Terrestrial and Aquatic Ecosystems At Regional Scales. Ecol. Appl. 16, 2123–2142. https://doi.org/10.1890/1051-0761(2006)016[2123:MDITAA]2.0.CO;2

Breiman, L., 2001. Random Forests. Mach. Learn. 45, 5–32.

Bruland, A., Gregory, L., Curtis, J., Stephen, C., 2006. Spatial variability of denitrification potential and related soil properties in created, restored, and paired natural wetlands. Wetlands 26, 1042–1056.

DelGrosso, S.J., Parton, W.J., Mosier, a R., Ojima, D.S., Kulmala, a E., Phongpan, S., 2000. General model for N2O and N2 gas emissions from soils when comparing observed and gas emission rates from irrigated field soils used for model testing NO2. Global Biogeochem. Cycles 14, 1045–1060. https://doi.org/10.1029/1999GB001225

Dewitz, J., 2019. National Land Cover Database (NLCD) 2016 Products: U.S. Geological Survey data release. https://doi.org/https://doi.org/10.5066/P96HHBIE

Dubrovsky, N.M., Burow, K.R., Clark, G.M., Gronberg, J.M., P.A., H., Hitt, K.J., Mueller, D.K., Munn, M.D., Nolan, B.T., Puckett, L.J., Rupert, M.G., Short, T.M., Spahr, N.E., Sprague, L.A., Wilber, W.G., 2010. The quality of our Nation's waters—Nutrients in the Nation's streams and groundwater, 1992–2004.

Erickson, M.L., Elliott, S.M., Christenson, C.A., Krall, A.L., 2018. Predicting geogenic Arsenic in Drinking Water Wells in Glacial Aquifers, North-Central USA: Accounting for Depth-Dependent Features. Water Resour. Res. 54, 10,172-10,187. https://doi.org/10.1029/2018WR023106

Faunt, C.C., Belitz, K., Hanson, R.T., 2009. Development of a three-dimensional model of sedimentary texture in valley-fill deposits of Central Valley, California, USA. Hydrogeol. J. 18, 625–649. https://doi.org/10.1007/s10040-009-0539-7

Ganot, Y., Holtzman, R., Weisbrod, N., Russak, A., Katz, Y., Kurtzman, D., 2018. Geochemical Processes During Managed Aquifer Recharge With Desalinated

Seawater. Water Resour. Res. 54, 978–994. https://doi.org/10.1002/2017WR021798

Gift, D.M., Groffman, P.M., Kaushal, S.S., Mayer, P.M., 2010. Denitrification Potential , Root Biomass , and Organic Matter in Degraded and Restored Urban Riparian Zones. Restor. Ecol. 18, 113–120. https://doi.org/10.1111/j.1526-100X.2008.00438.x

Gorski, G., Dailey, H., Fisher, A.T., Schrad, N., Saltikov, C., 2020. Denitrification during infiltration for managed aquifer recharge: Infiltration rate controls and microbial response. Sci. Total Environ. 727. https://doi.org/10.1016/j.scitotenv.2020.138642

Gorski, G., Fisher, A.T., Beganskas, S., Weir, W., Redford, K., Schmidt, C., Saltikov, C., 2019. Field and laboratory studies linking hydrologic, geochemical, and microbiological processes and enhanced denitrification during infiltration for managed recharge. Environ. Sci. Technol. 53, acs.est.9b01191. https://doi.org/10.1021/acs.est.9b01191

Grau-Martínez, A., Folch, A., Torrentó, C., Valhondo, C., Barba, C., Domènech, C., Soler, A., Otero, N., 2018. Monitoring induced denitrification during managed aquifer recharge in an infiltration pond. J. Hydrol. 561, 123–135. https://doi.org/10.1016/j.jhydrol.2018.03.044

Groffman, P.M., Law, N.L., Belt, K.T., Band, L.E., Fisher, G.T., 2004. Nitrogen Fluxes and Retention in Urban Watershed Ecosystems. Ecosystems 7, 393–403. https://doi.org/10.1007/s10021-003-0039-x

Hansen, A.T., Dolph, C.L., Foufoula-Georgiou, E., Finlay, J.C., 2018. Contribution of wetlands to nitrate removal at the watershed scale. Nat. Geosci. 11, 127–132. https://doi.org/10.1038/s41561-017-0056-6

Harms, T.K., Wentz, E.A., Grimm, N.B., 2009. Spatial heterogeneity of denitrification in semi-arid floodplains. Ecosystems 12, 129–143. https://doi.org/10.1007/s10021-008-9212-6

Harrison, M.D., Groff, P.M., Mayer, P.M., Kaushal, S.S., Newcomer, T.A., 2011.

Denitrifi cation in Alluvial Wetlands in an Urban Landscape. J. Environ. Qual. 40, 634–646. https://doi.org/10.2134/jeq2010.0335

Harter, T., Lund, J.R., Darby, J., Fogg, G.E., Howitt, R., Jessoe, K.K., Pettygrove, G.S., Quinn, J.F., Viers, J.H., 2012. Addressing Nitrate in California's Drinking Water with a focus on Tulare Lake Basin and Salinas Valley Groundwater. Rep. State Water Resour. Control Board Rep. to Legis. 1–78.

Hatch, C.E., Fisher, A.T., Revenaugh, J.S., Constantz, J., Ruehl, C., 2006. Quantifying surface water-groundwater interactions using time series analysis of streambed thermal records: Method development. Water Resour. Res. 42, 1–14. https://doi.org/10.1029/2005WR004787

Hopfensperger, K.N., Schwarz, K., Kirtman, E.R., Hopfensperger, K.N., Schwarz, K., Kirtman, E.R., Hopfensperger, K.N., Schwarz, K., Kirtman, E.R., 2014a. Effects of seasonal variation and land cover on riparian denitrification along a mid-sized river. J. Freshw. Ecol. 29, 457–473. https://doi.org/10.1080/02705060.2014.933717

Hopfensperger, K.N., Schwarz, K., Kirtman, E.R., Hopfensperger, K.N., Schwarz, K., Kirtman, E.R., Hopfensperger, K.N., Schwarz, K., Kirtman, E.R., 2014b. Effects of seasonal variation and land cover on riparian denitrification along a mid-sized river. J. Freshw. Ecol. 29, 457–473. https://doi.org/10.1080/02705060.2014.933717

Inwood, S.E., Tank, J.L., Bernot, M.J., 2007. Factors controlling sediment denitrification in midwestern streams of varying land use. Microb. Ecol. 53, 247–258. https://doi.org/10.1007/s00248-006-9104-2

Jasechko, S., Perrone, D., Befus, K.M., Bayani Cardenas, M., Ferguson, G., Gleeson, T., Luijendijk, E., McDonnell, J.J., Taylor, R.G., Wada, Y., Kirchner, J.W., 2017. Global aquifers dominated by fossil groundwaters but wells vulnerable to modern contamination. Nat. Geosci. 10, 425–429. https://doi.org/10.1038/ngeo2943

Kaushal, S.S., Belt, K.T., 2012. The urban watershed continuum : evolving spatial

and temporal dimensions. Urban Ecosyst. 15, 409–435. https://doi.org/10.1007/s11252-012-0226-7

Kaushal, S.S., Gro, P.M., Band, L.E., Elliott, E.M., Shields, C.A., Kendall, C., 2011. Tracking Nonpoint Source Nitrogen Pollution in Human-Impacted Watersheds. Environ. Sci. Technol. 45, 8225–8232. https://doi.org/10.1021/es200779e

Knoll, L., Breuer, L., Bach, M., 2019. Large scale prediction of groundwater nitrate concentrations from spatial data using machine learning. Sci. Total Environ. 668, 1317–1327. https://doi.org/10.1016/j.scitotenv.2019.03.045

Koch, J., Stisen, S., Refsgaard, J.C., 2019. Modeling Depth of the Redox Interface at High Resolution at National Scale Using Random Forest and Residual Gaussian Simulation Water Resources Research. Water Re 55, 1451–1469. https://doi.org/10.1029/2018WR023939

Kocis, T., Dahlke, H., 2017. Availability of high-magnitude streamflow for groundwater banking in the Central Valley, California. Environ. Res. Lett. 12. https://doi.org/10.1088/1748-9326/aa7b1b

Kolbe, T., De Dreuzy, J.R., Abbott, B.W., Aquilina, L., Babey, T., Green, C.T., Fleckenstein, J.H., Labasque, T., Laverman, A.M., Marçais, J., Peiffer, S., Thomas, Z., Pinay, G., 2019. Stratification of reactivity determines nitrate removal in groundwater. Proc. Natl. Acad. Sci. U. S. A. 116, 2494–2499. https://doi.org/10.1073/pnas.1816892116

Liu, W., Xiong, Z., Liu, H., Zhang, Q., Liu, G., 2016. Agriculture , Ecosystems and Environment Catchment agriculture and local environment affecting the soil denitri fi cation potential and nitrous oxide production of riparian zones in the Han River Basin , China. Agric. Ecosyst. Environ. 216, 147–154. https://doi.org/10.1016/j.agee.2015.10.002

Liu, Yuanyuan, Liu, C., Nelson, W.C., Shi, L., Xu, F., Liu, Yunde, Yan, A., Zhong, L., Thompson, C., Fredrickson, J.K., Zachara, J.M., 2017. Effect of Water Chemistry and Hydrodynamics on Nitrogen Transformation Activity and Microbial Community Functional Potential in Hyporheic Zone Sediment

Columns. Environ. Sci. Technol. 51, 4877–4886. https://doi.org/10.1021/acs.est.6b05018

Mcnicol, G., Bulmer, C., Amore, D.D., Sanborn, P., Saunders, S., Giesbrecht, I., 2019a. Large , climate-sensitive soil carbon stocks mapped with pedology-informed machine learning in the North Pacific coastal temperate rainforest. Environ. Res. Lett. 14.

Mcnicol, G., Bulmer, C., Amore, D.D., Sanborn, P., Saunders, S., Giesbrecht, I., 2019b. Large , climate-sensitive soil carbon stocks mapped with pedology-informed machine learning in the North Pacific coastal temperate rainforest Large , climate-sensitive soil carbon stocks mapped with pedology- informed machine learning in the North Paci f.

Newcomer, T.A., Kaushal, S.S., Mayer, P.M., Shield, A.R., Canuel, E.A., Groffman, P.M., Gold, A.J., 2012. Influence of natural and novel organic carbon sources on denitrification in forest , degraded urban , and restored streams. Ecol. Monogr. 82, 449–466.

Nolan, B.T., Fienen, M.N., Lorenz, D.L., 2015. A statistical learning framework for groundwater nitrate models of the Central Valley, California, USA. J. Hydrol. 531, 902–911. https://doi.org/10.1016/j.jhydrol.2015.10.025

Nolan, B.T., Gronberg, J.M., Faunt, C.C., Eberts, S.M., Belitz, K., 2014. Modeling nitrate at domestic and public-supply well depths in the central valley, California. Environ. Sci. Technol. 48, 5643–5651. https://doi.org/10.1021/es405452q

O'Geen, a. T., Saal, M., Dahlke, H., Doll, D., Elkins, R., Fulton, A., Fogg, G., Harter, T., Hopmans, J.W., Ingels, C., Niederholzer, F., Solis, S.S., Verdegaal, P., Walkinshaw, M., 2015. Soil suitability index identifies potential areas for groundwater banking on agricultural lands. Calif. Agric. 69, 75–84. https://doi.org/10.3733/ca.v069n02p75

Orr, C.H., Predick, K.I., Stanley, E.H., Rogers, K.L., 2014. Spatial Autocorrelation of Denitrification in a Restored and a Natural Floodplain. Wetlands 34, 89–100.

https://doi.org/10.1007/s13157-013-0488-8

Parton, W.J., Holland, E. a., Del Grosso, S.J., Hartman, M.D., Martin, R.E., Mosier, a. R., Ojima, D.S., Schimel, D.S., 2001. Generalized model for NOx and N2O emissions from soils. J. Geophys. Res. 106, 17403. https://doi.org/10.1029/2001JD900101

Schmidt, C.M., Fisher, A.T., Racz, A., Wheat, C.G., Los Huertos, M., Lockwood, B., 2011a. Rapid nutrient load reduction during infiltration of managed aquifer recharge in an agricultural groundwater basin: Pajaro Valley, California. Hydrol. Process. 26, 2235–2247. https://doi.org/10.1002/hyp.8320

Schmidt, C.M., Fisher, A.T., Racz, A.J., Lockwood, B.S., Huertos, M.L., 2011b. Linking denitrification and infiltration rates during managed groundwater recharge. Environ. Sci. Technol. 45, 9634–9640. https://doi.org/10.1021/es2023626

Sebilo, M., Mayer, B., Nicolardot, B., Pinay, G., Mariotti, A., 2013. Long-term fate of nitrate fertilizer in agricultural soils. Proc. Natl. Acad. Sci. U. S. A. 110, 18185–18189. https://doi.org/10.1073/pnas.1305372110

Seitzinger, S., Harrison, J.A., Böhlke, J.K., Bouwman, A.F., Lowrance, R., Peterson, B., Tobias, C., Drecht, G. Van, 2006. Denitrification Across Landscapes and Waterscapes: a Synthesis. Ecol. Appl. 16, 2064–2090.

Šimek, M., Cooper, J.E., 2002. The influence of soil pH on denitrification: Progress towards the understanding of this interaction over the last 50 years. Eur. J. Soil Sci. 53, 345–354. https://doi.org/10.1046/j.1365-2389.2002.00461.x

Soil Survey Staff, Natural Resource Conservation Service, 2016. Soil Survey Geographic (SSURGO) Database [WWW Document]. URL https://sdmdataaccess.sc.egov.usda.gov (accessed 11.3.17).

Tesoriero, A.J., Terziotti, S., Abrams, D.B., 2015. Predicting Redox Conditions in Groundwater at a Regional Scale. Environ. Sci. Technol. 49, 9657–9664. https://doi.org/10.1021/acs.est.5b01869

Tomich, T.P., Brodt, S.B., Dahlgre, R.A., Scow, K.M., 2016. The California nitrogen

assessment: Challenges and solutions for people, agriculture, and the environment, First. ed. University of California Press, Oakland, CA.

Wang, B., Hipsey, M.R., Ahmed, S., Oldham, C., 2018. The Impact of Landscape Characteristics on Groundwater Dissolved Organic Nitrogen: Insights From Machine Learning Methods and Sensitivity Analysis. Water Resour. Res. 54, 4785–4804. https://doi.org/10.1029/2017WR021749

Wheeler, D.C., Nolan, B.T., Flory, A.R., DellaValle, C.T., Ward, M.H., 2015. Modeling groundwater nitrate concentrations in private wells in Iowa. Sci. Total Environ. 536, 481–488. https://doi.org/10.1016/j.scitotenv.2015.07.080

Zarnetske, J.P., Bouda, M., Abbott, B.W., Saiers, J., Raymond, P.A., 2018. Generality of Hydrologic Transport Limitation of Watershed Organic Carbon Flux Across Ecoregions of the United States. Geophys. Res. Lett. 45, 11,702-11,711. https://doi.org/10.1029/2018GL080005

Table 3-S1 Summary of denitrification data used to create model

	Experiment al scale	n[a]	ΔNO_3 [b] (mg/L)	$[NO_3]_s$ (mg/L)	$[DOC]_s$ (mg/L)	TOC[c] (% wt)	TN (% wt)	Clay (%)	Silt (%)	Sand (%)	SRT (hrs)
Site 1	ercolation tes	6	0.2	23.15	26.01	0.04	0.01	2.11	4.28	93.6	1.69
			-1.1	-1.11	-1.06						-0.9
	IAR operatio	62	0.24	0.96	15.18	0.34	0.03	5.57	3.91	90.52	13.36
			-1.12	-1.82	-7.3	-0.07	-0.01	-1.55	-1.03	-2.54	-14.31
Site 2	olumn studi	53	0.32	3.15	1.32	0.36	0.03	7.62	9.67	82.71	14.29
			-1	-2.06	-0.36						(6.00 - 42.86)[d]
Site 3	olumn studi	23	1.59	31.19	29.79	0.57	0.05	15.67	39.62	44.71	50
			-1.7	-0.95	-3.89						(9.09 - 81.81)[d]
	ercolation tes	6	0.9	23.96	1.94	0.57	0.05	15.11	31.52	53.37	39.51
			-0.98	-1	-0.24						-2.88
Site 4	olumn studi	37	0.27	2.83	1.57	0.18	0	15.6	16.25	68.14	12.86
			-0.72	-0.82	-0.84						(6.67 - 28.13)[d]

[a] number of individual measurements of nitrate removal

[b] median values are reported for each experiment, and standard deviations are given in parentheses

[c] soil properties (TOC, TN, %Clay, %Silt, and %Sand) were measured once for each experiment except MAR operations, therefore they do not have a measure of variance

[d] during the column experiments, SRT was manipulated to determine the effect on denitrification, therefore ranges are reported

Table 3-S2 Estimated runoff nitrate concentrations

NLCD Code	Land use	$[NO_3]_s$ (mg/L)
11	Open Water	1
21	Developed, Open Space	5
22	Developed, Low Intensity	5
23	Developed, Medium Intensity	5
24	Developed, High Intensity	5
31	Barren Land (Rock/Sand/Clay)	1
41	Deciduous Forest	1
42	Evergreen Forest	1
43	Mixed Forest	1
52	Shrub/Scrub	1
71	Grassland/Herbaceous	1
81	Pasture/Hay	5
92	Cultivated Crops	15
90	Woody Wetlands	1
95	Emergent Herbaceous Wetlands	1

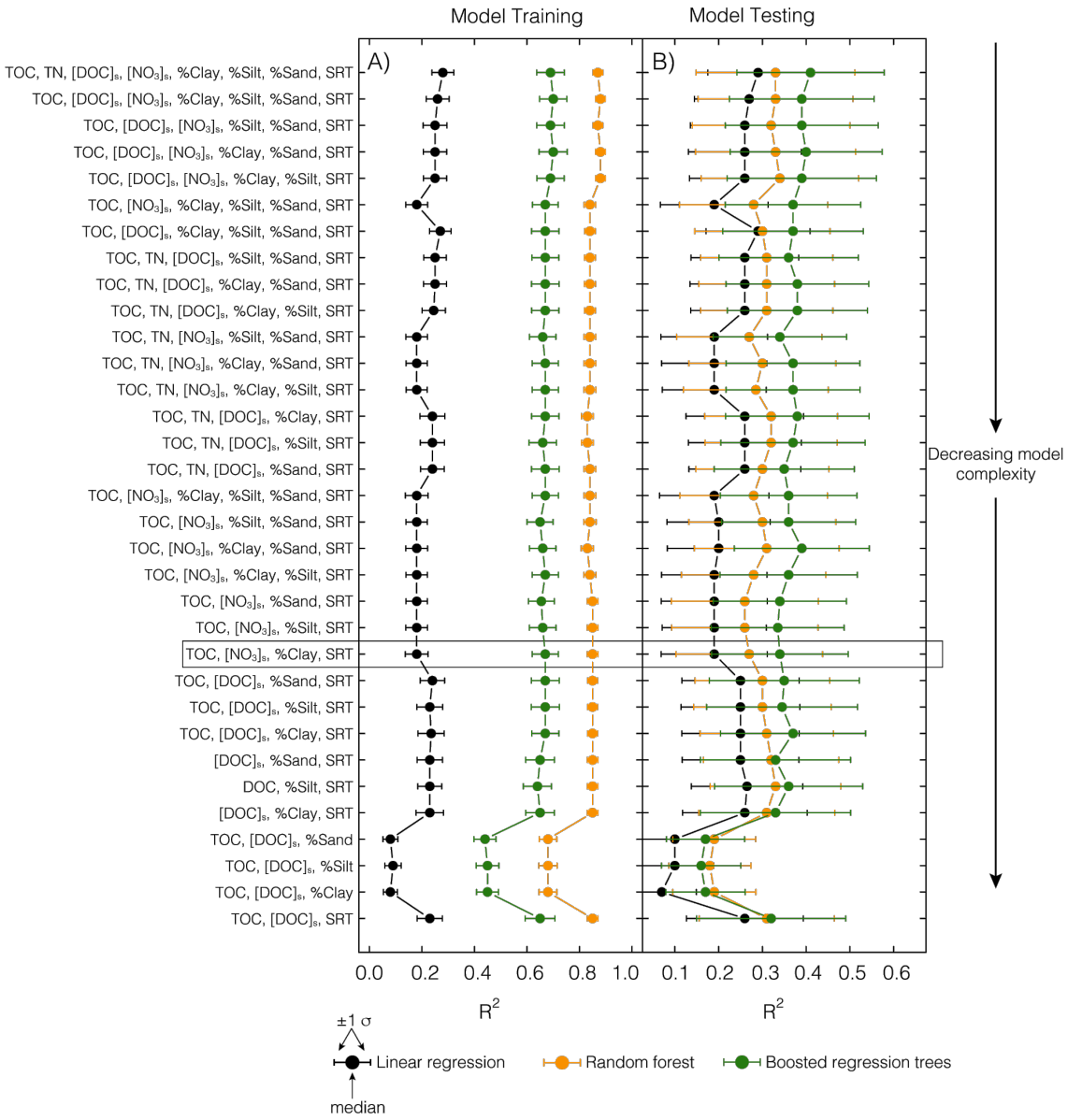

Figure 3-S1 Median R^2 statistics for 1000 realizations of 33 different predictor combinations to test the sensitivity of the training-testing split for three modeling approaches. Model complexity generally decreases going down. Error bars represent +/- 1 standard deviation. Box shows preferred covariate set using four parameters.

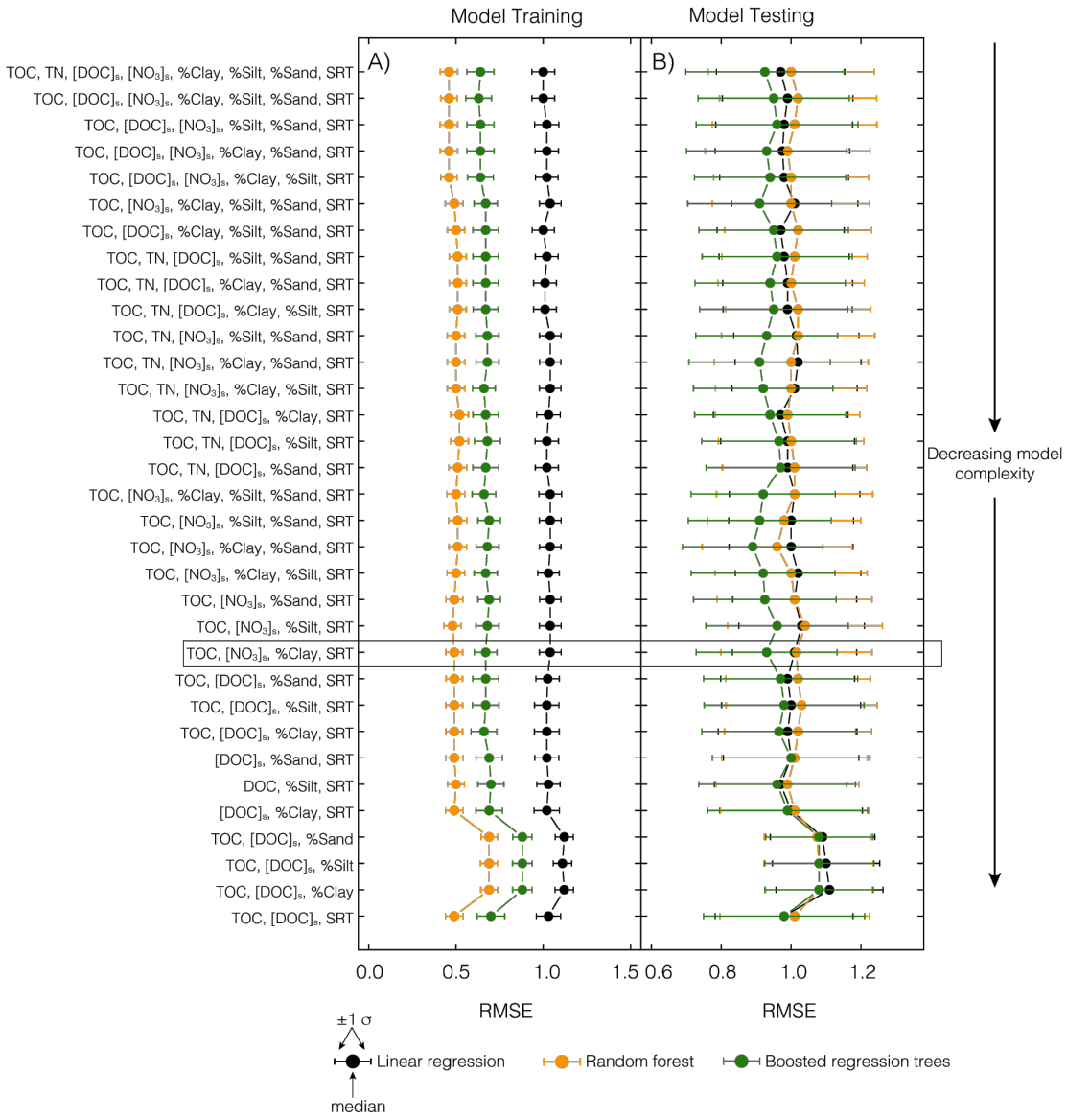

Figure 3-S2 Median RMSE for 1000 realizations of 33 different predictor combinations to test the sensitivity of the training-testing split for 3 different modeling approaches. Model complexity generally decreases going down. Error bars represent +/- 1 standard deviation. Box shows preferred covariate set using four parameters.

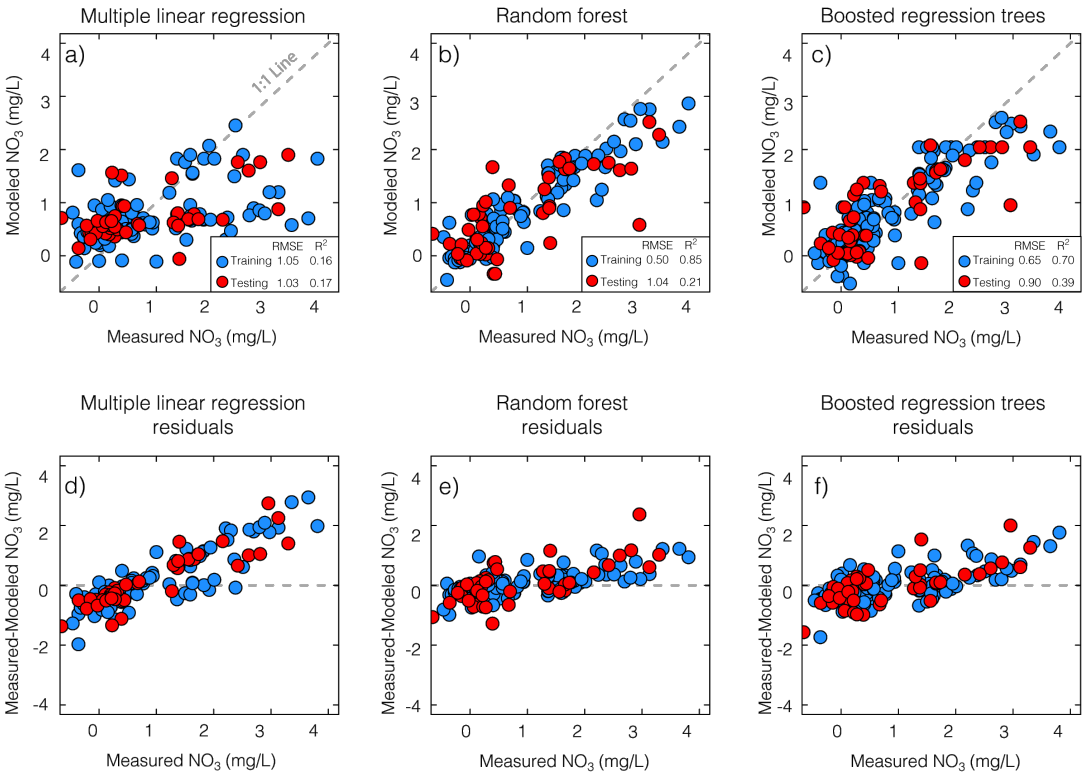

Figure 3-S3 Model performance for predictor set (%Clay, TOC, SRT, and $[NO_3]_s$) that showed median model performance in the testing dataset for random forest and boosted regression trees

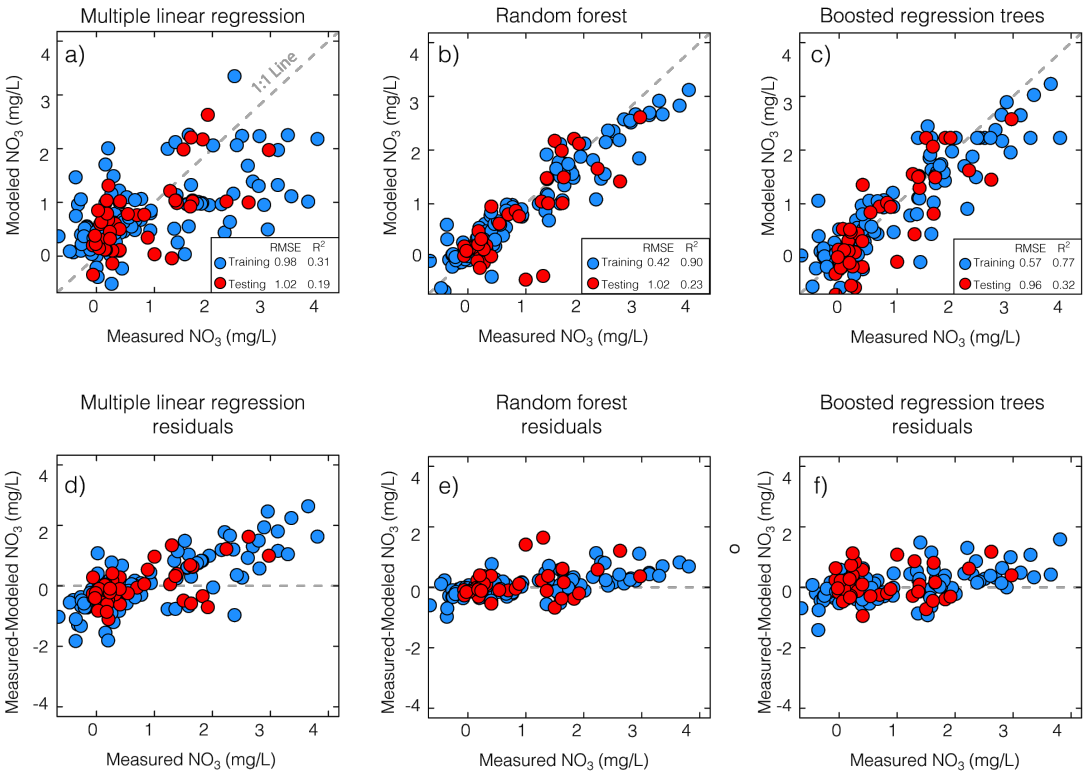

Figure 3-S4 Model performance for full predictor set (%Sand, %Silt, %Clay, TOC, TN, SRT, $[DOC]_s$, and $[NO_3]_s$) that showed median model performance in the testing dataset for random forest and boosted regression trees

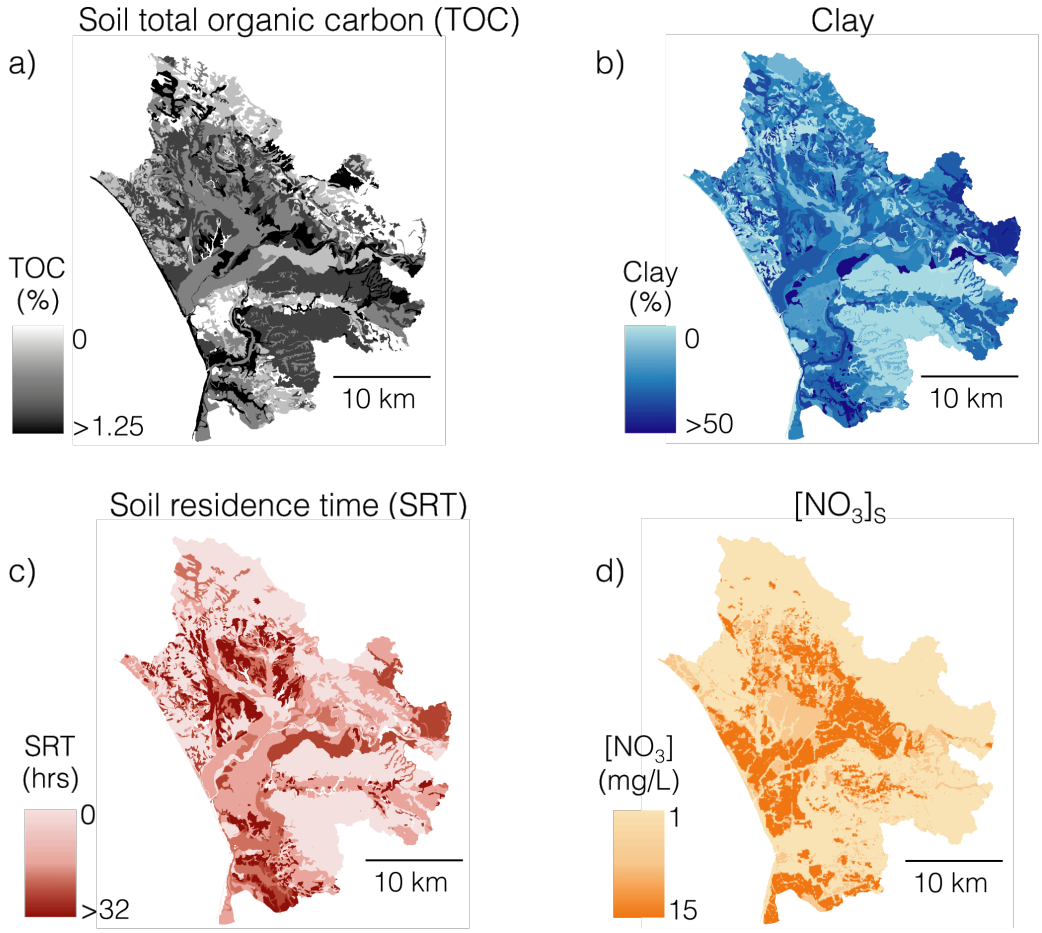

Figure 3-S5 Maps of predictor variables used for the final model. Soil total organic carbon (a), Percent Clay (b), soil residence time (c), and initial nitrate concentration, $[NO_3]_S$ (d).

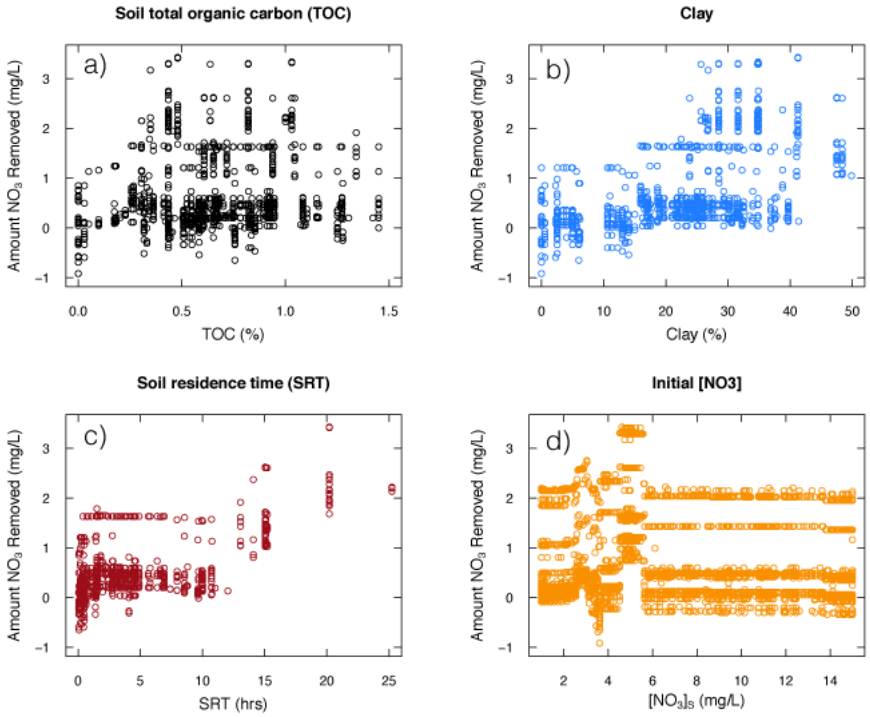

Figure 3-S6 Cross plots of the response variable Amount of [NO3] removed against the four predictor variables used for spatial model a) TOC b) clay c) SRT and d) $[NO_3]_S$. For clarity 5% of the total data are shown.

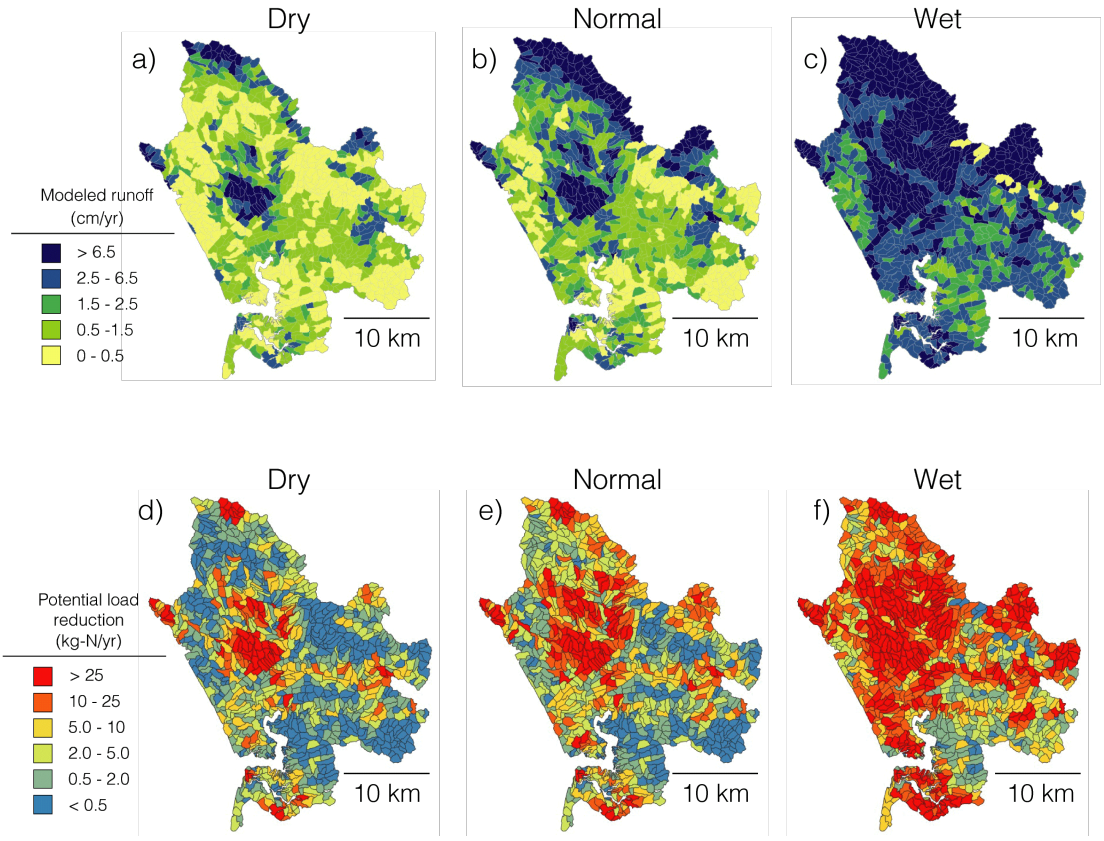

Figure 3-S7 Modeled hillslope runoff from (Beganskas et al., 2019a) for (a) "dry", (b) "normal", and (c) "wet" precipitation scenarios and corresponding potential nitrate load reduction for (d) "dry", (e) "normal", and (f) "wet" precipitation

Chapter Four

HYDROLOGIC REGIMES DRIVE NUTRIENT EXPORT BEHAVIOR IN HUMAN IMPACTED WATERSHEDS

In Prep: Gorski G., Zimmer M. A., (2020) Hydrologic regimes drive nutrient export behavior in human impacted watersheds.

Abstract

Nitrogen export from agricultural landscapes has detrimental effects on downstream human and ecosystem health. Identifying mitigation strategies and measuring their efficacy requires a better understanding of the underlying hydrologic drivers of nitrate mobilization. Currently there is a mismatch in time scale between hydrologic drivers (e.g., storms, high flow periods), which are on the order of days, events, and seasons, and common measurement schemes, which are often weekly or monthly. However, the recent deployment high frequency (daily) in-situ nitrate sensors facilitates the tracking of high temporal resolution water quality dynamics not previously possible. We analyzed daily nitrate concentration (c) and discharge (Q) data over a four-year period (2016-2019) from five nested, agricultural watersheds in the Midwestern United States. We partitioned the hydrograph into stormflow and baseflow periods and examined the nitrate export patterns of those periods separately through the analysis of their concentration-discharge c-Q relationships. Baseflow showed consistently positive c-Q chemodynamic slope, while stormflow c-Q relationships showed a much weaker chemostatic pattern. This suggests that water source contributions during baseflow are nonstationary. Anomalous flow periods during baseflow conditions greatly influenced overall c-Q patterns, suggesting that understanding event-scale characteristics is critical when interpreting seasonal or annual patterns. The watersheds span two distinct landforms shaped by differences in geologic history resulting in natural sol properties that necessitated different drainage infrastructure across the study area. The density of built drainage infrastructure was a

strong predictor of c-Q relationship and nitrate load, with more drainage infrastructure associated with higher loads and more chemostatic export patterns across all watersheds. This suggests that how humans 'replumb' the subsurface in response to geologic conditions has implications for hydrologic connectivity, homogenization of source areas, and subsequently nutrient export.

4.1 Introduction

Excess nutrient export can have detrimental effects on human health and ecosystem function, by contaminating drinking water (Weyer et al., 2001) and contributing to harmful algal blooms (Howarth, 2008), hypoxia (Jenny et al., 2016), and loss of species diversity in receiving bodies (Diaz and Rosenberg, 2008). For example, the Upper Mississippi River Basin contributes the majority of nutrients exported to the Gulf of Mexico (Turner et al., 2012), which experiences expansive eutrophication and dead zones each spring and summer (Rabalais et al., 2010). Mitigating these negative effects requires a deeper understanding of the complicated connections between anthropogenic, hydrologic, and biogeochemical forcings that drive nutrient mobilization and retention in contributing watersheds.

An effective method for disentangling these driving factors is examining the relationship between solute concentration and stream discharge (c-Q relationships) as a means for characterizing a watershed's tendency to transport or retain nutrients (Godsey, 2009; Thompson et al., 2011). When viewed in log-log space, solute concentration and discharge often vary linearly according to a slope (b), which can be

used to describe the relative tendency of a contributing area to transport or retain the solute (Basu et al., 2010; Musolff et al., 2017). Slopes near zero ($|b| \leq 0.2$) indicate chemostatic behavior in which solute concentration varies little in response to changes in discharge. Chemostatic conditions can arise when contributing areas have uniform solute concentrations, as is often seen with nitrate (NO_3^-) in areas with intensive agriculture (Bieroza et al., 2018; Thompson et al., 2011). In contrast, chemodynamic behavior is characterized by slopes different from zero in which the solute concentration is sensitive to changes in discharge. Chemodynamic conditions can arise from source areas with more heterogeneous solute concentrations which may become activated under different hydrologic conditions (i.e. variations in Q) (Dupas et al., 2019). The c-Q relationship can be characterized as an enrichment pattern if the slope is positive ($b > 0.2$) or a dilution pattern if the slope is negative ($b < -0.2$).

Given the connection between c-Q relationships and the controlling processes, researchers have calculated c-Q relationships across river systems to better understand the role of fluctuating source area contributions to riverine transport. For example, c-Q relationships were used to examine the effects of decadal shifts in land use and agricultural practices on nitrogen loading in a series of nested agricultural catchments (Ehrhardt et al., 2019). In that study, the authors observed a systematic shift from chemodynamic to chemostatic export patterns as a result of an increase in agricultural intensity. Additionally, c-Q relationships have been used to infer information about changes in solute source regions and flow paths in response to precipitation patterns and climatic forcings (Lloyd et al., 2016; Musolff et al., 2017).

The accessibility of data from high frequency sensor networks allows us to explore these relationships at a time scale previously difficult to observe. Most studies investigate c-Q relationships at annual or inter-annual time scales or by aggregating discrete data points (Botter et al., 2019; Ehrhardt et al., 2019; Minaudo et al., 2019) . Recent studies have recognized that c-Q relationships vary as a function of flow percentile (Diamond and Cohen, 2018; Marinos et al., 2020; Moatar et al., 2017; Zimmer et al., 2019). However, few studies have investigated event-scale c-Q relationships (Dupas et al., 2016; Rozemeijer et al., 2010). Without this fine temporal scale information, it is difficult to understand when exactly solutes are exported and if stormflow of similar magnitudes across different seasons have similar export dynamics. Here, we use publicly available daily measurements of discharge and NO_3^- concentration to investigate c-Q dynamics at event and seasonal scales, and spatial and temporal patterns of NO_3^- export in agricultural watersheds.

4.1 Methods

4.2.1 Site description

The Raccoon River watershed drains 8870 km^2 of low-relief, heavily agricultural area in central Iowa, USA typical of much of the Midwestern United States (Figure 4-1). It is made up of the North Raccoon River watershed (USGS HUC: 07100007) and the South Raccoon River watershed (USGS HUC: 07100006).

The area is subdivided into a series of five nested watersheds shown in Figure 1; the Upstream Sac City (*USC*) and the Middle Redfield (*MRF*) on the North Raccoon

River, the Upstream Panora (*UPN*) on the Middle Raccoon River, the Middle Jefferson (*MJF*) on the South Raccoon River, and the Downstream Van Meter (*DVM*), which is below the confluence of the three major tributaries draining the area. The *MJF* is inclusive of *USC*; *MRF* is inclusive of *UPN*, and *DVM* is inclusive of the entire Raccoon River watershed. Like much of the Midwest, agricultural production is the dominant land use in all five watersheds ranging from 85-92% of land use (Table S2), the vast majority of which is corn (*Zea mays L.)* and soybeans (*Glysine max L.)*.

The Raccoon River watershed is marked by a stark divide in landforms driven by Quaternary glaciations, with the majority of the area underlain by glacial sediments deposited by the Des Moines Lobe during the last glaciation of the region approximately 12,000 years ago (Prior, 1991). These areas are characterized by poorly developed surface drainage networks and ephemeral surface water bodies. As a result, extensive tile drainages, ditches, and canals have been installed and constructed in the latter half of the 20th century to drain excess water from the subsurface (Figure 4-1). The southwestern portion of the Raccoon River watershed lies within the Southern Iowa Drift Plain, an area that was shaped by 500,000-year-old glacial advances that extended south into present day Missouri (Prior, 1991). This portion of the watershed is characterized by steeper topography and more well-developed drainage networks, which require less drainage infrastructure such as tile drains, ditches, and canals. *UPN*, *MRF*, and *DVM* drain areas that overlay both the Des Moines Lobe and the Southern Iowa Drift Plain.

The Raccoon River watershed is characterized by cold dry winters and warm wet summers, with an average annual precipitation of 850 mm (1981-2010; PRISM), the majority of which falls between April and October as rain.

4.2.2 Datasets

We analyzed in situ mean daily nitrate (NO_3^-) concentration (c) and discharge (Q) data from the outlet of each watershed at gaging stations maintained by the U.S. Geologic Survey for *USC* (05482300), *MRF* (05483600), *MJF* (05482500), and *DVM* (05484500), and from the Iowa Institute of Hydraulic Research (IIHR) for *UPN* (WQS0032). To retrieve data, we used the dataRetrieval package in R (v 3.6.0) through the National Water Information System (De Cicco et al., 2018). Data for *UPN* was obtained directly from the IIHR. We analyzed daily discharge and NO_3^- data from January 2016 to December 2019, during which discharge records were complete for all sites and nitrate records had > 88% coverage for all sites except *UPN*, which had 72% coverage (Table 4-S1). At each gaging station, NO_3^- concentrations were measured at 15-minute resolution (5-min for *UPN*) using Hach Nitratax plus sc probes (Hach, Loveland, CO) and aggregated to daily average NO_3 concentration for this study.

To analyze land use characteristics for each watershed, we downloaded land use data from the National Landcover Database at a 30 m x 30 m resolution (Dewitz, 2019). Land use data were binned into four categories; water/wetlands, developed, forested/barren/shrubs, and crops (including pasture). Data for landforms, drainage infrastructure, and stream network were downloaded from the Iowa Department of Natural Resources. We downloaded daily precipitation data for the four-year period of

analysis (2016-2019) for four sites within the Raccoon River watershed from the NOAA National Centers for Environmental Information.

4.2.3 Event identification

We separated the discharge time series into baseflow and stormflow through semi-automating storm event identification using the following criteria: 1) $dQ/dt \geq$ 1e-4 cfs/second for the rising limb of the event, 2) $\max(Q_{event}) \geq 0.01 * \max(Q_{record})$, and 3) the event duration $\geq$ 3 days. The end of each event was determined when either the event falling limb $dQ/dt \geq 0$ or discharge returned to pre-event levels. For some, such as events that showed up as shoulder peaks on larger events, or those with indistinct peaks, visual inspection and subjective decisions were required (Figure 4-S1). The criteria were derived from similar studies (Dupas et al., 2016; Knapp et al., 2020; Rozemeijer et al., 2010), and exact thresholds for the criteria were tuned and adapted for the structure and dynamics of the watersheds' hydrographs to ensure the selection of peaks. Time periods identified as storm events were classified as stormflow, and all other times were classified as baseflow.

We note that this classification scheme differs from traditional baseflow separation techniques that use graphical, geochemical or isotopic approaches to identify the baseflow component in the hydrograph (Hooper and Shoemaker, 1986; Klaus and McDonnell, 2013). Baseflow separation techniques have shown that a large fraction of event water is derived from baseflow(Schilling and Zhang, 2004). Our goal is not to contradict or supplant this finding, but rather to illustrate how a simple

partitioning of the hydrograph based on peaks in discharge can result in a deeper understanding of nutrient export dynamics.

4.2.4 Characterizing export patterns

Export patterns (chemostatic, dilution, or enrichment) were calculated for stormflow, baseflow, and the full record (herein referred to as stormflow+baseflow) for the full period of analysis and on a seasonal basis. Concentration-discharge relationships for baseflow and stormflow+baseflow periods were calculated by aggregating data for the time period of interest. Stormflow c-Q relationships were calculated in two ways; first by aggregating data over the time period of interest, and second, by calculating c-Q relationships for each individual event and averaging those values over all events (Figure 4-S4). The former will be referred to as bulk stormflow c-Q characteristics, and the later will be referred to as event-averaged c-Q characteristics.

Seasonal and annual calculations were made based on the water year which begins on October 1st, and the year was divided seasonally into fall (October, November, December), winter (January, February, March), spring (April, May, June), and summer (July, August, September).

4.2.5 Load estimations

Cumulative NO_3^- load estimates were calculated for each hydrologic regime (stormflow, baseflow, stormflow+baseflow) on an annual and seasonal basis as:

$$\sum_{i=1}^{n} {}^{c_i Q_i}/_{f} \quad [4.2]$$

where c_i and Q_i are the daily NO_3^- concentration and discharge values, and f is the fraction of data coverage for the period of interest. If data were missing during a period, baseflow and stormflow loads were calculated based on their fractional contribution during the periods with data. All annual periods had $f > 0.75$, but some seasonal periods had low coverage, for seasonal periods where $f \leq 0.75$ no load estimate was calculated.

4.3 Results and Discussion

4.3.1 Annual, seasonal, and event variation in flow and nitrate concentration

In all five watersheds, 44-52% of the analysis period was classified as stormflow, with an average of 14-17 storm events per year (Table 4-1). While the proportion of stormflow periods was similar between watersheds, the fraction of flow that was partitioned into stormflow and baseflow varied considerably between watersheds. *MJF* and *USC* had the highest proportion of stormflow, with 77.0 and 73.4% of annual flow classified as stormflow, respectively, compared to 62.4 and 63.9% in *UPN* and *MRF*, respectively (Table 4-1). This observation is consistent with the higher density of drainage infrastructure (e.g. canals, tile drainage) in *USC* and *MJF* leading to quicker routing of high flows to the stream channel compared to more developed, natural drainage networks in *UPN* and *MRF*.

Flow in all watersheds exhibited strong seasonality, with an average of 42.9% of total flow delivered in the spring. Summer months contributed the least to overall discharge with an average of 17.3% across all watersheds. Despite differences in

overall flow between the seasons, spring and summer showed a similar number of events across all watersheds (average of 5.5 in spring and 4.4 in summer; Student's t-test; $p > 0.01$), suggestive that spring events were higher magnitude. Differences in event size between the two seasons is likely due to spring snowmelt, rain on snow events which can produce excess runoff, and increased crop growth in the summer months leading to more water retention.

The outlet of the largest watershed showed mean NO_3^- concentrations of 7.2±3.1 mg/L during 2016-2019. The heavily tile-drained *USC* watershed showed the highest average NO_3^- concentration (9.56±3.09 mg/L), while *MRF*, which has the least drainage infrastructure, showed the lowest (6.77±2.51 mg/L; Table 4-S3). This is consistent with observations of increased stream NO_3^- concentrations at the outlets of heavily tile-drained Iowa watersheds compared to those with more natural drainage structures (Schilling et al., 2012).

In all watersheds, NO_3^- concentrations were higher during stormflow periods than baseflow periods, and differences were statistically significant (Student's t-test; $p < 0.01$) for all watersheds, except *USC*, which has the highest drainage infrastructure density (Figure 1). NO_3^- concentrations exhibited pronounced seasonality in both stormflow and baseflow, with annual maxima during the spring and minima during the summer months (Figure 4-S2).

Spring highs are most likely driven by the timing of growing season fertilizer, and nutrient flushing associated with heavy spring rains (Royer et al., 2006; Van Meter et al., 2020). Summer lows often occur during low flow periods which are associated

with contributions from groundwater flowpaths with longer residence times, more streambed-water interaction, and warmer temperatures, all positively associated with biological nitrogen uptake activity (e.g. denitrification and assimilation) that can lower NO_3^- concentrations (Moatar et al., 2017). High flow periods reduce the ability of these biological processes to impact NO_3^- concentrations (Rodríguez-Blanco et al., 2015; Royer et al., 2006). This seasonality of NO_3^- concentration has been previously observed in the Raccoon River watershed (Schilling and Zhang, 2004), as well as other agricultural catchments in the Midwest (Dupas et al., 2017; Pellerin et al., 2014; Van Meter et al., 2020).

4.3.2 Shifting hydrologic regimes drive c-Q patterns across watersheds

Concentration-discharge relationships showed a distinct difference between bulk stormflow and baseflow periods, with stormflow periods showing lower b values across all five watersheds (Figure 4-2). Enriching chemodynamic export patterns ($b > 0.2$) were observed during baseflow periods in all watersheds (Figure 4-2A-E), with *UPN* showing the strongest enrichment signal ($b = 0.79$) and *USC* showing the weakest ($b = 0.21$). The observation that low flow periods tend to exhibit more chemodynamic behavior than high flow periods is consistent with other studies that have partitioned the hydrograph seasonally (Ehrhardt et al., 2019), by breakpoint analysis (Marinos et al., 2020), or by median discharge (Moatar et al., 2017), suggesting that this is a general feature of watershed hydrologic routing.

In *MJF*, a period of anomalously low flow (mean = 96 cfs; < 0.1 flow percentile) and low nitrate concentration (mean = 0.05 mg/L; < 0.1 NO_3^- concentration percentile) from 07/26/2017-10/19/2017 had a dramatic impact on the baseflow c-Q relationship (Figure 4-S3D). Inclusion of the data from this period resulted in b = 1.42, indicating very strong enrichment behavior. Removal of the data from this period decreased the b value to 0.42. The ability of a single anomalous period to influence the overall characterization of a hydrologic system highlights the difficulty of representing nutrient export behavior based on a single parameter fit across several seasons and flow regimes (Diamond and Cohen, 2018; Dupas et al., 2017; Marinos et al., 2020). While we do not include this period in further discussion of nutrient export behavior, we do include it in our estimates of annual and seasonal nitrate load, though it has little effect on our overall load estimates.

Seasonal analysis of baseflow c-Q relationships shows that the strongest chemodynamic enrichment patterns occur in the summer across all watersheds, while the most chemostatic season is generally the spring (Figure 4-2). This pattern varies somewhat throughout the smaller watersheds (e.g. *UPN* and *USC*; Figure 4-2A-B) but is exemplified in *DVM*, which integrates the signal from the other four watersheds (Figure 4-2E). The summer baseflow period in *DVM* is strongly enriching (b = 0.75), while in spring, baseflow is chemostatic (b = 0.08). This pattern is driven by differences in baseflow NO_3^- concentration from spring to summer, suggesting differences in the sourcing or internal processing of baseflow from one season to the next (Richardson et al., 2020).

Regardless of season, storms contribute flow to streams generally through shallow, quick flow paths that intersect high nitrate stores in these agriculturally intensive landscapes (Buda and DeWalle, 2009; Mellander et al., 2012). Seasonally averaged stormflow periods generally show chemostatic patterns throughout the year and bulk annual stormflow b values range from 0.05 – 0.30, suggesting that stormflow periods may exhibit weak chemodynamic behavior (Figure 4-2). The b values of individual storm events have approximately normal distributions with mean values from -0.02 to 0.02, but there are individual events which show strong chemodynamic behavior ($|b| > 1$) (Figure 4-S4).

4.3.3 Seasonal patterns in nitrate load across watersheds

Partitioning the hydrograph into stormflow and baseflow periods allows the identification of periods which contribute disproportionately to watershed NO_3^- export (Figure 4-3). Annual average NO_3^- export across the study watersheds ranged from 4216±768 kg-N/km^2/yr in *USC* to 2222±371 kg-N/m^2/yr in *MRF*.

Spring stormflow periods accounted for the largest contribution to annual load across all watersheds with an average of 37.5±11.5% for all years. Spring stormflow contributions showed a large spatiotemporal range, from 19.7% in *UPN* in 2016 to 59.8% in *DVM* in 2017. Summer stormflow loads also showed considerable variation, with an average contribution of 9.4% of annual load, but ranging from < 1% (19.4 kg-N/km^2/yr) in 2017 to 18.3% (711 kg-N/km^2/yr) in 2018.

These observed ranges in NO_3^-loads are largely driven by observed variation in summer precipitation (Figure 4-1). For example, in the summer of 2017, which had an anomalously low NO_3 load, there were fewer precipitation events than average. Specifically, there was an average of 1.8 events across the watersheds with zero events identified in *USC* and *MJF*. In contrast, there was an average of 6.0 events across all five watersheds in summer 2018. Additionally, the events in summer 2017 were approximately 22% the size of the events in summer 2018. This variability highlights the difficulty in predicting loads across seasons, hydrologic regimes and watersheds.

Baseflow loads were more consistent between seasons, rarely making up > 15% of the annual load in each watershed. Baseflow loads typically peaked in the spring months, likely due to a seasonally high water table, which increased shallow groundwater contribution to streams (Jiang et al., 2010; Molenat et al., 2008). Additionally, spring fertilizer application and plowing can increase surface leaching, increasing the nitrate pool in the shallow subsurface (Royer et al., 2006).

4.3.4 Nutrient export is driven by the spatial distribution of land use types and hydrologic infrastructure

There is a systematic trend toward higher NO_3^- load in watersheds with a higher density of built drainage infrastructure (Figure 4-4), consistent with other studies (Basu et al., 2010; Musolff et al., 2015; Schilling and Zhang, 2004). The slope of the relationship between NO_3^- load and drainage infrastructure density is much shallower for baseflow than for stormflow given the greater range in observed stormflow load across the watersheds (Kennedy et al., 2012). Drainage structures and tile drains route

water from high NO_3^- source areas directly to the stream, decreasing travel time and bypassing riparian areas that are highly active in nutrient processing (Dosskey et al., 2010). These structures are common features in agricultural landscapes and show strong correlation to the amount of cropped area across the five watersheds analyzed ($R^2 = 0.95$).

The short circuiting of subsurface flow paths and increased cropped area drives watershed nutrient export patterns towards chemostatic behavior by homogenizing the source regions and limiting nutrient cycling during transport (Marinos et al., 2020; Musolff et al., 2015; Thompson et al., 2011). These patterns are most clear during storm periods in the spring months, when tile drains likely have their greatest influence on hydrologic routing. During these periods, stormflow NO_3^- loads are strongly correlated with drainage infrastructure density ($R^2 = 0.88$; Table S4) and stormflow export regimes are chemostatic (average b = 0.15).

In contrast, summer baseflow periods showed the strongest chemodynamic enrichment patterns with average b = 0.73 across all watersheds. The NO_3^- load during these periods is most strongly correlated with the percentage of cropped area within 100 m of the stream ($R^2 = 0.94$; Table 4-S4). This suggests that summer chemodynamic regimes are driven by low flow, low NO_3^- periods where source areas that are proximal to the stream are contributing more significantly to discharge (Molenat et al., 2008). This is further supported by the strong correlation between baseflow NO_3^- loads and cropped area within 100 m of the stream ($R^2 = 0.90$; Table 4-S4). Lower density of

agricultural activity in riparian areas (Table 4-S2), leads to more heterogeneous source regions, which promotes load nitrate load and the observed chemodynamic behavior.

Seasonal and annual c-Q slopes across all hydrologic regimes show only weak correlations with watershed area suggesting that drainage infrastructure, and the distribution and intensity of agriculture are the dominant drivers of NO_3^- export regime in these watersheds, consistent with a recent study of 33 agricultural watersheds in the Midwest (Marinos et al., 2020). Our results show that both conditions that lead to high NO_3^- loads, whether hydrologic (i.e. stormflow) or landscape (i.e. increases in drainage infrastructure and agricultural intensity) are associated with chemostatic behavior. This trend is in line with the idea that landscapes with such agricultural intensity are a saturated solute source whose delivery is flow-limited (Thompson et al., 2011).

4.4 Conclusions

Detailed analysis of event, seasonal, and annual NO_3^- export demonstrated that all five heavily agricultural watersheds have similar temporal patterns of NO_3^- load with highs in spring stormflow and lows in summer baseflow. Spring storm flows were largely chemostatic and account for ~40% of annual loads, while low summer flows drive baseflow periods of chemodynamic enrichment, suggesting that the systems dynamically, but predictably, shift between NO_3^- export patterns in response to hydrologic forcing. There was a systematic trend toward more chemostatic behavior and higher NO_3^- loads with increasing density of drainage infrastructure and agricultural land use across the five watersheds, emphasizing the anthropogenic

controls on nitrate export in these watersheds. During baseflow conditions, land use near the stream has a large impact on NO_3^- loads indicating that buffer strips or other near stream near-stream management practices might reduce loads during these periods.

Analysis of a specific low-flow period demonstrated that a single anomalous period has the power to significantly affect our classification of export patterns and influence our understanding of watersheds as a whole. This highlights the dynamic nature of these systems and argues for event, seasonal, and longer-term analyses of nutrient export, particularly when attempting to measure the efficacy of management practices such as reductions in fertilizer application or buffer strips. High resolution hydrochemical observations allow the measurement of storm events which facilitate more accurate estimates of NO_3^- loads that were previously measured using regression-based techniques with sparse sample resolution. This study demonstrates the utility of high spatial and temporal resolution water quality sampling to disentangle the key factors controlling watershed nutrient export as well as the important role of state and federal water quality monitoring programs in addressing important water quality issues.

ACKNOWLEDGEMENTS

The authors would like to thank the Iowa Institute of Hydraulic Research for generously providing data.

FUNDING

This work was supported by the National Science Foundation Graduate Research Fellowship Program.

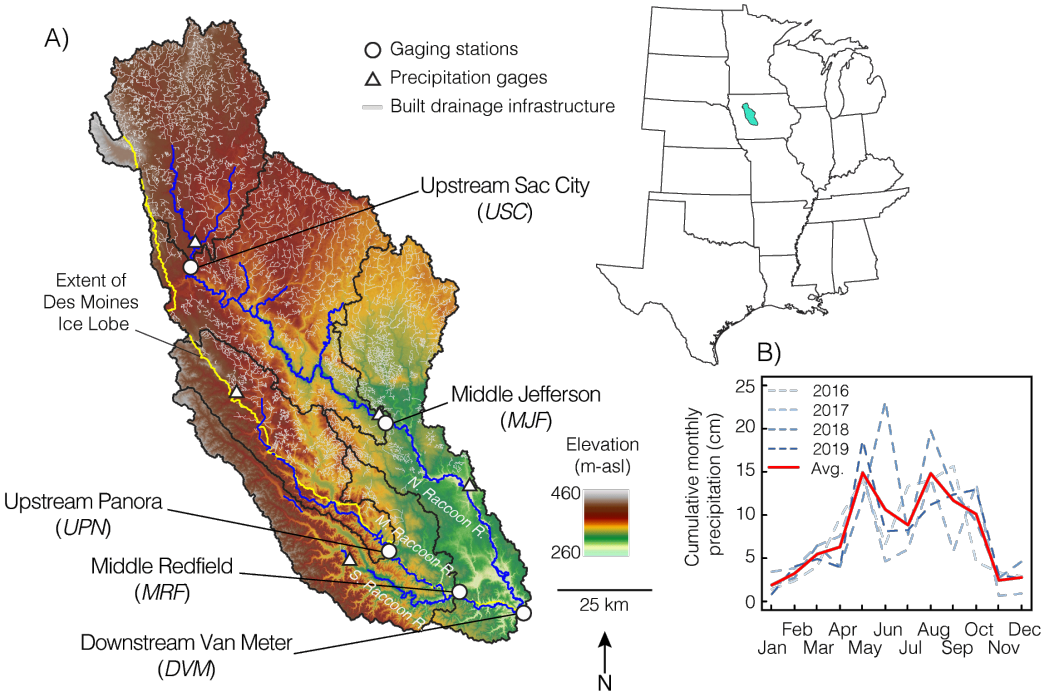

Figure 4-1 A) Map of five watersheds (black outlines) analyzed in central Iowa along the North, Middle and South Raccoon Rivers. *MJF* is inclusive of *USC*, *MRF* is inclusive of *UPN*, and *DVM* is inclusive of the entire watershed pictured. The yellow line maps the extent of the Des Moines Lobe in the last glaciation. Areas to the southwest of the line lie in the Southern Iowa Drift Plain. Built drainage infrastructure is shown in gray. Gaging stations (white circles) are along the North and Middle Raccoon Rivers (blue lines), the *DVM* gaging station is below the confluence of the branches of the Raccoon Rivers. Four precipitation gages are shown with white triangles. Precipitation data were averaged on a monthly basis across the four-year study period (2016-2019), and shown in (B); the red line indicates the monthly averages across the four years.

Table 4-1 – Watershed hydrologic characteristics

Watershed	Area	Stormflow discharge[a]	Baseflow discharge[a]	Stormflow events	OND	JFM	AMJ	JAS
	(km^2)	(%)	(%)	(events/yr)	(events/yr)	(events/yr)	(events/yr)	(events/yr)
UPN	1116	62.4	32.3	14.3	3.3	1.3	5	5
		-9.3	-5.5	-1.7	-1.5	-0.6	-0.8	-2.2
USC	1840	73.4	26.6	15	3	3	5.8	3.3
		-3.5	-3.6	-3.6	-1.4	-1.8	-2.5	-2.8
MRF	2548	63.3	36.8	16.8	3.8	2.3	5	5.8
		-4.9	-4.1	-1.3	-1	-1	-0.8	-1.7
MJF	4188	77	23.1	14.3	3.7	2.3	5.5	3.8
		-6.1	-5.3	-3.9	-1.6	-1.9	-1.3	-3.3
DVM	8870	72.9	27.1	15.8	3	2.3	6.3	4.3
		-6.7	-4.6	-5.1	-1.9	-1	-1.3	-2.8

[a] as a percent of total annual discharge, standard deviations are reported in parentheses

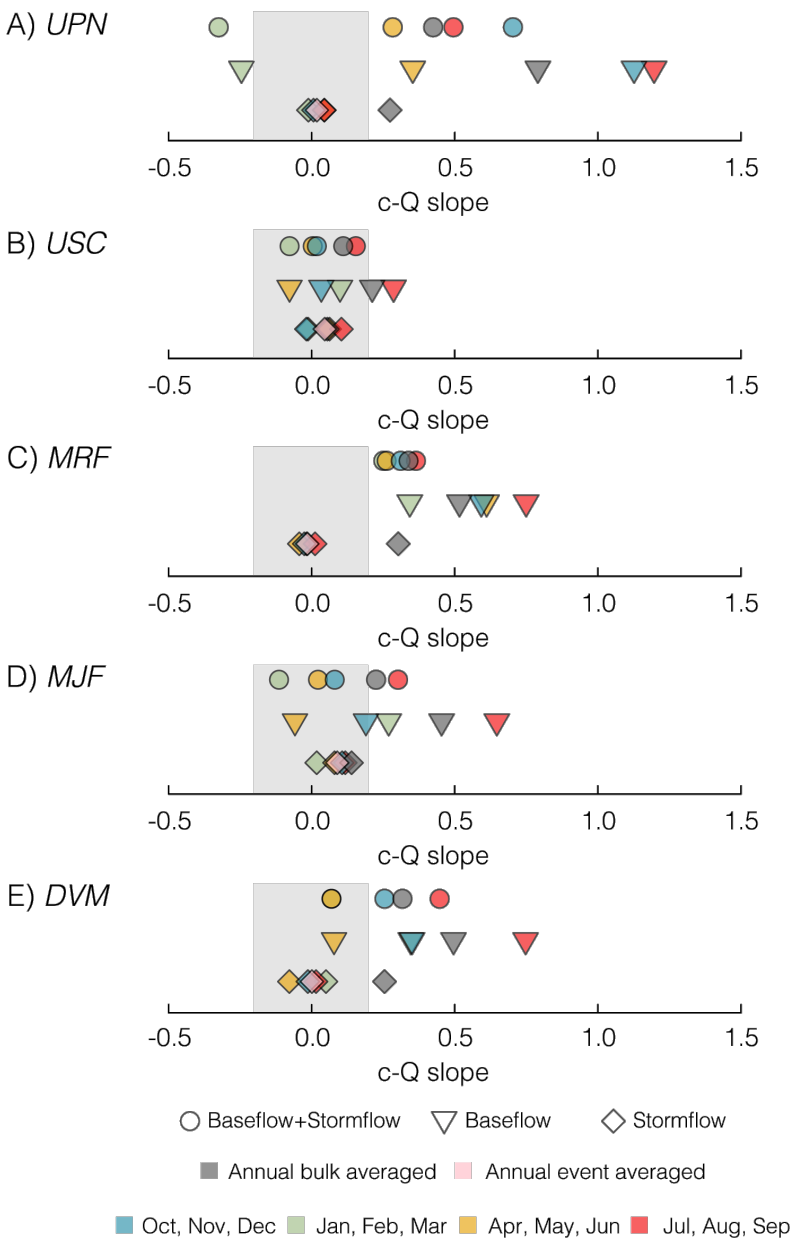

Figure 4-2 Concentration-discharge slopes in each watershed calculated independently for stormflow (diamonds), baseflow (triangles), and stormflow+baseflow (circles). Bulk annual slopes (dark gray) and seasonal slopes were calculated for fall (blue), winter (green), spring (yellow), and summer (red). Mean stormflow slopes were calculated as the mean of individual c-Q slopes (pink diamond), and as the c-Q slope of all stormflow data (dark gray diamond). Gray boxes indicate chemostatic behavior ($|b| \leq 0.2$).

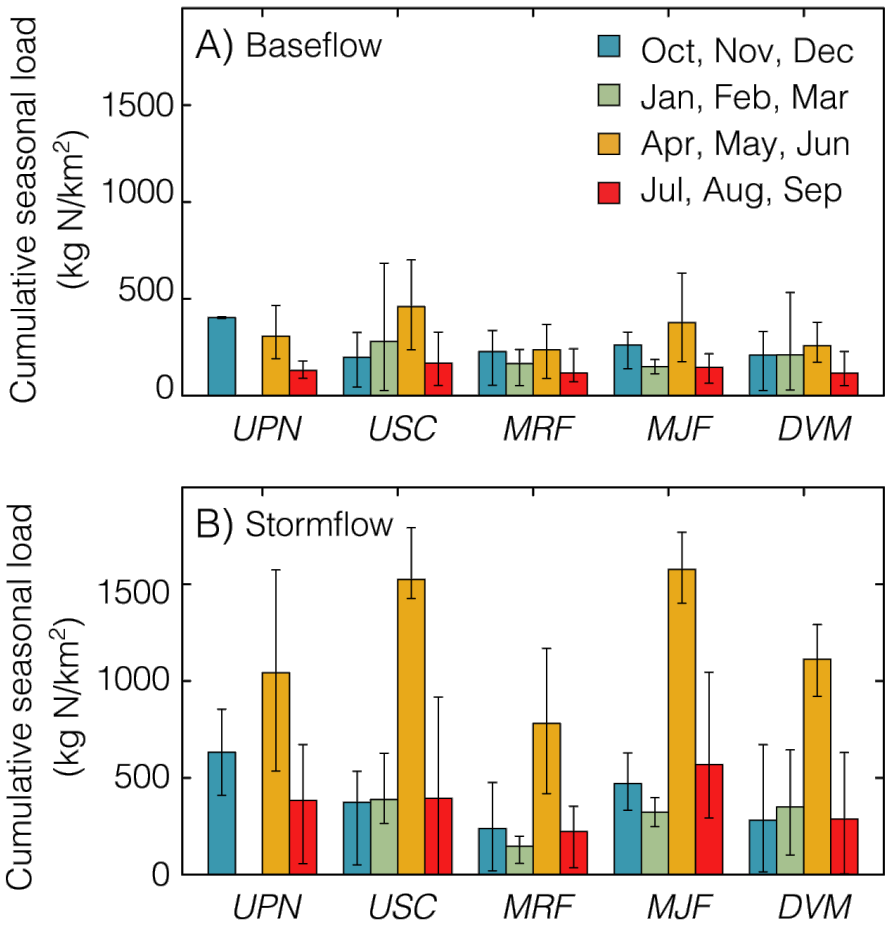

Figure 4-3 Seasonal NO_3 load (kg-N/km^2) normalized by watershed area, averaged over the four years of analysis (2016-2019) for each watershed for baseflow periods (A) and stormflow periods (B). Error bars show the range of loads measured over the four-year period.

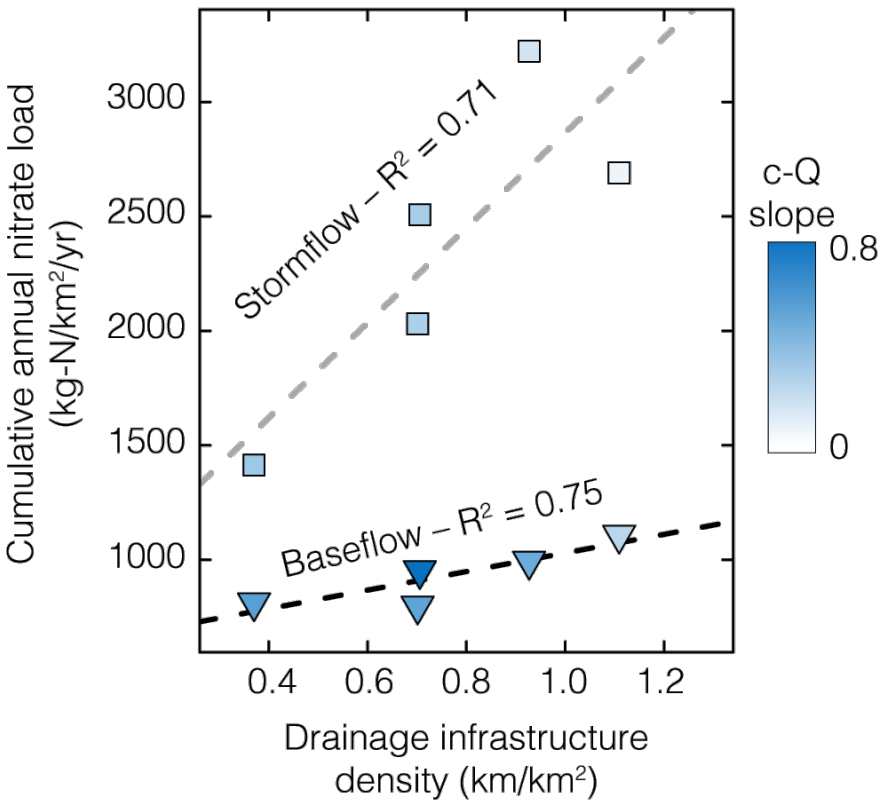

Figure 4-4 For all five watersheds, cumulative annual load exported during stormflow (squares) and baseflow (triangles) periods as a function of the drainage infrastructure density. Shapes are colored by the average c-Q slope for stormflow and baseflow periods with darker blues associated with more chemodynamic export regimes.

REFERENCES

Basu, N.B., Destouni, G., Jawitz, J.W., Thompson, S.E., Loukinova, N. V., Darracq, A., Zanardo, S., Yaeger, M., Sivapalan, M., Rinaldo, A., Rao, P.S.C., 2010. Nutrient loads exported from managed catchments reveal emergent biogeochemical stationarity. Geophys. Res. Lett. 37, 1–5. https://doi.org/10.1029/2010GL045168

Bieroza, M.Z., Heathwaite, A.L., Bechmann, M., Kyllmar, K., Jordan, P., 2018. The concentration-discharge slope as a tool for water quality management. Sci. Total Environ. 630, 738–749. https://doi.org/10.1016/j.scitotenv.2018.02.256

Botter, M., Burlando, P., Fatichi, S., 2019. Anthropogenic and catchment characteristic signatures in the water quality of Swiss rivers: A quantitative assessment. Hydrol. Earth Syst. Sci. 23, 1885–1904. https://doi.org/10.5194/hess-23-1885-2019

Buda, A.R., DeWalle, D.R., 2009. Dynamics of stream nitrate sources and flow pathways during stormflows on urban, forest and agricultural watersheds in central Pennsylvania, USA. Hydrol. Process. 3292–3305. https://doi.org/10.1002/hyp.7423

De Cicco, L.A., Hirsch, R.M., Lorenz, D., Watkins, W.D., 2018. dataRetrieval: R packages for discovering and retrieving water data available from Federal hydrologic web services. https://doi.org/10.5066/P9X4L3GE

Dewitz, J., 2019. National Land Cover Database (NLCD) 2016 Products: U.S. Geological Survey data release. https://doi.org/https://doi.org/10.5066/P96HHBIE

Diamond, J.S., Cohen, M.J., 2018. Complex patterns of catchment solute–discharge relationships for coastal plain rivers. Hydrol. Process. 32, 388–401. https://doi.org/10.1002/hyp.11424

Diaz, R.J., Rosenberg, R., 2008. Spreading dead zones and consequences for marine ecosystems. Science (80-.). 321, 926–929.

https://doi.org/10.1126/science.1156401

Dosskey, M.G., Vidon, P., Gurwick, N.P., Allan, C.J., Duval, T.P., Lowrance, R., 2010. The role of riparian vegetation in protecting and improving chemical water quality in streams. J. Am. Water Resour. Assoc. 46, 261–277. https://doi.org/10.1111/j.1752-1688.2010.00419.x

Dupas, R., Abbott, B.W., Minaudo, C., Fovet, O., 2019. Distribution of landscape units within catchments influences nutrient export dynamics. Front. Environ. Sci. 7, 1–8. https://doi.org/10.3389/fenvs.2019.00043

Dupas, R., Jomaa, S., Musolff, A., Borchardt, D., Rode, M., 2016. Disentangling the influence of hydroclimatic patterns and agricultural management on river nitrate dynamics from sub-hourly to decadal time scales. Sci. Total Environ. 571, 791–800. https://doi.org/10.1016/j.scitotenv.2016.07.053

Dupas, R., Musolff, A., Jawitz, J.W., Rao, P.S.C., Jäger, C.G., Fleckenstein, J.H., Rode, M., Borchardt, D., 2017. Carbon and nutrient export regimes from headwater catchments to downstream reaches. Biogeosciences 14, 4391–4407. https://doi.org/10.5194/bg-14-4391-2017

Ehrhardt, S., Kumar, R., Fleckenstein, J.H., Attinger, S., Musolff, A., 2019. Trajectories of nitrate input and output in three nested catchments along a land use gradient. Hydrol. Earth Syst. Sci. 23, 3503–3524. https://doi.org/10.5194/hess-23-3503-2019

Godsey, S.E., 2009. Concentration-discharge relationships reflect chemostatic characteristics of US catchments. Hydrol. Process. 1844–1864. https://doi.org/10.1002/hyp.7315

Hooper, R.P., Shoemaker, C.A., 1986. A Comparison of Chemical and Isotopic Hydrograph Separation. Water Resour. Res. 22, 1444–1454. https://doi.org/10.1029/WR022i010p01444

Howarth, R.W., 2008. Coastal nitrogen pollution: A review of sources and trends globally and regionally. Harmful Algae 8, 14–20. https://doi.org/10.1016/j.hal.2008.08.015

Jenny, J.P., Normandeau, A., Francus, P., Taranu, Z.E., Gregory-Eaves, I., Lapointe, F., Jautzy, J., Ojala, A.E.K., Dorioz, J.M., Schimmelmann, A., Zolitschkal, B., 2016. Urban point sources of nutrients were the leading cause for the historical spread of hypoxia across European lakes. Proc. Natl. Acad. Sci. U. S. A. 113, 12655–12660. https://doi.org/10.1073/pnas.1605480113

Jiang, R., Woli, K.P., Kuramochi, K., Hayakawa, A., Shimizu, M., Hatano, R., 2010. Hydrological process controls on nitrogen export during storm events in an agricultural watershed. Soil Sci. Plant Nutr. 56, 72–85. https://doi.org/10.1111/j.1747-0765.2010.00456.x

Kennedy, C.D., Bataille, C., Liu, Z., Ale, S., VanDeVelde, J., Roswell, C.R., Bowling, L.C., Bowen, G.J., 2012. Dynamics of nitrate and chloride during storm events in agricultural catchments with different subsurface drainage intensity (Indiana, USA). J. Hydrol. 466–467, 1–10. https://doi.org/10.1016/j.jhydrol.2012.05.002

Klaus, J., McDonnell, J.J., 2013. Hydrograph separation using stable isotopes: Review and evaluation. J. Hydrol. 505, 47–64. https://doi.org/10.1016/j.jhydrol.2013.09.006

Knapp, J., von Freyberg, J., Studer, B., Kiewiet, L., Kirchner, J., 2020. Concentration-discharge relationships vary among hydrological events, reflecting differences in event characteristics. Hydrol. Earth Syst. Sci. Discuss. 1–27. https://doi.org/10.5194/hess-2019-684

Lloyd, C.E.M., Freer, J.E., Johnes, P.J., Collins, A.L., 2016. Using hysteresis analysis of high-resolution water quality monitoring data, including uncertainty, to infer controls on nutrient and sediment transfer in catchments. Sci. Total Environ. 543, 388–404. https://doi.org/10.1016/j.scitotenv.2015.11.028

Marinos, R.E., Van Meter, K.J., Basu, N.B., 2020. Is the River a Chemostat?: Scale Versus Land Use Controls on Nitrate Concentration-Discharge Dynamics in the Upper Mississippi River Basin. Geophys. Res. Lett. https://doi.org/10.1029/2020gl087051

Mellander, P.E., Melland, A.R., Jordan, P., Wall, D.P., Murphy, P.N.C., Shortle, G., 2012. Quantifying nutrient transfer pathways in agricultural catchments using high temporal resolution data. Environ. Sci. Policy 24, 44–57. https://doi.org/10.1016/j.envsci.2012.06.004

Minaudo, C., Dupas, R., Gascuel-Odoux, C., Roubeix, V., Danis, P.A., Moatar, F., 2019. Seasonal and event-based concentration-discharge relationships to identify catchment controls on nutrient export regimes. Adv. Water Resour. 131, 103379. https://doi.org/10.1016/j.advwatres.2019.103379

Moatar, F., Abbot, B.W., Minaudo, C., Curie, F., Pinay, G., 2017. Elemental properties, hydrology, and biology interact to shape concentration-discharge curves for carbon, nutrients, sediment, and major ions. Water Resour. Res. 1270–1287. https://doi.org/10.1002/2016WR019635

Molenat, J., Gascuel-Odoux, C., Ruiz, L., Gruau, G., 2008. Role of water table dynamics on stream nitrate export and concentration in agricultural headwater catchment (France). J. Hydrol. 348, 363–378. https://doi.org/10.1016/j.jhydrol.2007.10.005

Musolff, A., Fleckenstein, J.H., Rao, P.S.C., Jawitz, J.W., 2017. Emergent archetype patterns of coupled hydrologic and biogeochemical responses in catchments. Geophys. Res. Lett. 44, 4143–4151. https://doi.org/10.1002/2017GL072630

Musolff, A., Schmidt, C., Selle, B., Fleckenstein, J.H., 2015. Catchment controls on solute export. Adv. Water Resour. 86, 133–146. https://doi.org/10.1016/j.advwatres.2015.09.026

Pellerin, B.A., Bergamaschi, B.A., Gilliom, R.J., Crawford, C.G., Saraceno, J., Frederick, C.P., Downing, B.D., Murphy, J.C., 2014. Mississippi river nitrate loads from high frequency sensor measurements and regression-based load estimation. Environ. Sci. Technol. 48, 12612–12619. https://doi.org/10.1021/es504029c

Prior, J.C., 1991. Landforms of Iowa. University of Iowa Press, Iowa City, IA.

Rabalais, N.N., Díaz, R.J., Levin, L.A., Turner, R.E., Gilbert, D., Zhang, J., 2010.

Dynamics and distribution of natural and human-caused hypoxia. Biogeosciences 7, 585–619. https://doi.org/10.5194/bg-7-585-2010

Richardson, C.M., Zimmer, M.A., Fackrell, J.K., Paytan, A., 2020. Geologic controls on source water drive baseflow generation and carbon geochemistry: evidence of nonstationary baseflow sources across multiple subwatersheds. Water Resour. Res.

Rodríguez-Blanco, M.L., Taboada-Castro, M.M., Taboada-Castro, M.T., Oropeza-Mota, J.L., 2015. Relating nitrogen export patterns from a mixed land use catchment in NW Spain with rainfall and streamflow. Hydrol. Process. 29, 2720–2730. https://doi.org/10.1002/hyp.10388

Royer, T. V., David, M.B., Gentry, L.E., 2006. Timing of riverine export of nitrate and phosphorus from agricultural watersheds in Illinois: Implications for reducing nutrient loading to the Mississippi River. Environ. Sci. Technol. 40, 4126–4131. https://doi.org/10.1021/es052573n

Rozemeijer, J.C., Van Der Velde, Y., Van Geer, F.C., De Rooij, G.H., Torfs, P.J.J.F., Broers, H.P., 2010. Improving load estimates for NO3 and P in surface waters by characterizing the concentration response to rainfall events. Environ. Sci. Technol. 44, 6305–6312. https://doi.org/10.1021/es101252e

Schilling, K., Zhang, Y.K., 2004. Baseflow contribution to nitrate-nitrogen export from a large, agricultural watershed, USA. J. Hydrol. 295, 305–316. https://doi.org/10.1016/j.jhydrol.2004.03.010

Schilling, K.E., Jindal, P., Basu, N.B., Helmers, M.J., 2012. Impact of artificial subsurface drainage on groundwater travel times and baseflow discharge in an agricultural watershed, Iowa (USA). Hydrol. Process. 26, 3092–3100. https://doi.org/10.1002/hyp.8337

Thompson, S.E., Basu, N.B., Lascurain, J., Aubeneau, A., Rao, P.S.C., 2011. Relative dominance of hydrologic versus biogeochemical factors on solute export across impact gradients. Water Resour. Res. 47, 1–20. https://doi.org/10.1029/2010WR009605

Turner, R.E., Rabalais, N.N., Justić, D., 2012. Predicting summer hypoxia in the northern Gulf of Mexico: Redux. Mar. Pollut. Bull. 64, 319–324. https://doi.org/10.1016/j.marpolbul.2011.11.008

Van Meter, K.J., Chowdhury, S., Byrnes, D.K., Basu, N.B., 2020. Biogeochemical asynchrony: Ecosystem drivers of seasonal concentration regimes across the Great Lakes Basin. Limnol. Oceanogr. 65, 848–862. https://doi.org/10.1002/lno.11353

Weyer, P.J., Cerhan, J.R., Kross, B.C., Hallberg, G.R., Kantamneni, J., Breuer, G., Jones, M.P., Zheng, W., Lynch, C.F., 2001. Municipal drinking water nitrate level and cancer risk in older women: The Iowa women's health study. Epidemiology 12, 327–338. https://doi.org/10.1097/00001648-200105000-00013

Zimmer, M.A., Pellerin, B., Burns, D.A., Petrochenkov, G., 2019. Temporal variability in nitrate-discharge relationships in large rivers as revealed by high-frequency data. Water Resour. Res. https://doi.org/10.1029/2018WR023478

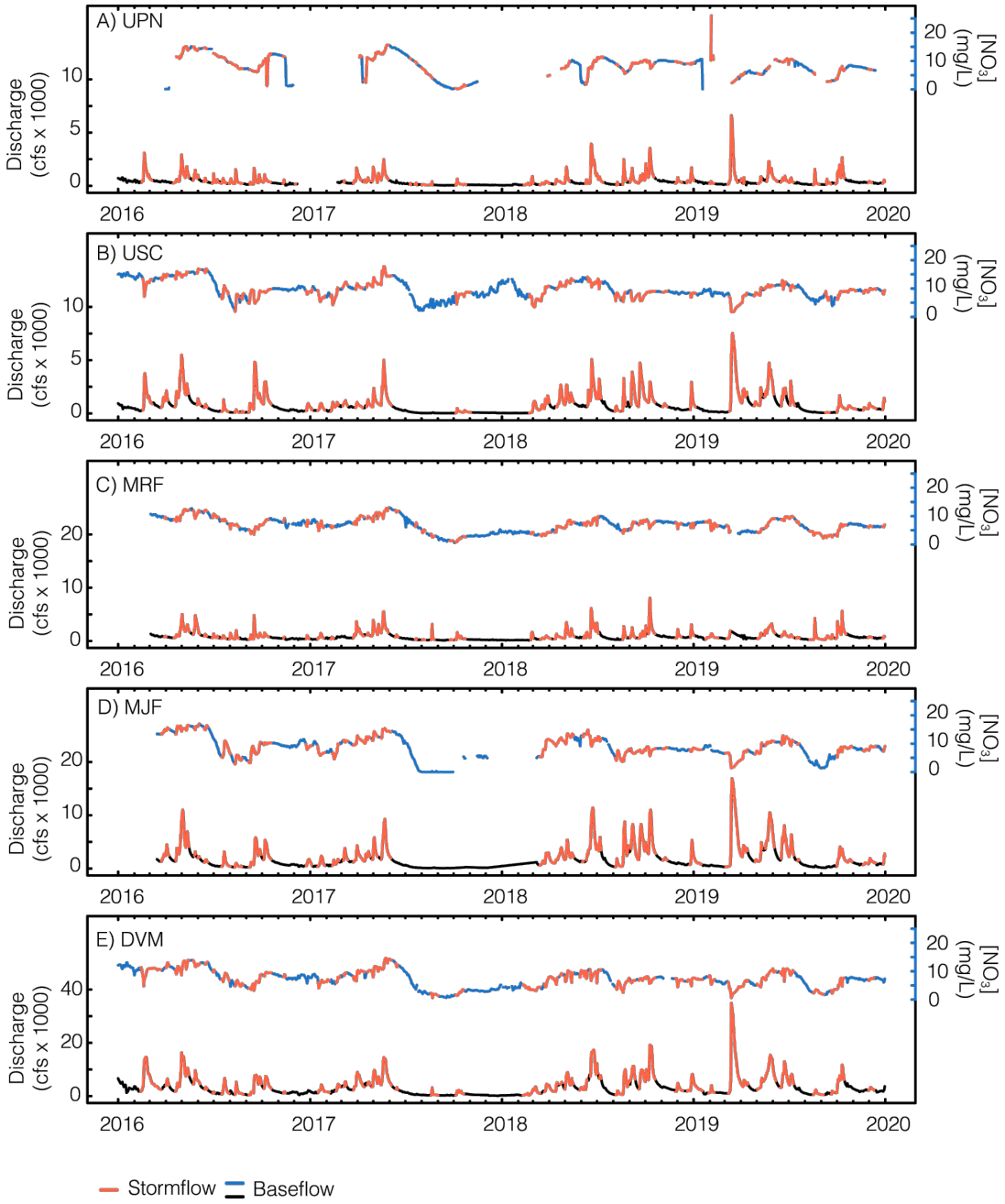

Figure 4-S1 Paired hydrographs and chemographs for the 5 study watersheds with identified events shown in red and baseflow shown in black (hydrograph) and blue (chemograph). Events were identified using the hydrograph, see section 2.X for details. The record begins in January 2016 and ends in December 2019.

Table 4-S1 – Data coverage by watershed

Watershed	Record start date	Record end date	n obs[a]	coverage[b]	largest gap
				(%)	(days)
UPN	3/31/16	12/13/19	971	71.8	127
USC	1/1/16	12/31/19	1451	99.4	7
MRF	3/3/16	12/31/19	1344	91.9	15
MJF	3/15/16	12/31/19	1229	88.7	94
DVM	1/1/16	12/31/19	1403	96.0	16

[a] Number of paired observations with discharge and $[NO_3]$

[b] Data coverage for discharge was complete for all stations, gaps were $[NO_3]$ non-reporting

Table 4-S2 – Watershed land cover characteristics

		Water		Developed		Forest		Crop		
Watershed	Area	Total	100 m buffer of stream	Total	100 m buffer of stream	Total	100 m buffer of stream	Total	100 m buffer of stream	Drainage infrastructure density
	(km^2)	(%)	(%)	(%)	(%)	(%)	(%)	(%)	(%)	(km/km^2)
UPN	1116	2	45	6	4	5	19	87	32	0.71
USC	1840	2	39	5	5	1	16	92	39	1.11
MRF	2548	2	46	5	3	8	20	85	31	0.37
MJF	4188	2	47	5	3	2	15	91	35	0.93
DVM	8870	2	52	5	3	4	16	88	28	0.70

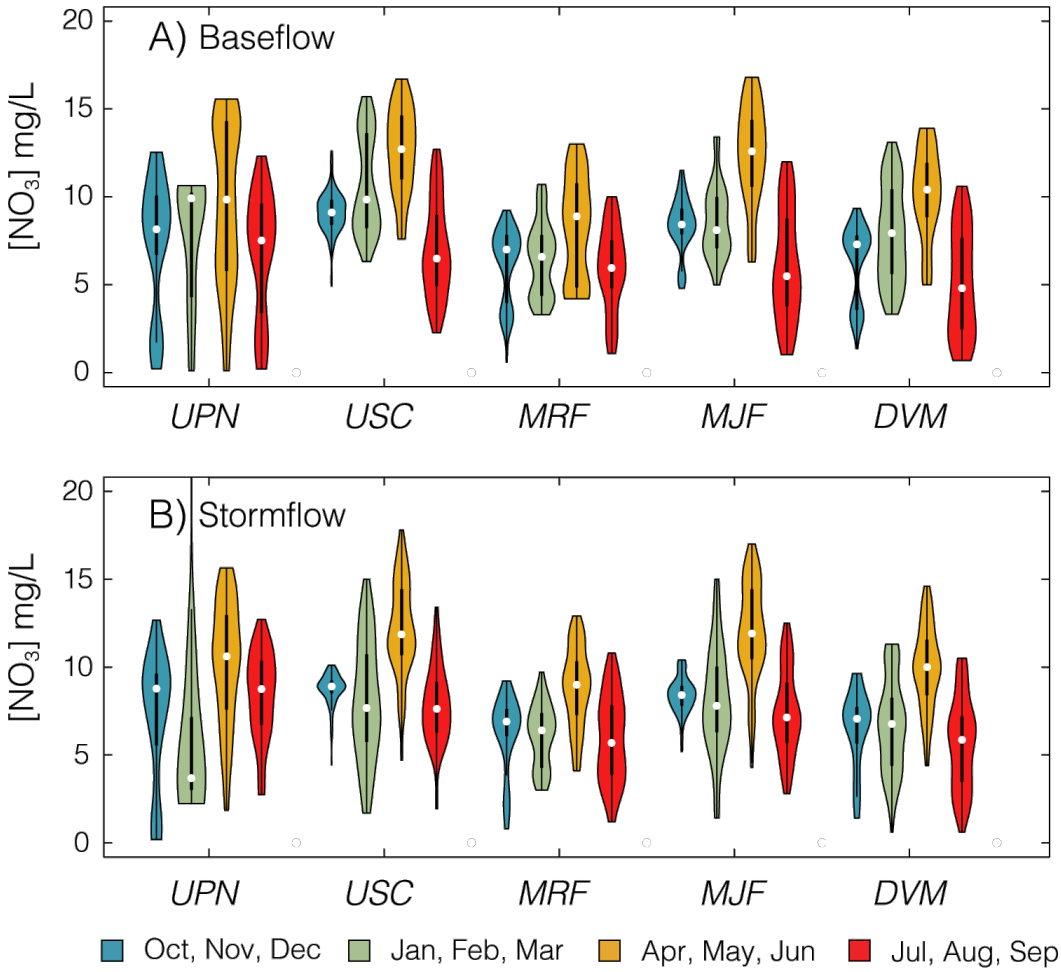

Figure 4-S2 Nitrate concentration by season for the five watersheds during baseflow (A) and event periods (B).

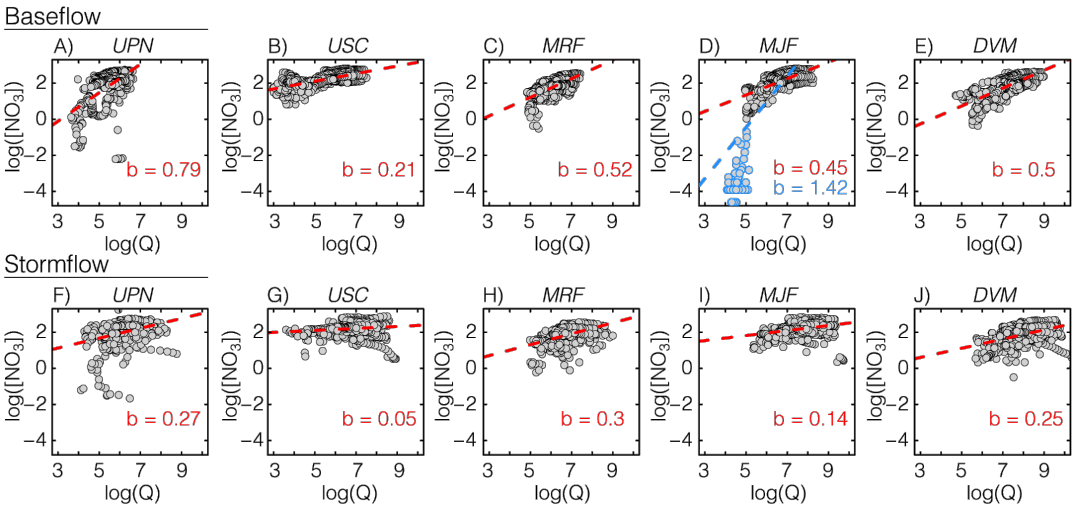

Figure 4-S3 Concentration-discharge plots for five studied watersheds during baseflow (A-E) and stormflow (F-J), with the slope shown in red. Panel D shows the baseflow for *MJF* with the low flow period from 7/27/17-10/19/17 when $[NO_3] < 0.5$ mg/L included (blue) and excluded (red). All slopes are statistically significant ($p < 0.01$)

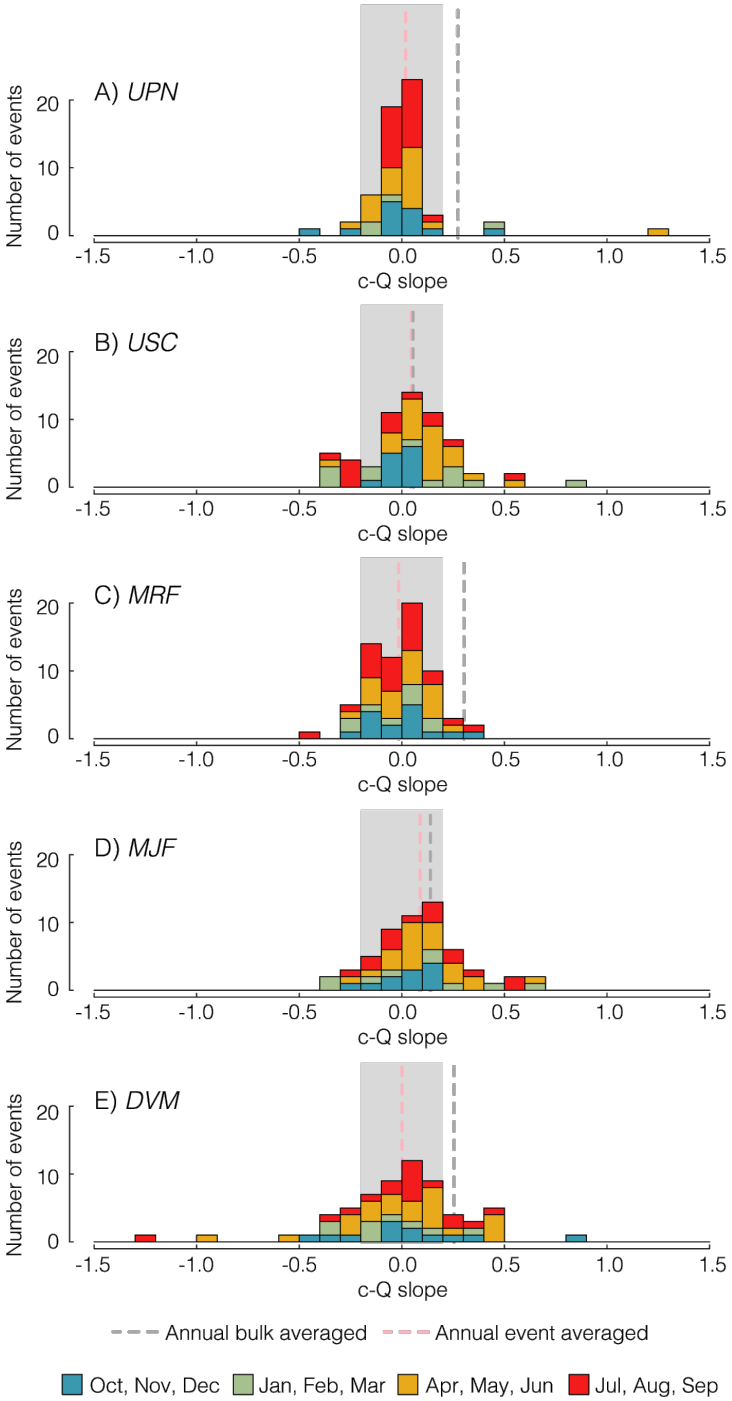

Figure 4-S4 Hisograms of event c-Q slope for each watershed colored by season. Gray dashed line shows the bulk stormflow c-Q slope and the pink dashed line shows the event-averaged c-Q slope. Gray boxes delineate chemostatic behavior ($|b| < 0.2$).

Table 4-S3 – Nitrate concentration and load for each watershed during baseflow and stormflow

	Baseflow+Stormflow		Baseflow		Stormflow	
Watershed	Nitrate concentration[a]	Cumulative annual load[b]	Nitrate concentration	Cumulative annual load	Nitrate concentration	Cumulative annual load
	mg/L	kg-N/km^2/yr	mg/L	kg-N/km^2/yr	mg/L	kg-N/km^2/yr
UPN	8.27	3457	7.89	953	8.66	2507
	(3.81)	(940)	(4.00)	(162)	(3.57)	(89)
USC	9.56	3799	9.53	1108	9.58	2690
	(3.09)	(1133)	(3.10)	(492)	(3.08)	(675)
MRF	6.77	2222	6.56	813	7.03	1413
	(2.51)	(371)	(2.43)	(208)	(2.59)	(215)
MJF	9.11	4216	8.68	994	9.52	3222
	(3.29)	(768)	(3.32)	(269)	(3.21)	(674)
DVM	7.24	2829	6.94	799	7.55	2031
	(3.07)	(654)	(3.08)	(287)	(3.02)	(412)

[a] mean value is reported for nitrate concentration, numbers in parentheses are the standard deviation

[b] mean annual cumulative load is reported, numbers in parentheses are the standard deviation